Experimental Testing Procedures to Investigate and Improve Insulated Rail Joint Design and Life Cycle

Thesis Submitted for the degree of Doctor of Philosophy

Department of Mechanical Engineering

The University of Sheffield

Philip Beaty, MEng

Academic Supervisors:

Professor R. Lewis

Dr. M. B. Marshall

Abstract

An insulated block joint (IBJ) is a mechanical joint which joins two abutting railway rails whilst keeping them electrically separate from each other. They are an integral component of block signalling systems as they allow for train detection within the network, however, they are a weak point in the system where failures can occur.

The aims of this research work were to develop test regimes to enable life cycle analysis of IBJs and use these tests to assess the performance of different materials and designs. This has been achieved by the use of specimen, component and full assembly level testing.

Specimen and component level shear testing has been carried out which has allowed for the assessment of different glues and insulating materials that are used in an IBJ and also has tested differing design principles. These experiments have been monitored using ultrasound techniques to investigate how failures within the insulating materials occur. It has been found that by using a full fit design with a glass fibre lining material an improvement in the shear strength of the IBJ can be obtained in comparison to a standard UK design.

A full scale testing regime was developed in order to cyclically load assembled IBJs and compare a new joint design with the standard design. The new test method enabled testing of the IBJs to failure and gave a good comparison between two joints. Ultrasonic monitoring techniques have been implemented based on knowledge gained in component level testing which has allowed for the assessment of de-bonding within the IBJs as the test is carried out.

Further specimen and full scale testing was carried out and a novel test regime was used to experimentally model lipping, the plastic flow of steel over the end of an IBJ causing electrical failure. This test regime allowed for the testing of different materials in both the endpost and the rail. By using a hardened rail steel or a hardened laser clad layer on the running surface of the rail it has been found that lipping performance can be improved greatly.

The work has led to the development of a new design of IBJ that incorporates material and design changes and aims to increase the life cycle of the IBJ by increasing static and dynamic stiffness and improving the rail material with respect to lipping performance. Further work on in service testing of laser cladding technology could be performed to further the work that has been achieved using twin disc testing.

Executive Summary

Introduction

The work presented in this thesis was carried out as part of a knowledge partnership between the University of Sheffield and L.B. Foster Rail Technologies (UK) Ltd. The aim of the work was to develop new methods of testing insulated block joints in order to understand their failure mechanisms. Following this, new designs and materials could be introduced which would increase the life cycle of these joints.

Research into this area is important. In the main UK rail network there are 80,000 IBJs (Insulated Block Joints) in service, 900 delay causing incidents are attributed to IBJs each year which results in a cost to the operator of £5,000,000 (1). Therefore, understanding and reducing these failures can lead to large savings for the rail operator.

Test Methods and Results

Three main test methods have been used to experimentally simulate different failures in IBJs. Shear testing has been used assess delamination and damage to the insulating layer, twin disc testing to assess lipping and full scale IBJ deflection testing to investigate the joint as a system.

Shear testing has been carried out at a specimen and a component level. Specimen tests were a good way to quickly and inexpensively compare and contrast the different materials used in the insulating layer of the joint. It was found that Temperange II adhesive was the best performing glue in these tests when used with any liner or when a liner is not included. Kevlar and glass fibre liner materials performed similarly in shear strength but both were better performing than the standard UK IBJ pultruded liner material. An increase in shear strength was seen when no liner was included in the bond between the adherends. Practically, this solution is not thought to be beneficial as there is then more of a reliance on the glue itself as an insulating material.

Component level shear testing was used to compare IBJ materials but also the design of the joint, full fit and wedge fit designs. This testing clearly showed that a full fit design using a flexible glass fibre liner showed better shear strength than the standard UK IBJ which is a wedge fit design using a pultruded glass fibre liner. The failures that occurred during these tests were either in the liner or at the bond between the liner and the rail. This suggests that any further design, material or manufacturing changes to improve the IBJ need to focus on this interface as the bond between the IBJ fishplate and the insulating liner is better than at the other interfaces.

Twin disc testing was successfully used in a novel way to experimentally model lipping over the endpost of an IBJ. Slots were cut into the surface of a disc cut from railway steel and filled with endpost materials. The testing simulated a wheel rolling over the endpost and generated lipping of the steel meaning that the gaps in the rail discs closed up. This would lead to an electrical failure in a real IBJ. Different endpost materials were tested and were found not to have a great effect on the rate or amount of lipping in the steel. Different rail steels were tested and it was seen that lipping was reduced when using harder and tougher steel grades. Further tests were therefore carried out on discs where a harder material had been laser clad onto the surface. This increased the performance of the discs and lipping was reduced dramatically.

The twin disc test results were compared with another method to experimentally model lipping. This test involved an endpost inserted into a full sized rail and a railway vehicle wheel was used to roll / slide over the rail and endpost. This full scale testing confirmed that a laser clad layer of harder material could be used to protect from failure by lipping. The test also gave confirmation that the twin disc test was a good method to assess the lipping performance of different rail materials.

Four point bending full scale deflection tests of IBJs were carried out to improve on current qualification testing methods and take IBJs to the point of failure. This was achieved and a standard UK IBJ was tested in comparison with a new design of joint. The two designs showed different final failure mechanisms with the new design of joint generally being stiffer and tougher than the standard joint. Video analysis was performed on the IBJs in the lab test and also on some plain rail in the same test set-up. This allowed non-intrusive measurement of the system which can also be carried out on in service IBJs. Plain rail was measured in the field and compared to the results gained from laboratory testing to assess the realism of the test set-up. It was concluded that the laboratory test set-up was a good and thorough method of testing and comparing joint designs in order to assess and improve design changes.

Ultrasonic techniques have been used in both the component shear testing and the full scale testing to analyse the interface between the components. The technique was successful at monitoring the insulating layer and assessing when delamination occurs in this layer. This is a useful set toward developing condition monitoring equipment for glued IBJs.

Conclusions and Further Work

This work has been successful in developing new test methods to experimentally investigate IBJ design and life cycle. Shear testing has resulted in a greater knowledge of the materials used in the joint and how they affect performance. Twin disc testing has led to the development of a method to test new rail steel and their effectiveness at preventing lipping from occurring. It has also shown that a harder, laser clad surface on the rail head could dramatically reduce the lipping seen and therefore reduce the potential for electrical failure. Full scale deflection testing has improved upon current test methods used and has taken IBJs to the point of failure. An Ultrasonic monitoring technique used during this testing has confirmed that condition monitoring of IBJs would be possible and will allow for the detection of delamination within the joint.

Further work should focus on the laser clad solution to lipping. This would include investigation into the design of the laser clad layer, where on the head of the rail this solution is applied and what happens at the transition between the laser clad layer and the normal rail steel. More laboratory testing should be carried out with a focus on the ultrasonic measurements so that this can be improved and a condition monitoring solution can be investigated further.

Contents

1 Introduction

1.1 Background

An insulated rail joint, or insulated block joint (IBJ), is a component in the railway signalling system that allows for the mechanical joining of two pieces of running rail whilst keeping the two rails electrically isolated from each other. The two rails are electrically separated from each other and the track split up into signalling blocks to allow the signalling system to tell where trains are on the network. This is achieved using track circuits and relays. A power source is connected to both running rails at one end of a track block and at the other end of the block both rails are connected via a relay. When the relay is energized the track block is unoccupied and a green signal aspect can be shown. When a train moves onto the track block the electrical circuit is shorted by the axle of the train and the relay becomes de-energised, causing a red signal aspect to be displayed. A diagram of this operation can be seen in Figure 1.

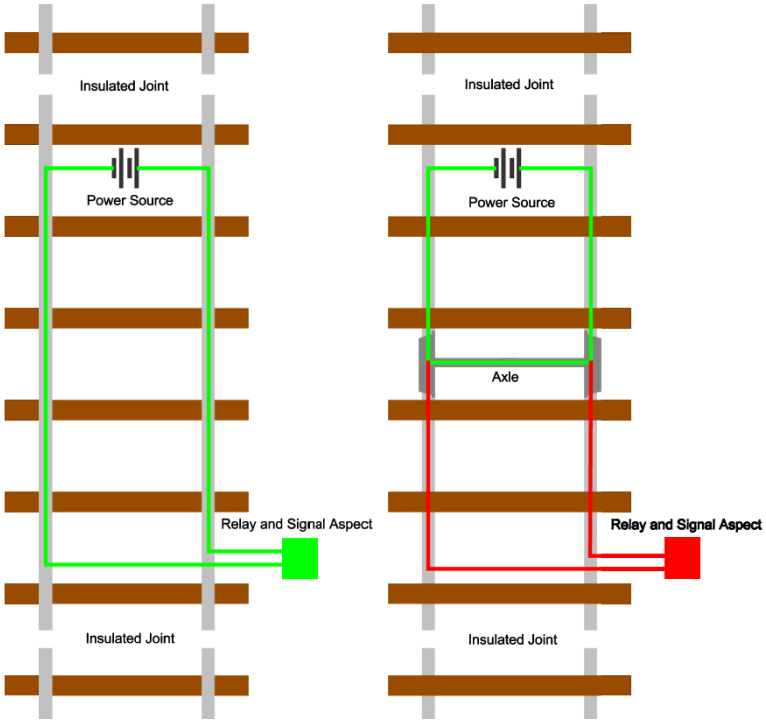

Figure 1: Image displaying the operation of a track circuit

An IBJ is generally constructed using a double lap joint design where two joint bars (fishplates) are fixed to either side of the adjoining rails. These fishplates are pinned or bolted into the rail and can be additionally secured using high strength glues. The fishplates are coated or encapsulated in an insulating material and an insulating endpost is inserted between the two rails to provide electrical isolation. A standard insulated joint set-up can be seen in Figure 2.

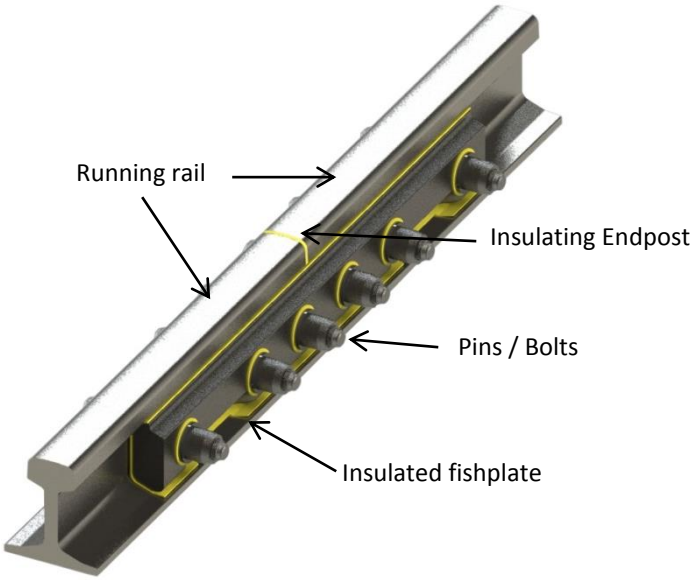

Figure 2: Standard insulated rail joint design

The IBJ inherently causes a weak point in the track structure where the bending strength of the track is generally lower than that of the surrounding rail. In a non-insulated standard UK joint, for example, the moment of inertia of the joint fishplates is only 29% of that of the parent rail. This leads to only around 90% of the bending moment being transferred across the joint (2). This can be improved upon using different joint designs or support situations, however, the weakness is still present. In addition to this weakness it has been found that dynamic impact loads on the IBJ can be up to three times higher than the static wheel loads (3). This is due to localised dipping of the railhead around the joint.

A discontinuity in the track structure coupled with high impact loads can lead to degradation and failure of the joint and also the surrounding supporting structure more quickly than the rest of the track. This causes replacement and maintenance work to be carried out that can be expensive and lead to delays in train operation.

In the UK network there are currently around 80,000 insulated joints. Over a two year period IBJs generally contribute towards 1,800 delay causing incidents, due to failures, at a cost of ten million pounds (1). Different failure modes are discussed in chapter 1.3.

1.2 IBJ Designs

Various IBJ designs are utilised in the railway industry around the world. These are tailored to the operating conditions of the railway and the standards that apply in the country of operation. Generally IBJs can be split into two categories; these are dry joints and glued joints. Dry joints are not glued into the track and rely upon the bolts holding the fishplates onto the rail for structural integrity whereas in a glued joint the fishplates are also glued to the rail to give further support.

Joints are usually designed with either four or six bolts or pins holding the fishplates in place. The longer six hole joints are thought to be stronger and stiffer, therefore lasting longer in service. Four hole joints, however, are shorter in length and can be used in curved track and in situations where

space is limited, within a points and crossing layout for example. Four hole joints are therefore still widely used on networks.

1.2.1 Dry Joints

Dry joints are generally manufactured using steel fishplates that are fully encapsulated in an insulating plastic based material, but fishplates manufactured from insulating materials, such as glass fibre re-enforced plastic, are also used. These joints can be installed into rail in-situ (in the field) and are used more commonly in switch and crossing and depot layouts where train movements are slower and joints have to be placed in more complex configurations.

The design and shape of dry joints follows the design principles of standard rail joints where a wedge fit principle is used and therefore the rail is guaranteed to be supported. A wedge fit design and an explanation of the terminology can be seen in Figure 3.

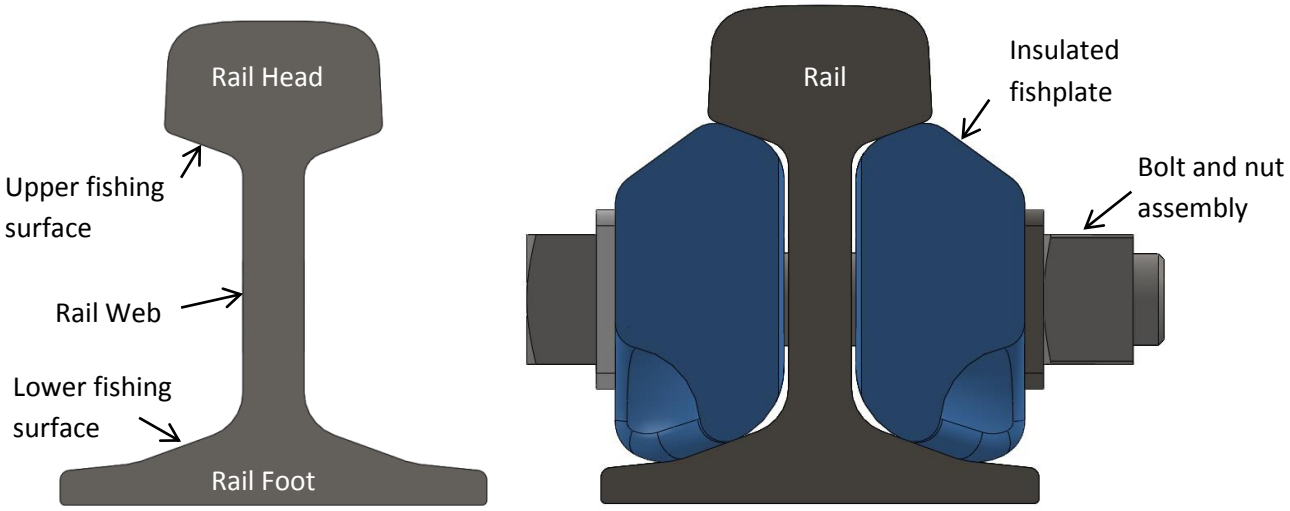

Figure 3: Image showing rail terminology and a wedge fit dry IBJ cross section

The wedge fit design of an IBJ means that only the fishing surfaces of the rail and the fishplates are in contact. The bolts can then be tightened to ensure the fishplates are fully supporting the rail and they are not loose in the assembly.

1.2.2 Glued Joints

Glued joints are generally assembled using fishplates that have an insulating liner between the steel fishplate and the rail rather than the fishplate being fully encapsulated. Glued joints are usually installed in a factory environment, where a clean atmosphere can be created, and more control can be offered. These joints are then welded into the parent rail in the field, usually by an aluminothermic welding method. Glued joints can be designed as wedge fit fishplates as discussed above, but are also designed as a full fit joint. Figure 4 shows a typical full fit glued joint design.

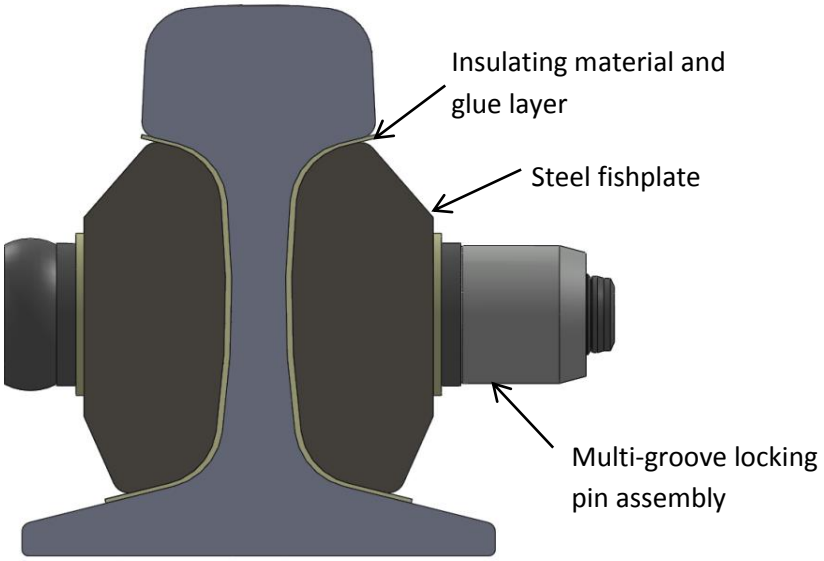

Figure 4: Full fit glued joint cross section

In a full fit joint the fishplate matches the shape of the rail web and fishing surfaces which aims to improve the glue bond between the two components. A full fit design requires improved accuracy and smaller manufacturing tolerances in the rail and the fishplate compared to a wedge fit fishplate design that can be made to fit in more cases.

1.2.3 Joint support design

The design of the support system of a joint also varies in different railway systems around the world. The simplest way to alter the support system of the joint is by altering where the sleepers lie underneath the joint. Standard practice in the UK is to suspend the insulated joint between two sleepers that are spaced at standard intervals, this allows automated maintenance practices to still be used around the joint. A supported joint can be created by placing the middle of the joint over a sleeper, or sometimes over two sleepers that are fastened together. This aims to give the joint more support, however, it disrupts the use of automated maintenance as sleepers are not distributed normally. This also alters the track stiffness which will affect other components and possibly lead to failures or degradation elsewhere in the system. The difference between these types of support situation can be seen in Figure 5.

Figure 5: Images showing a suspended joint (a) and a joint supported with two sleepers under the centre of the joint (b) (4)

1.3 Insulated Joint Failure Modes

Insulated joints can fail in a number of different ways which can usually be classified as either a mechanical or electrical failure. A mechanical failure can result from the failure of a component of the joint or the rail meaning the joint loses its structural integrity. A mechanical failure does not necessarily lead to a failure in the signalling system as the electrical isolation between the two adjoining rails may still be intact. An electrical failure of the joint will always lead to the failure of the signalling system as the electrical isolation between the two adjoining rails is lost. An electrical failure can result from a mechanical failure or can be caused by other factors.

The failure modes that are most common in the UK rail network can be seen in Figure 6 (5). These statistics cover all designs of IBJ currently in use on the UK network and there is currently no data (other than anecdotal evidence) to detail what the common failure modes of individual designs are.

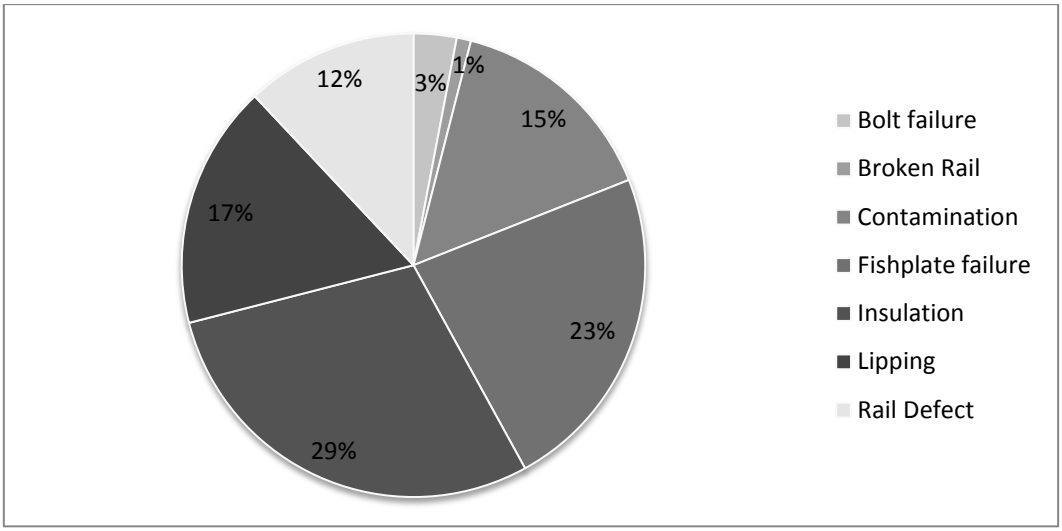

Figure 6: Breakdown of insulated joint failure modes in the UK rail network covering 1800 delay causing incidents in 2 years (5)

Both electrical and mechanical failures have the potential to cause delays in the running of railway operations. Depending on severity, mechanical failures can lead to speed restrictions or line closures until the fault is fixed. Electrical failures mean that signallers are unsure of the exact location of a train on that part of the network, which also leads to speed restrictions and a reduced capacity on the network.

1.3.1 Mechanical Failure

In the UK network, as illustrated in Figure 6, mechanical issues account for 39% of IBJ failures which include bolt failure, rail breaks, fishplate failure and rail defects. Mechanical failures can occur because of the high forces imparted on the joint by passing wheels. The forces at the area around the joint can be higher than those seen on a plain rail section due to the fact the joint is a discontinuity in the track as discussed in chapter 1.1. These high dynamic forces can over stress the components of the joint, leading to failure which usually occurs by fatigue. The image in Figure 7 shows the lower half of a broken fishplate that has fractured after large fatigue crack growth.

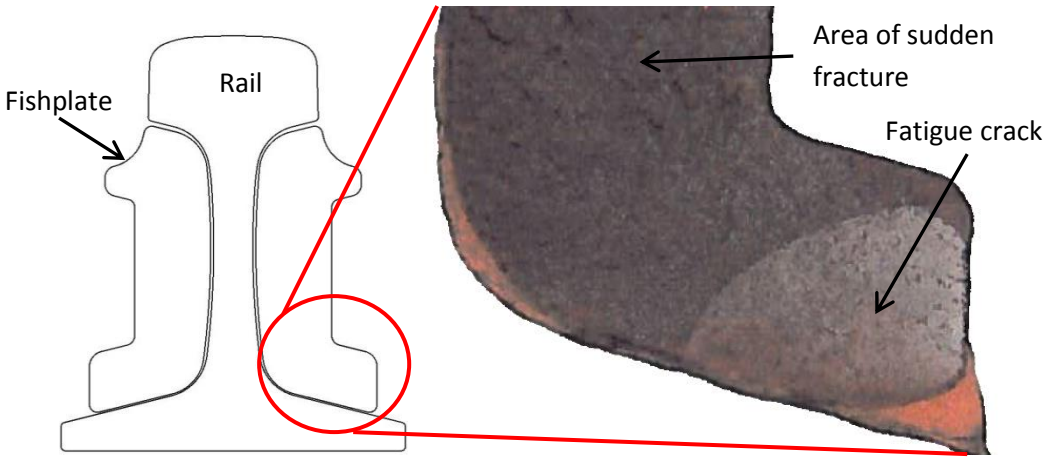

Figure 7: Fatigue failure of an IBJ fishplate (6)

It is estimated that the majority of mechanical failures occur in joints that have been in service for a long period of time and are of the dry joint design. These generally have a lower strength than glued joints.

1.3.2 Electrical Failure

Electrical failures account for 61% of IBJ failures in the UK, made up from contamination, insulation failure and lipping. Contamination is when a non-insulating material bridges the insulating gap between the two rail ends causing an electrical connection to be formed. The contaminating material could be general metallic debris on the trackside or wear debris from the head of the rail that builds up to form a bridge.

Insulation failure can occur in dry IBJs or glued IBJs that have become de-bonded where movement between the rail and the fishplate has worn away the insulation. This means the steel fishplate will act as a conductor between the two adjoining rails.

Lipping is defined as the plastic deformation or flow of the railhead over the endpost of the joint. The steel can be deformed by the high pressure applied by passing wheels and if the gap is completely closed up then electrical isolation is lost. An example of partial lipping can be seen in Figure 8 where the gap between the two rails has become narrower, damage to the railhead and the endpost can also be seen.

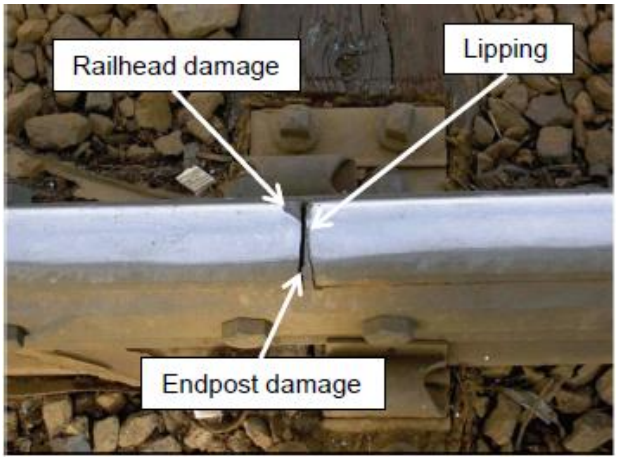

Figure 8: Image showing lipping of the rail head in an IBJ (7)

1.4 Aims of this work and contents

The aims of this work were to develop test regimes in order to assess the life cycle performance of IBJs and the merits of different designs or materials used in their construction. Some of the different failure modes mentioned in chapter 1.3 were investigated by the development of novel test methods. These failure modes were fishplate failure, insulation breakdown and de-bonding and lipping of the railhead over the endpost of the IBJ. Tests were carried out at specimen, component and full assembly level, depending on the failure mode being investigated. A further discussion of the test regimes employed and the justification for using these regimes can be found in chapter 4.

This thesis first outlines the current state of research in this field with a literature review focusing on different research areas in IBJs. A review of current qualification and quality testing methods for IBJs has then been conducted. The thesis then describes the test regimes that have been used to assess IBJ design and materials starting with specimen tests, then component testing and finally full scale assembly testing. Each of these sections is comprised of a method statement followed by results, discussion and conclusions. Final discussions and conclusions are then made with an overall view of all the testing performed.

2 Literature Review

Research has been carried out on various aspects of insulated rail joints which can generally be classified into categories including joint design and materials, support structure and vehicle / track interaction.

2.1 Joint Design and Materials

Insulated joint design has evolved over time since the introduction of track circuits. The first IBJs were dry joints where the fishplates were constructed from insulating materials such as high strength wood (2) and bone fibre (8). With the increase of axle loads and the introduction of continuously welded rail, which imparts more force into the joints, fishplates began to be constructed with different materials including glass fibre reinforced plastic and, eventually, steel fishplates with insulating liners have been introduced.

Many new designs of insulated joint have been developed and tested in order to try and improve the life of the joint and increase the joint strength so that it is closer to that of the parent rail. These designs generally focus on the improvement of the joint stiffness and therefore try to reduce the mechanical failures of the joint or electrical failure due to insulation breakdown. The designs do not generally improve the performance of the joint where other electrical failures occur, such as lipping.

IBJs were originally manufactured with four bolts to secure the fishplates into the rail, to keep the designs in line with non-insulating fishplates which have been around much longer and generally are of a four bolt design. To increase the stiffness and durability of joints longer fishplates were introduced that have six fasteners. The increase in length means that fishplates no longer fit in the gap between sleepers and therefore six hole plates have to provide space for the rail fastening system. An example of how this is achieved can be seen in Figure 9. Some joints are now designed with even longer fishplates requiring eight fasteners. A problem with this increase in length is the increase in cost of the IBJ where these spaces need to be provided, this also limits where the IBJ can be placed.

Figure 9: A six hole fishplate with material removed to allow fitment of the fastening system, in this case a Pandrol ‘e-clip’

Fishplates have been designed that have an increased cross section in their centre, therefore increasing the stiffness of the joint where it is most vulnerable. An example of this type of fishplate can be seen in Figure 10. This also increases the cost of the IBJ as a fishplate that is not uniform in cross section cannot be manufactured by standard rolling processes and has to be forged or machined which can be more expensive processes.

Figure 10: Fishplate strengthened in the centre to give higher modulus and reduced deflection (9)

Many IBJs utilise the standard fishplate design where a double lap joint is created by the fishplates either side of the rail. Attempts have been made to machine the rail so that it forms a lap joint itself. Figure 11 shows this type of joint where the traditional endpost is replaced by an insulating layer between the two rails that are forming a lap joint. Fishplates are still used to further secure the rails (10). This type of joint is used on networks where very high train loads are expected as they are stiffer than standard joints, they are however, much more expensive than normal fishplated versions. This design also does not help to alleviate many of the electrical failures that can occur due to lipping or contamination etc.

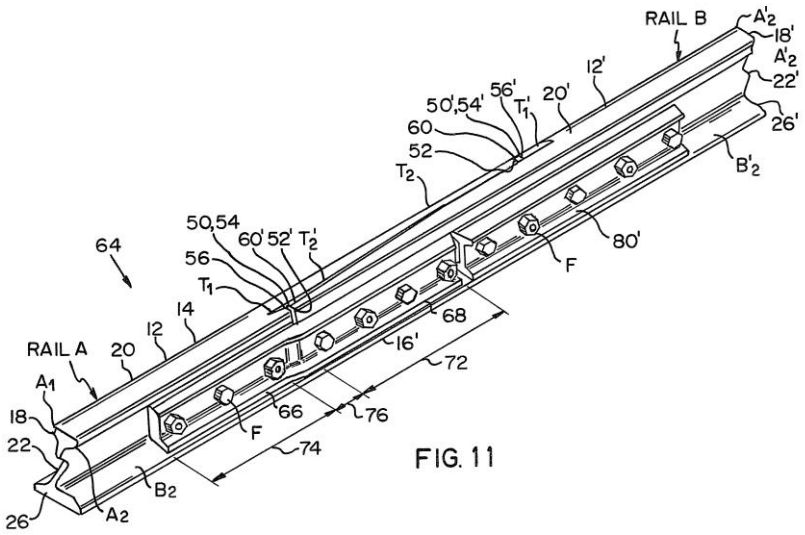

Figure 11: Long Angle Projection joint used in the USA (10)

Other studies have focused on improving the materials used in IBJ design to improve the joint's stiffness and life. Ceramic materials can have high strength and good electrically insulating properties, they have been used as part of rail joint design to improve the strength of the joint and also provide a method of monitoring the joint in service (11). Ceramics have also been investigated for use as an endpost material. LB Foster have investigated the use of ceramic material in endposts in order to increase the compressive strength of the endpost and thus reduce stresses in the

fishplates and glue layer. This approach has been modelled using finite element analysis and stresses are seen to be reduced (12). In other studies ceramics have been brazed onto steels to act as more of a structural component in the joint rather than just an insulating separator (13). Ceramics are a good material to use in compression as they have a high compressive strength but could be problematic if the IBJ starts to lose it's structure. If the IBJ starts to delaminate then higher impact forces are imparted on the joint and ceramic materials perform poorly under impact loads.

Other improvements in materials have been made in the steel fishplates. Standard fishplate steels are no longer used to manufacture IBJs and companies are now using micro-alloyed or heat treated steels that are stronger and more resistant to bending. Research has been undertaken to understand the failures of some steel fishplates due to fatigue cracking, see Figure 7. It was found that large amounts of decarburisation were causing a reduction in fatigue strength (6). This emphasises the importance of manufacturing control as well as material selection.

In an attempt to eradicate failure by contamination at the foot of the rail and electrical failure due to material build up between the joined rails, a few different methods are now employed. An endpost with specially designed lips and covers which increases the distance of the tracking path is sometimes used in the UK (14). UK railways including London Underground have tried to tackle the issue by increasing the endpost thickness, again in order to increase the distance between the two rail ends. Standard UK endposts are 6mm in thickness and endposts up to 12mm have been installed (15). The technique employed by LB Foster in the USA is to fully coat the joint in paint after installation which can be seen in Figure 12. This works for a new IBJ but paint can easily be worn away on the bottom of the joint by contact and abrasion by the ballast underneath.

Figure 12: Installed IBJs painted to stop failure by contamination (16)

To improve the joint stiffness additional products have been used to supplement the IBJ, the 'Hercules' joint (17) is an example of this and can be seen in Figure 13. This type of product increases the section modulus of the joint and increases the stiffness to try to stop the joint being a weak point in the track. This type of design, however, cannot be used in every location due to it's size and the fact that it may obstruct sleeper placement. It can also lead to an increased risk of electrical failure due to contamination build up or insulation failure as there is a higher area of insulated surface.

Figure 13: 'Hercules' insulated rail joint support plates (17)

2.2 Support Structure

The support structure around a joint in the rail is important because the joint itself does not have the same strength as the surrounding rail as discussed in chapter 1.1. A study has shown that poorly supported track around the IBJ due to unsatisfactory drainage, problems with rail fasteners or substructure degradation leads to a distressed or failed IBJ (3).

To counter this weakness in the rail, the support structure underneath the joint can be changed in order to support the rail more continuously. It has been calculated that the maximum vertical bending moment in a plain section of rail (non-jointed) is around 13% higher when the load is situated midway between the sleepers than when situated over the sleeper (18). As discussed in chapter 1.2.3, insulated joints are sometimes situated over the sleeper so that more support is provided. This does, however, cause problems in the fact that the connection between the rail and the sleeper has to be insulated. Also, double support sleepers as shown in Figure 5 are not favoured by most railways due to the inability to use mechanised track maintenance equipment at their location.

Investigations have been carried out to determine the effect of sleeper width on the support of an insulated joint (19). In this study finite element analysis was used to show that increasing the sleeper width decreases the deflection of the joint and the shear stress in the glue layer, in this study the joint was supported over the sleeper. This result is backed up by field testing of standard width sleepers against wider sleepers (3). This testing also shows that ballast degradation can be reduced by increasing the sleeper width. Using wider sleepers would be advantageous around the IBJ but would also lead to problems with mechanised track laying and maintenance.

One method of supporting a joint has been trialled where a sleeper is fixed to the adjacent sleeper underneath the rail joint, an image of this sleeper configuration can be seen in Figure 14. This method aims to increase the support area and also increase the rigidity of the joint's support (20). The advantage with this method is that it allows normal maintenance of the track with the use of mechanised equipment. It was proved that this method could lead to an increase in time between maintenance operations and therefore lower the life cost of a rail joint. The problem with this

method was making sure that the concrete used to join the sleepers does not crack as it is exposed to the high dynamic forces imparted on the rail.

Figure 14: A joint supporting sleeper arrangement where two adjacent sleepers are fastened together (20)

Another method that has been developed to continuously support the IBJ is the sleeper plate. These have been designed so that a sleeper can be placed directly underneath the joint whilst ensuring this does not affect the electrical isolation of the two rails. A three sleeper plate has also been developed to allow all three adjacent sleepers to support the rail as shown in Figure 15 (21).

Figure 15: Three sleeper insulated plate used to support the IBJ (3)

2.3 Wheel / Rail Interaction

The large pressure that is generated between the wheel and the rail can cause many problems for an insulated joint. A known problem at an IBJ is material deformation, or plastic flow, of the rail head because of this pressure. Deformation of the rail head occurs in the longitudinal, lateral and vertical directions, examples of this can be seen in Figure 16.

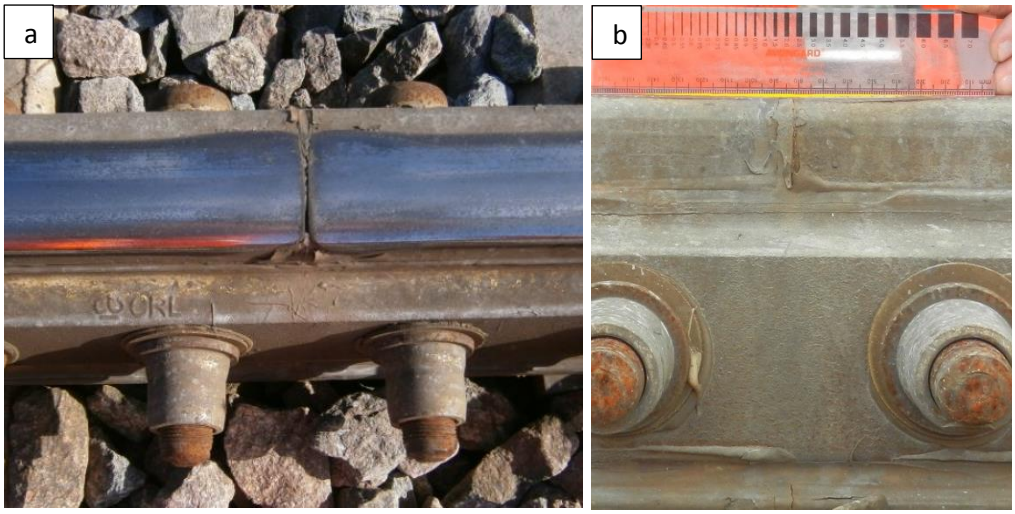

Figure 16: Image (a) showing longitudinal and lateral deformation (lipping and bulging) and (b) showing vertical deformation (dipping - highlighted)

The vertical deformation of the railhead leads to a dip in the track around the endpost of the joint. Track irregularities such as this have been investigated and studies show that dips in the track, caused by IBJs, squats and aluminothermic welds etc., can lead to high dynamic forces being imparted to the rail (22). These high impact and bending forces then affect the joint by increasing the stress in the fishplates and the glue layer which become more liable to failure. These forces can also affect the track structure and sub-structure which can lead to an exacerbation of the dip because of mechanisms such as ballast degradation or rail pad wear. It is therefore important to design a joint that can resist these forces when dipping occurs or improve the support structure as discussed in chapters 2.1 and 2.2. This is also why it is important to conduct full scale testing of a joint which is carried out as part of this research. Because welds in the track can cause high impact forces similar to an IBJ it is usual to attempt to place IBJs as far from welds as possible. Flash butt welding when installing an IBJ may be advantageous to aluminothermic welding as this process is less likely to cause a defect in the track that would affect the IBJ.

Longitudinal plastic deformation of the steel railhead, known as lipping, can close the insulating gap between the two abutting rails. If lipping is left without maintenance the gap can close up fully and the electrical isolation of the two rails is lost, resulting in signalling failure. To stop lipping and maintain a healthy gap between the two rails the lipping is generally ground off during track maintenance and the resulting gap filled with epoxy resin (1). Although this temporarily fixes lipping it does not address any damage due to vertical deformation of the railhead and the track will remain dipped after this repair process.

Studies into lipping have generally focused on three areas; field testing or field studies, full scale lab testing and numerical and computer modelling. A field study on the Swedish rail network gathered data on the deterioration of IBJs over a number of years (7) (23). This study highlights the railhead damage around an IBJ. It has been found that this occurs more rapidly in a newly installed joint and slows over time as the railhead becomes more resistant due to work hardening. The track dip has also been investigated which has been shown to increase in magnitude over time. Some microstructural characterisation has been carried out on field tested joints, but this has shown little data on the material flow pattern of the rail and how this flow occurs (24).

Methods have been trialled to reduce lipping which include changing the shape of the railhead and coating the railhead with a stronger material. Stronger and harder materials coating the railhead have been shown to lead to less damage in service including reduced material flow (24). Other studies have been carried out that suggest a laser clad layer on the rail surface would provide more protection against rolling contact fatigue and other damage to the railhead (25). The shape of the railhead has been machined into a dip around the joint in one study which has the effect of taking the area of critical strain away from the end of the rail (26). This should reduce lipping as it takes away a possible cause, however, introducing a dip into the track will lead to other problems as discussed above. This testing has been carried out using full scale test rigs, but field tests are advantageous because they represent the real conditions the joint will face. However, laboratory tests allow the acceleration of testing and can be less expensive alternatives to field testing. Some full scale testing methods have not been able to model lipping, but have given useful data for comparison with numerical models investigating plastic strain accumulation (27).

Computer modelling studies have discovered that the contact pressure between the rail and the wheel increases when the wheel passes over the endpost of an IBJ which could be a cause of material flow in this area (28) (29). This increase in contact pressure seems quite obvious as the contact area between the wheel and rail decreases as the wheel rolls of the edge of the rail over the endpost. Similar modelling studies using finite element and numerical techniques have investigated the effect of changing the endpost thickness on contact forces between the wheel and rail. It has been found that damage to the railhead at an IBJ will occur more quickly where a thicker endpost is used. This is due to an increase in the effective strain and plastic strain magnitudes with an increase in endpost thickness (7) (22) (30). In terms of lipping it is hard to judge the overall effect of changing the endpost thickness because although lipping may occur more quickly it also has a larger gap to close with a thicker endpost.

The wheel-rail contact and the effect it has on plastic deformation in the rail has been studied using a scaled experimental test. Twin disc testing has experimentally modelled ratchetting (the accumulation of plastic deformation) of the steel railhead. Twin disc testing can apply a tractive force (slip) to the rail which results in the ratchetting behaviour that can be seen in Figure 17. Laser cladding of harder materials has also been applied to twin disc test samples with rail steel as the base material in order to reduce ratchetting and increase the fatigue strength of the discs (31) (32). Modelling and analysis has also been conducted of rail coated with high strength materials which concludes this can be used to reduce RCF and increase wear resistance (33). These methods could be utilised at the rail ends at an IBJ to limit the extent of lipping and increase the service life of an insulated joint.

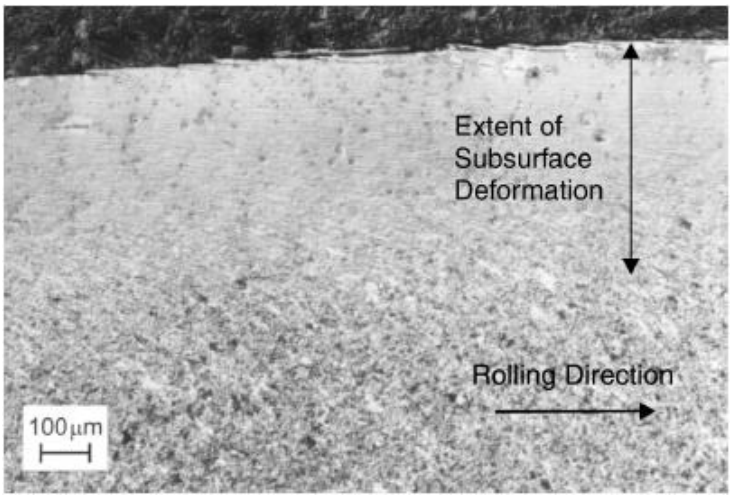

Figure 17: Steel ratchetting formed through twin disc testing with 3% slip (34)

2.4 Summary

The literature review has provided a background of the research carried out associated with IBJs that is currently available to the author. Many differing designs and materials are used in IBJ manufacture, however, specific results are not available on the performance of these. Specimen, component and assembly testing that will assess and rank differing materials and designs is therefore required to understand and improve upon the life cycle of an IBJ. This work will also contribute towards the current aims of Network Rail where IBJs are concerned. These aims include manufacture of an IBJ with comparable stiffness to plain rail, with stiffness not deteriorating during the life of the IBJ and the investigation of different insulating materials (35).

Lipping, a very common cause of failure, has been researched through analytical, numerical, and experimental modelling. To date no experimental modelling of this failure mode has provided results that can be used to determine the effect of changing materials of the IBJ on lipping performance. An aim of this work is to attempt to experimentally model lipping using twin disc testing which is a novel approach to this problem.

Testing of the designs and products mentioned above has been carried out in service, by numerical analysis or in line with test regimes similar to those discussed in the next chapter. It can be noted that no literature has been found where condition monitoring is used to investigate the joint and the insulating layer.

3 Insulated Joint Test Regimes

As a structural part in a safety critical environment, insulated joints are subject to standards that are set either by railway operators or by the government of the country where the railway is located. To comply with these standards it is generally required to undertake qualification testing of new joint designs before they are placed in service. The qualification tests are usually formed of a number of static and dynamic loading scenarios and include electrical testing, both wet and dry, and tests of straightness and conformance with track clearances.

The tests that are carried out and the pass criteria vary depending on where the joint will be used in the track and what loads and environmental conditions it will be subjected to.

3.1 Static Testing

Static testing can be employed to test the stiffness of the joint and its resistance to loading. This is usually completed in the longitudinal direction, but is also carried out in the vertical direction. Longitudinal static testing is useful for simulating the forces that would be imparted on a joint due to rail expansion and contraction because of changing temperature. This is especially important if joints are to be installed in continuously welded rail as this situation can lead to large longitudinal forces.

The forces that are applied to the rail in order to pass qualification tests vary depending on rail size and the specific requirements of the operating railway. For example in the UK using the most common rail section the joint must be subjected to a 700 kN longitudinal force (36).

Static testing can also be used to test the vertical bending stiffness of a joint. In the qualification test regime for Australian IBJs it is required that a vertical load be applied up to 1900 kN or until the IBJ fails (37).

3.2 Dynamic / Cyclic Testing

The cyclic testing of a joint aims to model experimentally what happens in field service or to accelerate this process. Generally, joints are cyclically loaded in the vertical direction to simulate a wheel passing over the track. The loading configuration can be in three point or four point bending or is sometimes set-up so that a loaded wheel is rolled back and forth over the joint. The rail is usually supported statically at a spacing of anything up to 1.3 metres.

In Figure 18 a cyclic testing set-up is shown that simulates the vertical deflection of the joint both downwards (sagging) and upwards (hogging). Rail in service experiences this as a wheel passes over it.

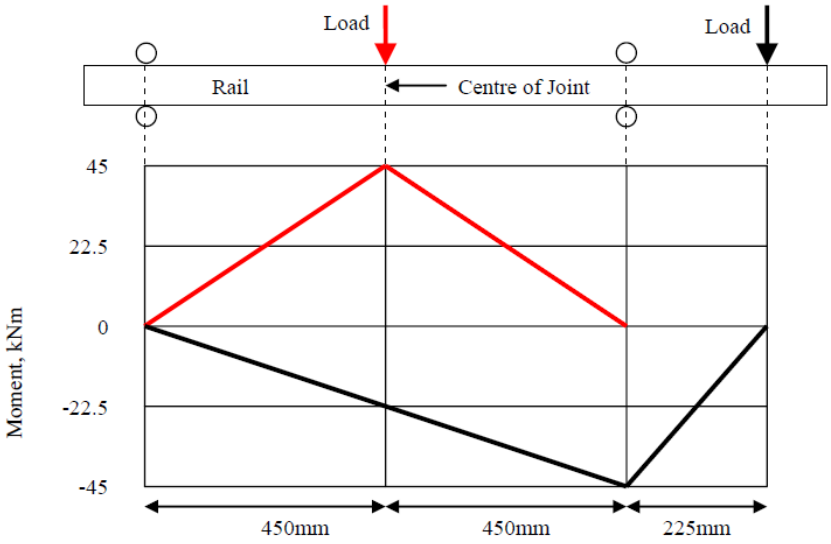

Figure 18: Test set-up for vertical cyclic loading of an IBJ

3.3 Electrical Testing

The electrical testing of a joint usually forms part of the qualification test of an IBJ for product acceptance purposes, but also part of the quality control process of manufactured IBJs. The testing process for qualification is generally more rigorous and can involve high impedance tests, lower voltage DC resistance testing and tests in various environmental conditions. In addition to the two rails being electrically isolated from each other, requirements are generally set for the fastening systems to be isolated from both the rails and the joint bars.

For quality control, DC resistance testing is usually required, in the UK a voltage of 500 VDC should be used to check the resistance between the two rails and also between the fasteners and the rails and the fishplates. For the manufactured joint to pass this test a resistance of at least 500kΩ should be achieved (38).

3.4 Summary

Although the test regimes mentioned above are useful for assessing the quality of an IBJ, and whether it is fit for purpose, they do not generally test joints sufficiently to enable a comparison or ranking between differing joint designs. One of the aims of this work, to test a fully assembled IBJ and compare designs, will stress the joint to a higher degree therefore enabling this comparison and life cycle assessment.

4 Justification for Experimental Analysis

Various tests were devised to assess different failure modes in IBJs as discussed in the introduction. Specimen testing was carried out using a twin disc testing machine to experimentally model lipping of the railhead, different rail materials have been tested to assess their effect on this failure mode. This test method aimed to further research already carried out, as discussed in the literature review, where no experimental procedure has been successful in modelling lipping. This specimen testing for lipping was then compared to the results of a full scale lipping experiment that was designed to confirm results of earlier twin disc tests. Specimen testing was useful as it provided results more quickly enabling the testing of various materials and layouts. Comparing specimen test results with full scale testing was important to find out that the earlier tests gave a good representation of a real life scenario.

In both the twin disc and full scale experimental methods the endpost gap was measured to assess the lipping of the rail material over the endpost. Twin disc testing allowed for further analysis because the samples could be more easily sectioned which gave an insight into material flow below the surface of the rail. This has led to a greater understanding of the mechanism behind lipping.

Specimen testing was also carried out to assess the shear strength of different glue and insulating liner combinations. This gave an understanding of different material strengths and allowed for the ranking of materials which can be used in an IBJ assembly.

Component shear testing was used to evaluate the difference in joint design and materials used. This testing confirmed the specimen testing and also allowed for the trial of ultrasonic monitoring techniques that can be used in other test set-ups.

Full scale assembly testing was then used to confirm any advantage from a different IBJ design and compare new test methods with those currently used in qualification testing. This testing was static and dynamic and improved understanding of the joint and enabled more analysis than can normally be carried out under a more standardised qualification testing procedure. The full scale testing also made use of the ultrasonic techniques investigated in the component shear testing. This gave an understanding of the failure mode of different joint design and also helped investigate the possibilities of developing condition monitoring for glued IBJs.

The full scale test method that was devised was then compared to real field measurements of rail deflection. This allowed for the justification of this new test method and gives a comparison of real life scenario against what is seen in laboratory testing. The different testing modes and how they are related to the overall joint performance are outlined in Figure 19.

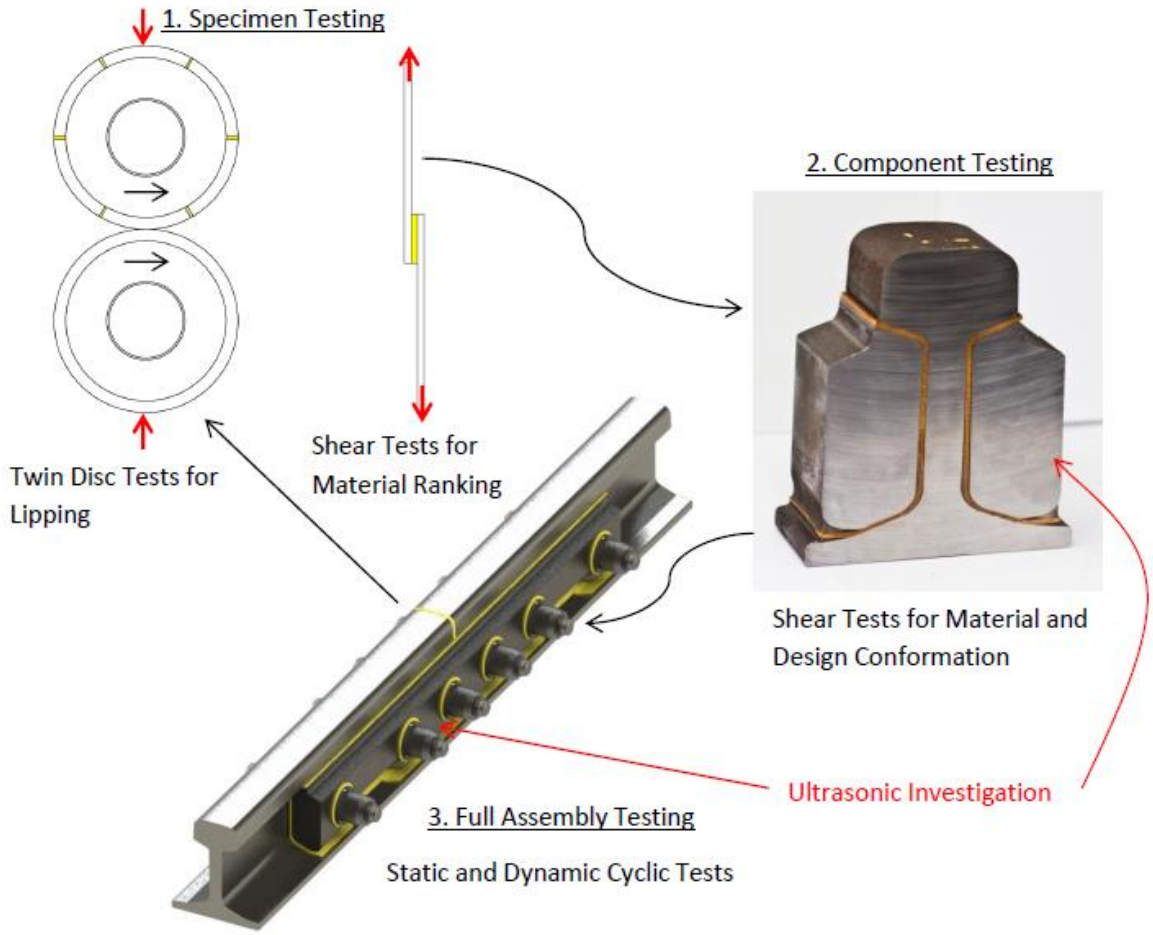

Figure 19: Variety of tests used to investigate IBJ design

5 Specimen Testing – Comparison of Materials

The insulating layer and the glue that hold a glued IBJ in place form an important structural material as well as being used to electrically insulate the components of the IBJ. Under normal conditions a joint can be subjected to tension due to longitudinal forces, bending due to vertical forces and torsion due to lateral forces. These different forces are mostly transferred from the rail to the fishplate by shear through the glue layer. Lap shear testing has therefore been used to compare the performance of different glue and insulating liner combinations.

The aim of the experiment was to rank different glues and insulating liners so that the best combination could be determined and this could then be investigated further and verified in component or full scale testing.

5.1 Method

The method for this testing was based upon a European standard shear testing arrangement (BS EN 1465: 2009 *Determination of tensile lap-shear strength of bonded assemblies*). This standard specifies the size of the steel pieces used and the size of the bonded area. The specified thickness of the bond was not adhered to due to the insulating liners that have been incorporated into the testing; these liners increase the overall thickness of the test specimen.

The shear test samples were tested using a hydraulic tensile test rig under displacement control. The samples were pulled apart at a constant rate of 0.01 mm/s. Readings of the force applied by the rig and the displacement of the test samples were taken throughout the test. The measurement of applied force was used to compare the shear strength of the samples. An image of the test set-up can be seen in Figure 20.

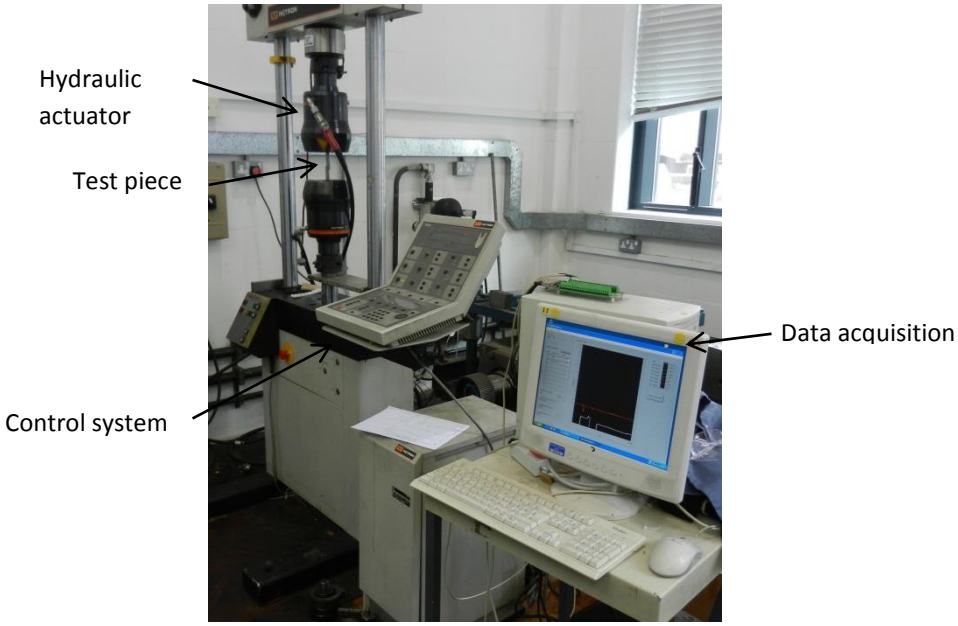

Figure 20: Image of the test set-up

5.1.1 Test Samples

Test samples were made to try to replicate the method used in manufacturing IBJs. The joint bar / rail in IBJs are gritblasted and degreased prior to bonding, it was not possible to gritblast the thin test sample steel and therefore surface preparation was carried out by roughening and cleaning the steel using p60 abrasive paper. The bonding surface was then cleaned with alcohol wipes. The steel samples were 100 x 25 x 1.6 mm in dimensions.

The insulating liner that electrically separates the steel was glued on to one steel piece and this was allowed to fully cure before the next steel piece was glued to this as can be seen in steps 1 and 2 in Figure 21. This method matches the general installation of glued IBJs where insulated fishplates are manufactured prior to installation into rail to manufacture a full joint. The overlap between the insulating liner and the steel is 12.5 mm.

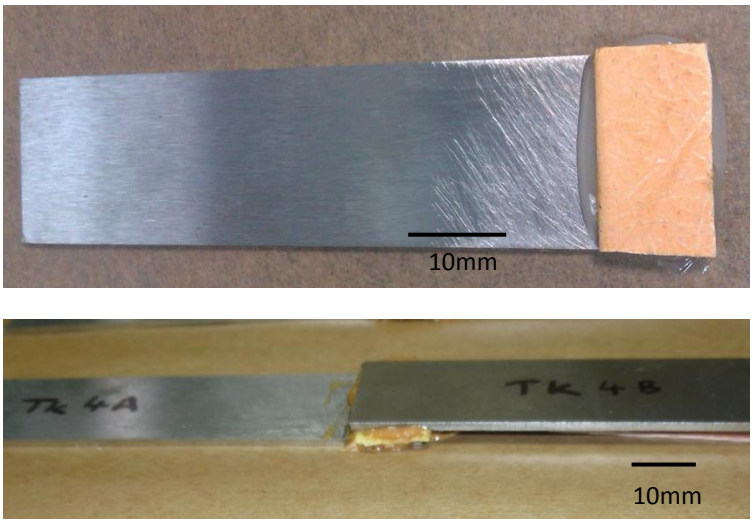

Figure 21: Step 1, top, bonding the liner onto a steel sample and step 2, above, bonding another steel sample to this.

During this process four different glues and three liners, including samples with no liner, were tested. Notation for the different glues can be seen below.

The different glues used were:

1. Huntsman Araldite adhesive (H)
2. Temperange II (T)
3. Edilon Dex-L 2k tix (E)
4. Permabond (P)

All of the glues used are two part epoxy systems made from a resin and a hardener and have been developed by the manufacturers specifically for use in IBJs.

The liners used were:

1. Pultruded glass reinforced polyester resin (stiff liner material) (P)
2. Glass fibre sheet (flexible woven mat) (G)
3. Kevlar sheet (flexible woven mat) (K)
4. No liner (N)

The three liner materials above are used in various IBJs around the world. At present there is no known IBJ that does not employ the use of an insulating liner.

For each combination of glue and liner tested five specimens were created so as to give a fair representation of the results.

After the glue had cured all the test samples were tested for electrical insulation using a Megger 500 V D.C. insulation testing kit, similar to that used for quality control testing of IBJs. All the test samples passed this testing, including the samples with no insulating liner.

Once the test samples had been created shims were then attached to the steel samples so that when the tensile load was applied it was applied in line with the bonded joint and the samples were tested in pure shear. An example of this can be seen in Figure 22.

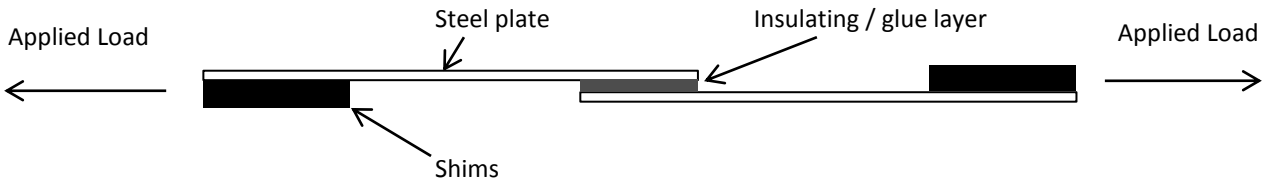

Figure 22: Diagram of specimen in the test set-up

5.2 Results and Discussion

5.2.1 Varying Insulating Liner Material

All four liner materials being tested were assembled into test specimens using one type of glue so that the liner could be assessed independently of the adhesive. The results of this can be seen in Figure 23, where the maximum applied force that could be held by the specimen is shown. The peak applied force directly relates to the shear strength of the samples due to the consistent bond area of each different sample. The spread of results is displayed in Figure 23 by the range bars.

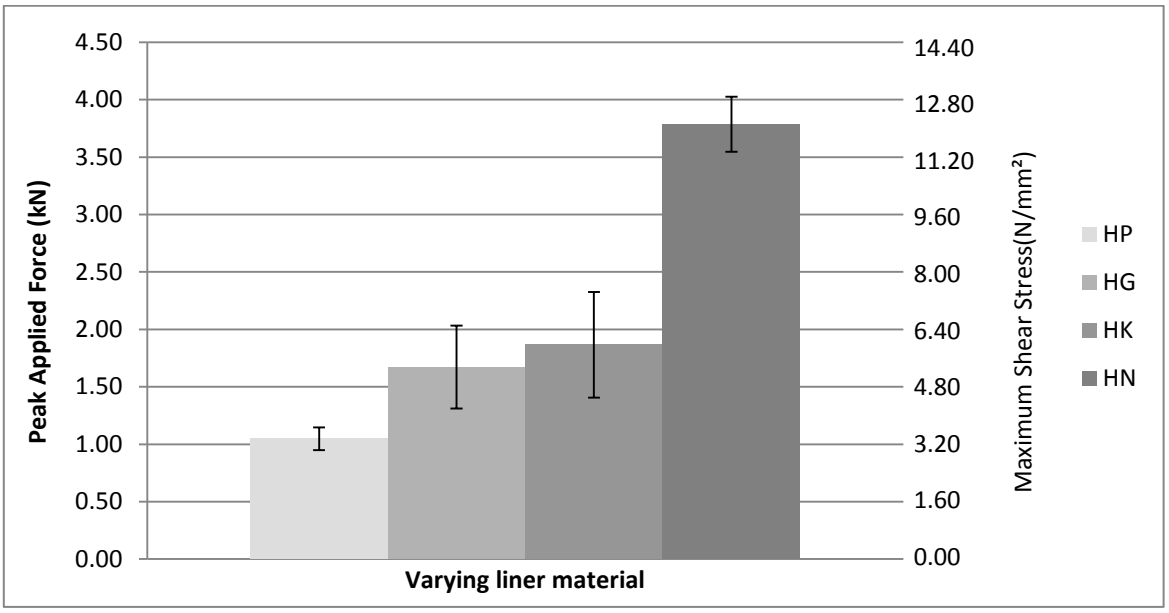

Figure 23: Results of varying the insulating liner material with range of results displayed (all samples using Huntsman Araldite adhesive)

Figure 23 shows that the pultruded glass fibre liner (HP) performs worse than the flexible glass fibre and Kevlar liners (HG and HK) which show fairly similar results. It is thought that this is because the flexible liners allow the glue to impregnate the weave of the fabric resulting in a better bond than can be obtained using the smooth pultruded material. This is backed up by the images in Figure 24 which show that there is more de-bonding of the glue from the liner when using the pultruded liner than using the flexible glass fibre liner. In the case of the flexible glass fibre liner it can be seen that the de-bonding occurs solely at the interface between the glue and the steel. The use of no liner (HN) has dramatically improved the shear performance of the specimens, indicating that the insulating liner creates a weakness in the joint.

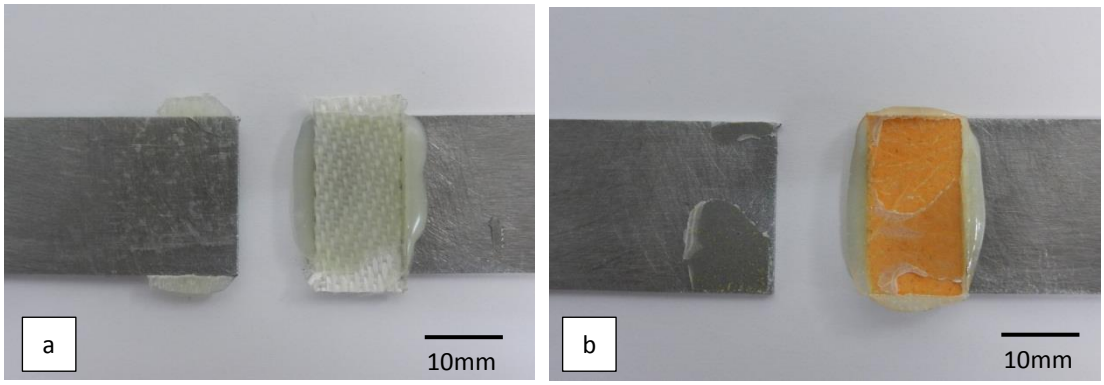

Figure 24: a) Specimen that has failed at the interface between the glue and the steel (HG) b) specimen that has failed more between at the interface between the glue and the insulating liner (HP)

5.2.2 Varying Glue Type

Changing the glue type also had a large effect on the performance of the test specimens. Figure 25 shows the performance of the four tested glues using flexible glass fibre, Kevlar and no liner. It can be seen that the Temperange II epoxy is the best in each situation. The Permabond adhesive displays the lowest strength in each situation and the Edilon and Huntsman glues are between these two. As confirmed in chapter 5.2.1 the lack of an insulating liner provides a specimen that has the best strength and the flexible glass fibre and Kevlar liners show a similar performance.

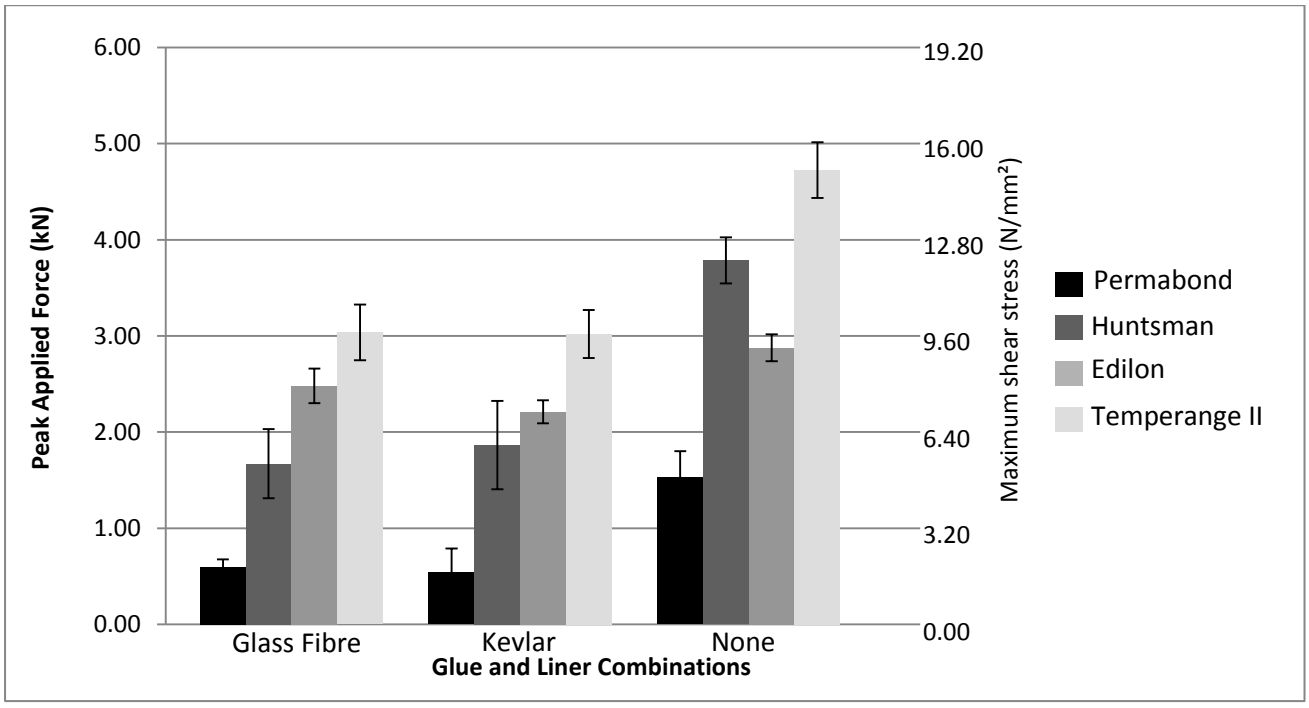

Figure 25: Results of varying the glue type used in the test specimens with the range of results displayed

A record of the displacement against load was gathered for each specimen. In all cases but one the failure of the bond between the steel occurred quite rapidly and after this failure the sample no longer supported any load, the samples mainly performed elastically. This did not occur in the

samples that were constructed using the Edilon adhesive with a Kevlar liner. As can be seen in the graphs in Figure 26, these samples reached a peak applied force, but were able to support a load after this was reached, displaying a more plastic behaviour.

It is worth noting that the errors in the test set-up could be up to 0.25 kN, this represents the 0.005% accuracy of the 50 kN load cell used. This error value is not displayed on the graphs in Figure 23 or Figure 25.

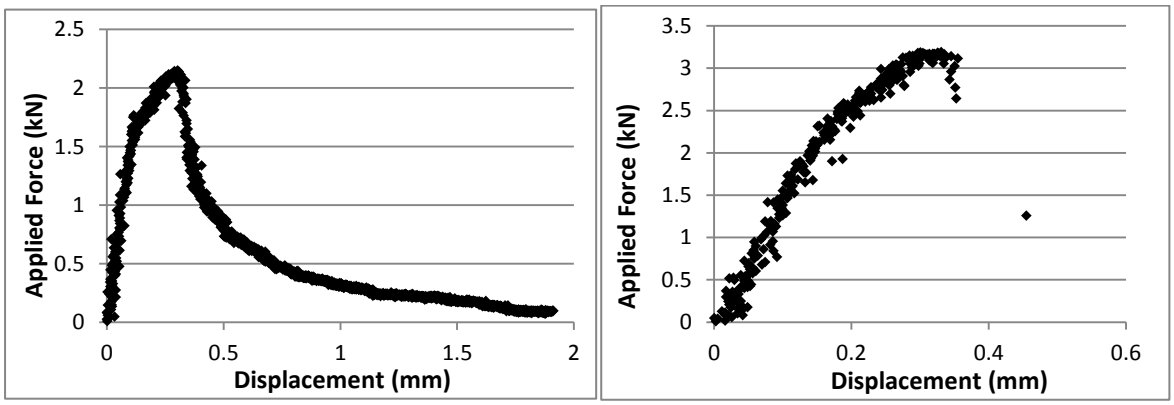

Figure 26: Left, graph showing Edilon/Kevlar specimen behaviour. Right, graph showing Temperange II/Kevlar behaviour (more typical failure type).

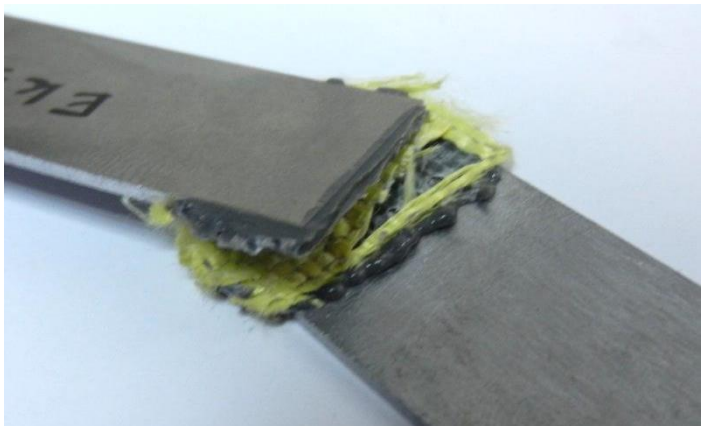

Figure 27: Edilon/Kevlar sample after testing

Figure 27 shows that partial de-bonding and failure of the liner material itself is responsible for the slow plastic failure of these samples once the peak applied force is reached. This type of failure could be advantageous in the context of a safety critical system such as an IBJ. If the failure is not sudden then the partial failure will be noticed and can then be rectified before full failure occurs.

5.3 Conclusions

Four different glue types and four different liner types were tested using the method described above. A number of conclusions can be drawn from this work.

- When there is no insulating layer in the construction of the specimen the shear strength is higher than with a liner included
- Glass fibre and Kevlar insulating liners perform similarly while the pultruded liner does not perform well compared to these
- The Temperange II glue performed better than the other glues
- The Edilon glue performed better than Huntsman glue when used with an insulating liner

6 Component Testing – Shear Testing of Glued IBJ Sections

This chapter aimed to further the work described in chapter 5, where specimens were tested in shear to assess the performance of different glues and insulating liners. The shear strength of the glue and liner are important because of the high forces imparted on the rail in the longitudinal, vertical and lateral directions. The aim of this testing was to assess the effect the design of the IBJ and the materials used have on its shear strength in the longitudinal direction.

6.1 Method

An IBJ was cut into test pieces between the fastening bolts or pins (swage fasteners) which were 60mm in width, a test piece can be seen in Figure 28. These test pieces were placed on a base that supported only the cross section of the fishplates. A further plate was placed on top of the test piece that rested only on the cross section of the rail. This set-up, which is shown in Figure 29, was then placed into a hydraulic test rig. Load was applied to the set-up at a rate of around 100 kN/minute until failure occurred so that the ultimate shear strength of the glue / insulating liner could be measured.

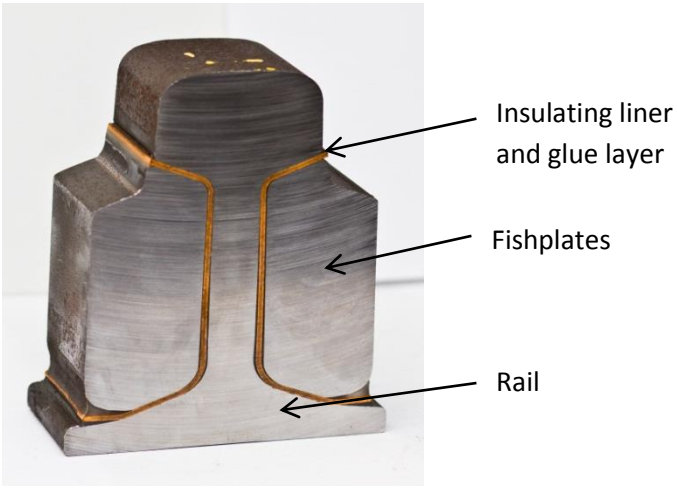

Figure 28: Shear test piece, sample number 1a, pre-testing.

The applied load was measured throughout the experiment which was used to determine the ultimate shear strength of the test pieces. The displacement of the fishplates with respect to the rail was also logged throughout the testing which provided an indication of the resilience and elasticity of the glue and liner combination.

This method can assess the performance of a design in shear but it does not fully represent what occurs in practice. This is because the clamping force, or preload, applied by the joint fasteners is taken away in this setup and the sample is not clamped in any other way. The lack of this clamping force will reduce the performance of the sample, however, the test can still be considered representative of an in service IBJ and is an excellent method of comparing and ranking designs and materials.

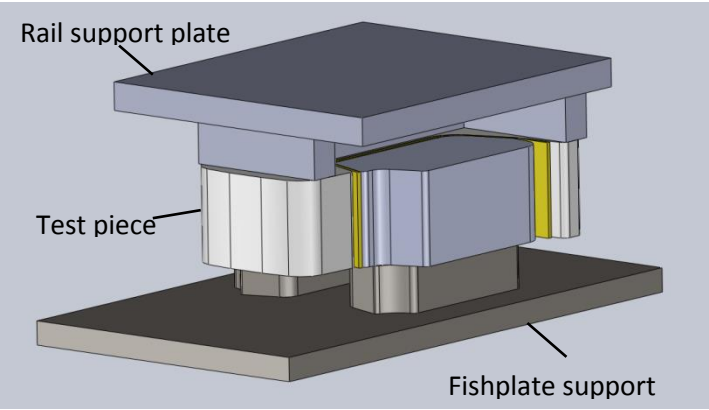

Figure 29: Shear test set-up

In addition to the force and displacement data gathered to analyse the performance of the test samples, ultrasonic technology was used to gain a better understanding of the failure process in the liner and glue. This was a novel approach to investigate what is happening in the glue layer and at the interfaces between components.

Ultrasonic transducers emit ultrasonic waves which travel through a body and are partially reflected where there is a change in the acoustic impedance, at a surface between one material and another. The acoustic impedance is the product of a material's density and the wave speed through that material. The reflection coefficient is a measure of the ultrasonic waves that are reflected at such an interface and it is dependent on the change in acoustic impedance between the two materials. Calculation of the reflection coefficient (R) can be seen in Equation 3, where *z* is the acoustic impedance, and the subscripts 1 and 2 denote the material above and below the interface (39) (40).

$$R_{12} = \frac{z_1 - z_2}{z_1 + z_2}$$

When sensors are attached to a glued IBJ the reflection coefficient of the interfaces between the metallic and insulating components can be measured during shear testing. When the interfaces de-bond during the test air gaps appear which alter the reflection coefficient due to a change in material at the interface and therefore the acoustic impedance. This gives the ability to determine which interfaces de-bond first during the test and, therefore, allows for the improvement of design. An illustration of the testing set-up can be seen in Figure 30; when an air gap forms, more of the incident wave is reflected back to the sensor.

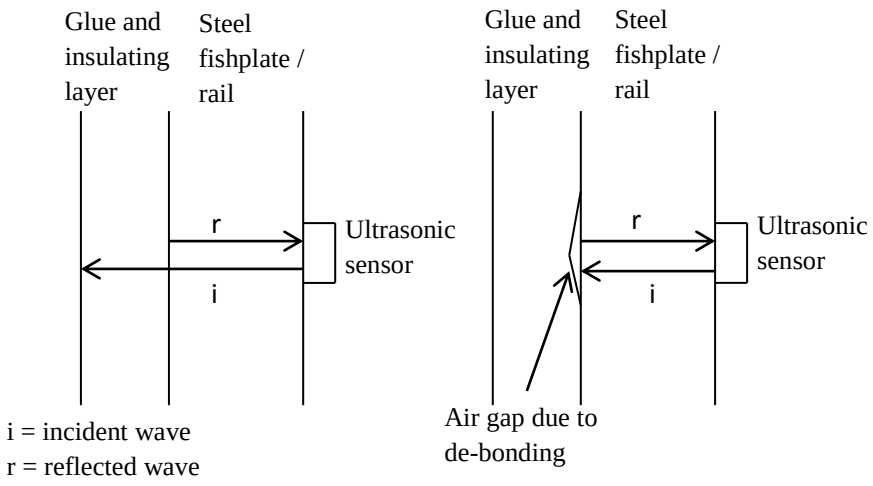

Figure 30: Ultrasonic technique to assess de-bonding of the glue layer during tests

6.1.1 Test Samples

The test samples were manufactured in an environmentally controlled workshop to the standards that are currently applied to the manufacture of glued IBJs in the UK. The fishplates were prepared in three different designs, the current standard UK design, which is a wedge fit design, a full fit design with Kevlar insulating liner and a full fit design using a flexible glass fibre mat liner. A description of wedge fit and full fit fishplates can be found in chapter 1.2. These fishplates were then assembled into rail using various fastening systems which resulted in five differing joint designs, these are outlined in Table 1.

Differing fastening systems were used in an attempt to vary the thickness of the glue layer between the insulating liner and the rail. The 1.1/8" pins (swage fasteners) put the highest clamping force onto the joint upon installation, use of 1" pins reduced this clamping force and a further reduction resulted when using bolts tightened to a set torque. The lower clamping forces aim to squeeze less glue out of the gap when the fishplates are installed into the rail.

Joint No.	Liner Type	Design	Fixing
1	Pultruded glass fibre	Wedge fit	1.1/8" Pin
2	Kevlar	Full fit	1.1/8" Pin
3	Kevlar	Full fit	M29.5 Bolt
4	Glass fibre mat	Full fit	1.1/8" Pin
5	Kevlar	Full fit	1" Pin

Table 1: Details of test samples

Each fishplate and rail length used for the assembly of the test pieces was prepared using the same method to control the variables of the experiment. The glue used was also consistent throughout, although the glue used in the fishplate manufacture was different to the glue used in joint assembly. Both glues are approved for use by Network Rail.

Each joint design was made into two assemblies which were then cut into three test pieces each, every test piece has a thickness of 60mm. This gives six test pieces for each design in total that were labelled A to F, A, B and C being from one assembly and D , E and F being from the second. To gain

reliable results four test pieces of each design were tested, two from each assembly. One further test piece from each design had ultrasonic sensors attached to them. Slots were cut into the rail where necessary so the sensors were perpendicular to the surface that was being monitored, the position of the sensors can be seen in Figure 31. Two sensors were placed so that they were monitoring the web of the rail, one from the fishplate side (2) and the other from a slot in the rail web (3). Two other sensors were placed so as to monitor the upper (1) and lower (4) fishing surfaces.

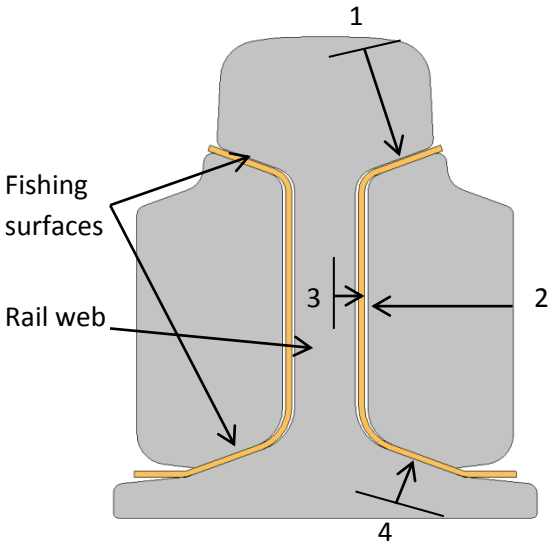

Figure 31: The position and direction of ultrasonic sensors placed on shear test samples

Each plain-wave ultrasonic sensor consisted of a 7 mm diameter piezoelectric element with a centre frequency of 10 MHz and a bandwidth of 3 MHz. The piezoelectric elements were both emitting and receiving elements and the sensors were operated using a PC mounted ultrasonic pulsar and receiver. This enabled the elements to send ultrasonic waves through the test samples, controlled by the PC, and read the reflected waves and covert these to electrical signals which were then sent back to the PC. By taking a reference signal before testing the change in reflection signal and therefore the reflection coefficient were gained.

6.2 Results and Discussion

6.2.1 Overview

A brief overview of the results of this shear testing can be seen in Table 2. The peak applied force is the highest force reached by the hydraulic actuator during the test. This is then converted to ultimate shear strength using the area of the bond between the fishplate and the rail, which in this case is 166.2 cm^2.

Sample No.	Peak Applied Force (kN)	Ultimate Shear Strength (N/mm^2)		% above or below bench mark	
1a	213.9	12.87	P	6.67	Standard pultruded glass fibre liner, 1.1/8" Pins
1b	230.9	13.89	P	15.14	
1d	209.6	12.61	P	4.52	
1e	166.0	9.99	F	-17.22	
2a	164.2	9.88	F	-18.12	Kevlar liner, 1.1'8" Pins
2b	133.7	8.04	F	-33.33	
2d	176.5	10.62	F	-11.99	
2e	225.1	13.54	P	12.25	
3a	150.0	9.03	F	-25.20	Kevlar liner, M29.5 Bolts, 700N.m
3b	164.6	9.90	F	-17.92	
3d	240.8	14.49	P	20.08	
3e	161.1	9.69	F	-19.66	
4a	215.8	12.98	P	7.61	Glass fibre liner, 1.1/8" Pins
4b	207.4	12.48	P	3.42	
4d	272.8	16.41	P	36.04	
4e	250.3	15.06	P	24.82	
5a	179.7	10.81	F	-10.39	Kevlar liner, 1" Pins
5b	176.0	10.59	F	-12.23	
5d	145.5	8.75	F	-27.44	
5e	147.2	8.86	F	-26.60	

Table 2: Results of shear testing showing maximum shear strength of each test piece

A similar test set-up to that used here is applied as a quality control technique in the USA. The test sets a bench mark of 12.07 N/mm^2 and therefore this is shown in the results in Table 2. Tests highlighted in green have a higher shear strength then the benchmark and those in red are lower. It can be seen in Table 2 that only one set of test pieces completely passed with respect to this benchmark. The glass fibre liner full fit design shows the best results from this testing, the standard joint comes second to this and the Kevlar based full fit designs are all similar and do not perform as well.

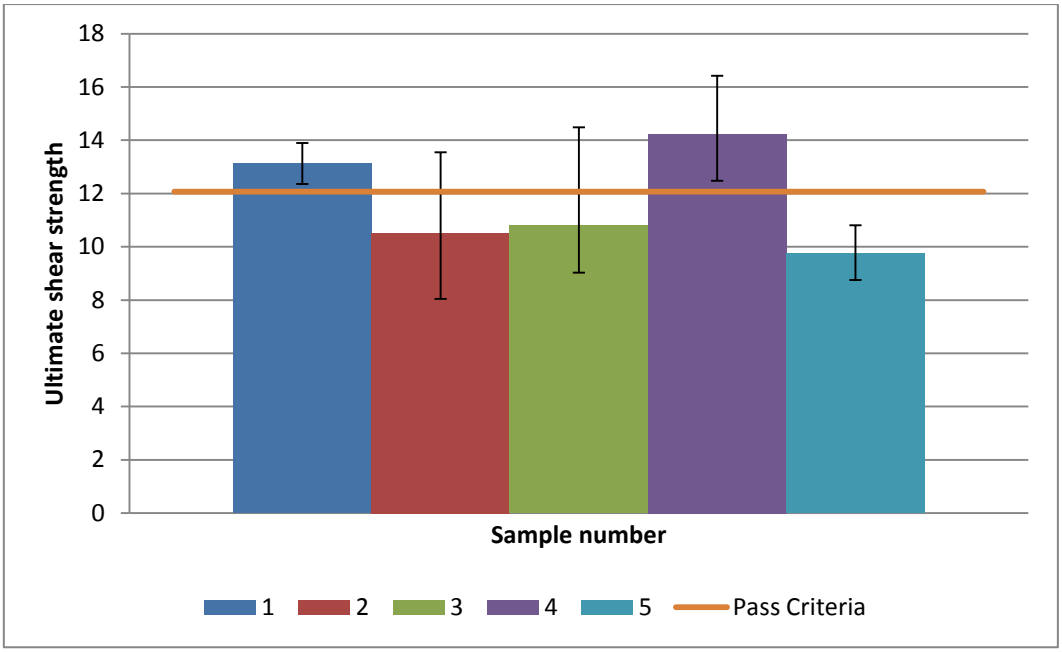

Figure 32: Bar chart showing average performance for each joint design with error bars to display the distribution of results of each set of test pieces

The chart in Figure 32 gives an overview of the average performance of each test piece design and the distribution of the results. The pass criterion of 12.07 N/mm^2 is shown on the chart. The glass fibre liner full fit type joint samples (number 4) are above the pass criterion for the entire range of results. The standard pultruded liner wedge fit joints are also above this mark, although with a lower average, when the lowest result is discounted (explained in chapter 6.2.2 below).

A typical result from the ultrasonic implementation of the test samples can be seen in Figure 33. The plot shows the force that is applied to the test sample over time and also the change in the reflection coefficient from the ultrasonic sensors. The sensors are labelled as per Figure 31. It can be seen that some reflection coefficient changes occur during the test, suggesting that de-bonding of the glue layer is taking place as discussed above in chapter 6.1. Upon failure of the sample the reflection coefficient changes more dramatically and over a greater number of sensors.

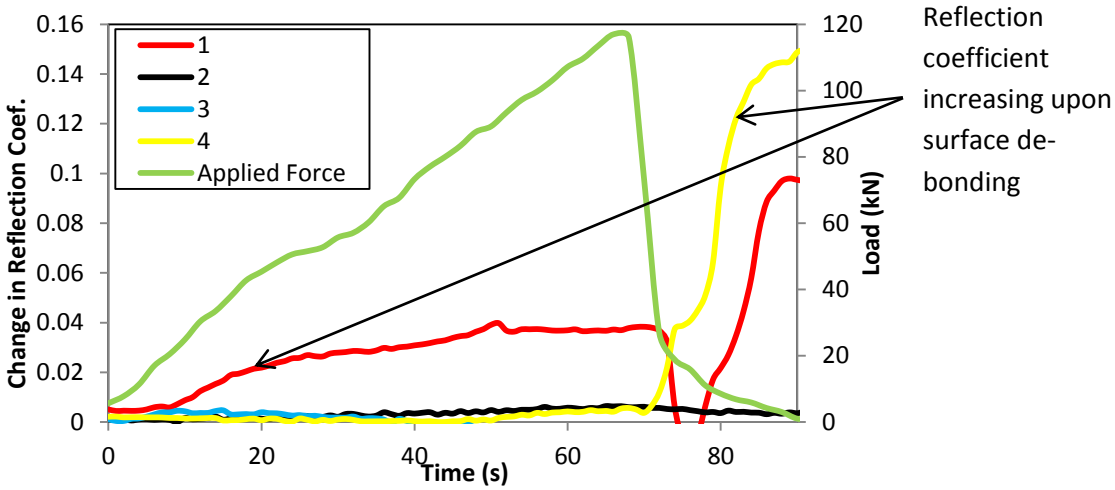

Figure 33: Plot showing the change in reflection coefficient of the ultrasonic sensors in comparison with the force applied to the test sample.

The ultrasonic results and an investigation of the different failure types in each IBJ design are carried out in more detail in the following chapters. It should be noted that the test samples that were ultrasonically instrumented all performed more poorly and failed at a lower peak force than similar samples that were not monitored in this way. This could be because of the length of time the samples were left for before testing, the non-monitored samples were tested very quickly after sectioning whereas the ultrasound samples were left for a longer period of time. During this time fluid or air that may have had time to ingress into sample after the cutting process to manufacture the samples may have caused oxidation to occur. This could have affected the bond strength between the glue and other components.

6.2.2 Standard UK Joint Design

The standard joint that is currently used throughout the UK network was tested as a control piece to determine possible benefits of differing designs, the results of the test can be seen in Table 3. If sample 1e is taken as an anomalous result (explained below) then the average shear strength of the samples is 13.12 N/mm^2. This value is above the benchmark set by glued joint quality inspection in the USA as discussed in chapter 6.2.1. Again green denotes a value higher than the benchmark and red indicates lower.

Sample No.	Peak Applied Force (kN)	Ultimate Shear Strength (N/mm^2)		% above or below bench mark*
1a	213.9	12.87	P	6.67
1b	230.9	13.89	P	15.14
1d	209.6	12.61	P	4.52
1e	166.0	9.99	F	-17.22

Table 3: Test results of standard UK joint design - type 1

Figure 34 shows that, at the web of the rail, failure has occurred within the pultruded liner. This means that the glue and the bond it makes with the rail, fishplate and liner are stronger than the liner itself. This indicates that the ultimate shear strength of this type of joint using a pultruded liner cannot be increased by using different glues because the liner is the weak point in the joint.

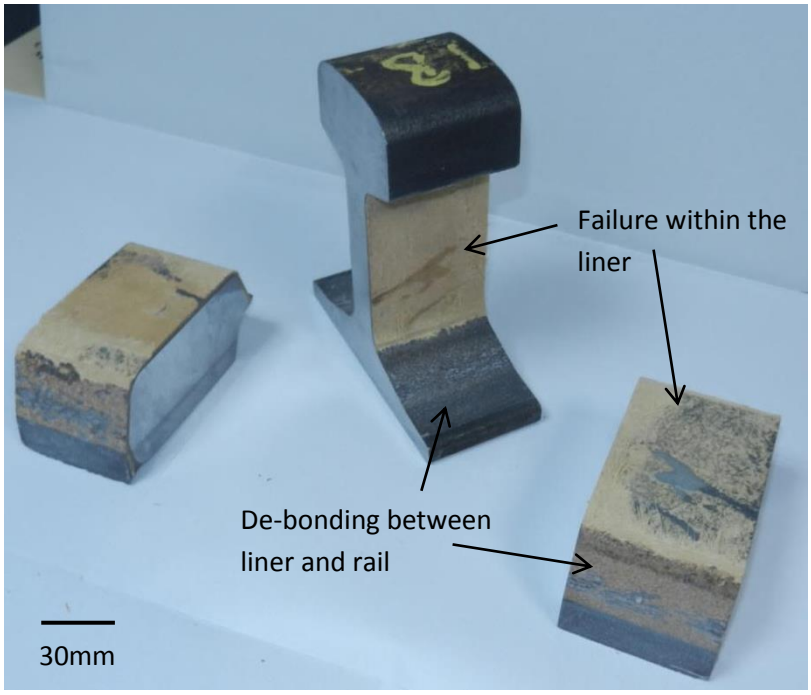

Figure 34: Test piece 1b showing failure in the insulating liner at the rail web

Although at the web of the rail the liner failed, at the fishing angles of the joint the failure occurred at the bond between insulating liner and the rail. This can be seen in Figure 34. The reason for this is that the joint is a wedge fit design and therefore a lot of pressure is exerted onto the fishing angles of the joint during assembly, forcing almost all of the glue out of this area. The observations made of Figure 34 can be compared to the ultrasonic data gathered from one of the test samples shown in Figure 35. The sensors directed at the web of the rail (2 and 3) show no change until the complete failure of the sample. The sensor directed at the upper fishing angle (1) shows a change in reflection coefficient before ultimate failure, suggesting that this surface de-bonded (as can be seen in Figure 34) prior to the failure of the sample.

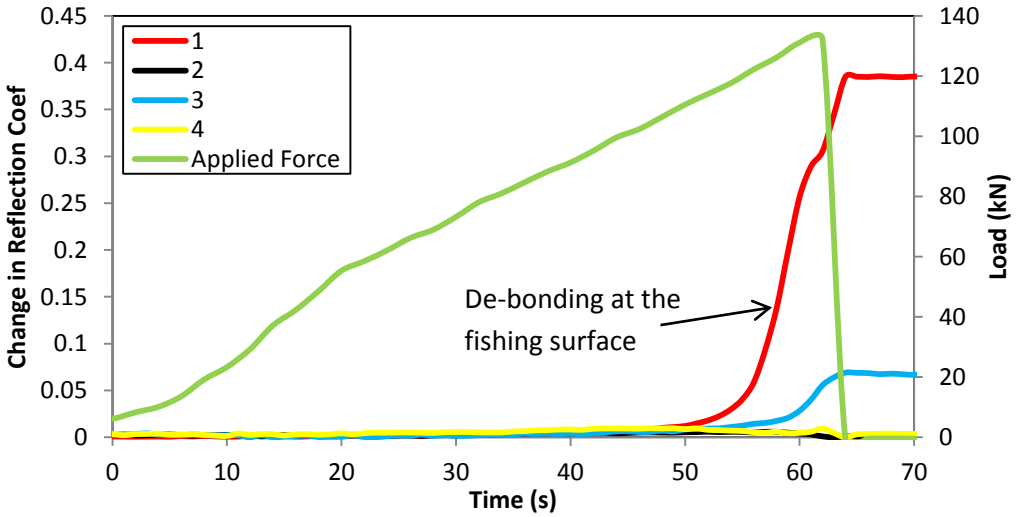

Figure 35: Plot showing ultrasonic and force data for standard UK IBJ design sample.

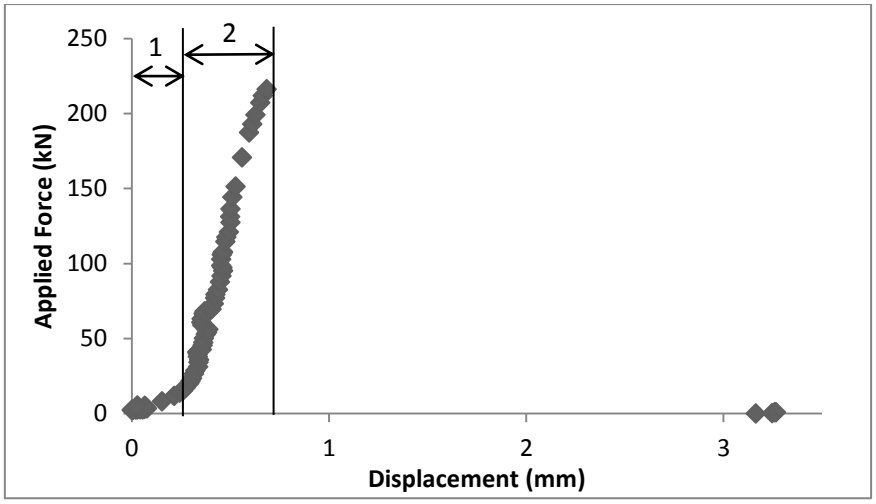

Figure 36: Graph showing applied force vs displacement for test piece 1a

The graph in Figure 36 shows how the fishplate displaced with respect to the rail when force was applied. In the case of these test samples the maximum displacement of the system was around 0.5mm. This is explained on the graph, region 1 is the where the test rig is bedding in and therefore discounted, region 2 is the 0.5 mm mostly elastic movement of the test sample. Failure occurred quickly at the peak applied force, as can be seen by the sudden change in displacement and applied force.

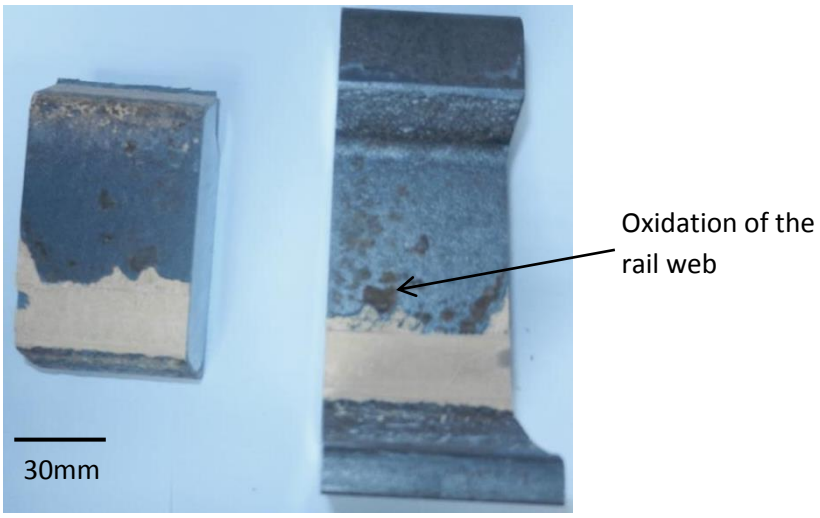

Figure 37: Oxidation of the rail web causing a weaker bond and failure at a low applied force

Sample 1e exhibited lower ultimate shear strength than the other samples of the same design and therefore the result was taken as being anomalous. This was because of a bond failure between the glue and the rail. Figure 37 shows that where this bond failure occurred, oxidation of the rail can be seen. It is hard to establish whether this oxidation occurred because the rail was unclean upon assembly or whether it was due to problems arising from the sectioning of the assembled joints into test pieces. In this process cutting fluid may have been able to penetrate the glue layer and cause the oxidation as may have happened in the ultrasonically implemented test samples described above.

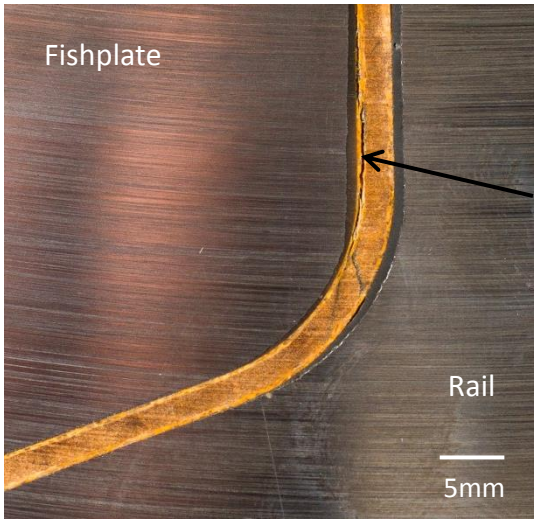

Figure 38: Close up of pultruded liner before testing

It should be mentioned that before testing was carried out cracks were found in the liners of the test pieces, this can be seen in Figure 38. These cracks are assumed to have been created when the joint was assembled due to the large clamping force that the swage fastening system applies to the joint.

6.2.3 Kevlar Insulated Full Fit Joints

Testing of full fit IBJ test samples with Kevlar insulating liners was carried out and the results of the testing can be seen in Table 4. As discussed previously the green highlighted results are above the USA benchmark (12.07 N/mm^2) and the red indicates a lower value of shear strength.

Sample No.	Peak Applied Force (kN)	Ultimate Shear Strength (N/mm^2)		% above or below bench mark*	
2a	164.2	9.88	F	-18.12	Kevlar liner, 1.1'8" Pins
2b	133.7	8.04	F	-33.33	
2d	176.5	10.62	F	-11.99	
2e	225.1	13.54	P	12.25	
3a	150.0	9.03	F	-25.20	Kevlar liner, M29.5 Bolts, 700N.m
3b	164.6	9.90	F	-17.92	
3d	240.8	14.49	P	20.08	
3e	161.1	9.69	F	-19.66	
5a	179.7	10.81	F	-10.39	Kevlar liner, 1" Pins
5b	176.0	10.59	F	-12.23	
5d	145.5	8.75	F	-27.44	
5e	147.2	8.86	F	-26.60	

Table 4: Results of Kevlar insulated joints – samples numbers 2, 3 and 5

The Kevlar insulated full fit joints were created using differing fastenings with the intention of creating three joint assemblies with different glue thickness between the insulating liner and the rail. After sectioning the joints into test pieces it became apparent that the glue thicknesses were very similar in all cases, this can be seen in Figure 39.

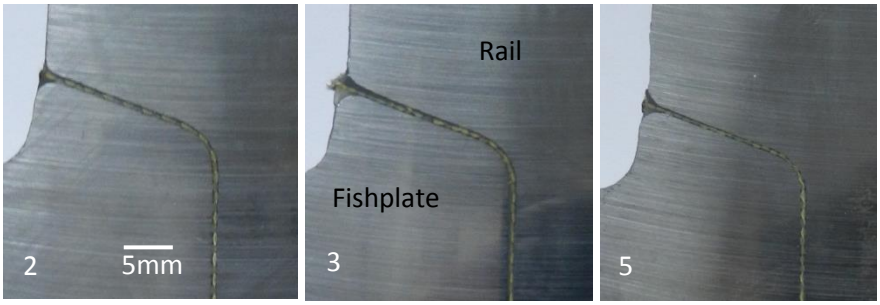

Figure 39: Glue layer thickness examination of Kevlar insulated full fit joints

Due to the fact that the glue layer thickness is constant in these test pieces they are all to be treated as the same design even though they have been installed using different fastenings. Table 4 shows that the results of these test pieces are all similar with the exception of two results that are higher than the others. The average ultimate shear strength of these samples not including the two anomalous higher results is 10.35 N/mm^2.

The failure of these test pieces was mainly due to de-bonding of the glue from the rail web. De-bonding of glue from the insulating liner on the rail side at the fishing surfaces was also seen. This is show in Figure 40.

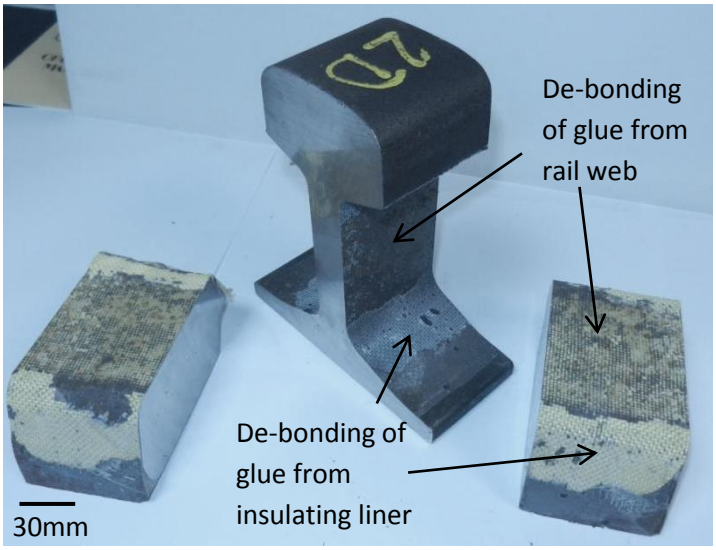

Figure 40: Sample 2d showing glue de-bonding from the rail web and insulating liner on the fishing surfaces

This de-bonding could be attributed to various mechanisms. Either there is not enough glue between the insulating liner and the rail as it is being squeezed out by the assembly process or the bond is affected by the surface preparation of the rail. The web of the rail after de-bonding can be seen in Figure 41, this shows that oxidation was found on the metal surface under the glue. This supports the theory that the surface preparation of the rail is not adequate and this is causing the glue to de-bond from the rail.

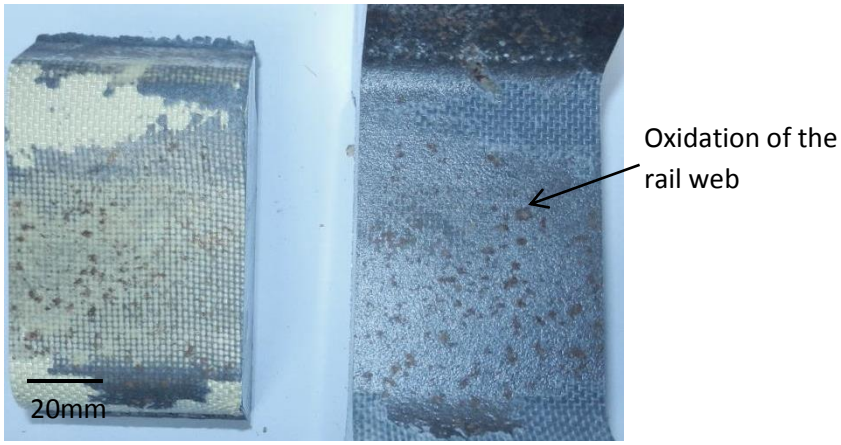

Figure 41: Oxidation present after testing of test piece 2B

The ultrasonic data collected from a Kevlar full fit joint can be seen in Figure 42. The plots show that the coefficient of reflection does not change greatly for the sensors focusing on the upper fishing surface (1) and the web of the rail from the fishplate side (2). The sensor looking at the web of the rail from the middle of the web displays a large change in the reflection coefficient as soon as the force is applied, this would suggest de-bonding at this surface which is backed up by the images in Figure 40 and Figure 41. At the interface between the glue, liner and rail at the upper fishing surface the reflection coefficient changes when the joint finally fails, this matches with the explanation of de-bonding at the fishing surfaces below and this behaviour is displayed in Figure 43.

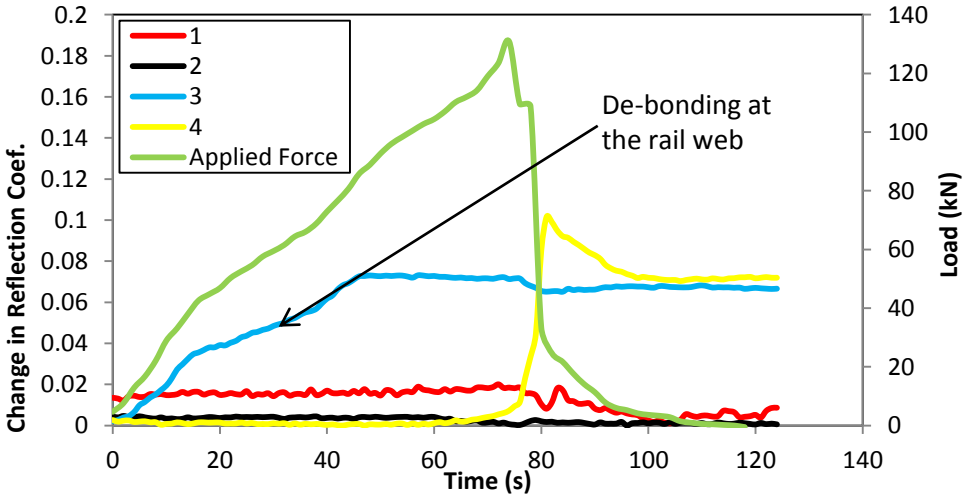

Figure 42: Plot showing ultrasonic and force data for a Kevlar full fit IBJ design

In some cases, at the fishing surfaces, the liner de-bonds from the glue on both sides. This failure occurs later than the de-bonding of the glue from the rail web. This is due to more glue being present between the liner and the rail at this part of the joint. This supports the theory that de-bonding of the glue and the rail web is due to there being too little glue in the assembly as much of it is squeezed out. This is shown in Figure 43.

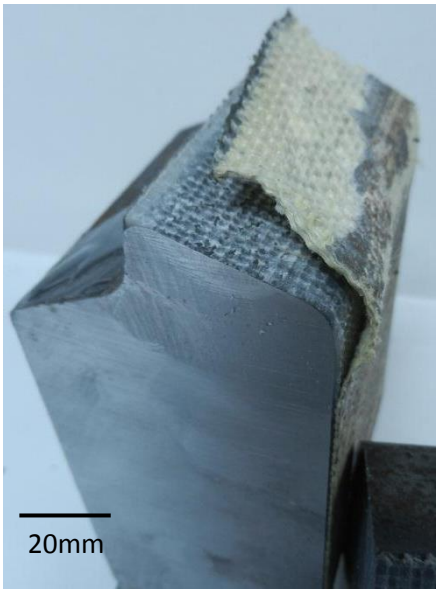

Figure 43: Liner de-bonding in test piece 2D

The maximum displacement of the Kevlar insulated test pieces was similar to that of the standard joints at around 0.5 mm, this can be seen in Figure 44. It is also visible from this graph that the failure mechanism was not as abrupt in these samples as for the standard test pieces. The applied force does not reduce fully after the main failure of the sample.

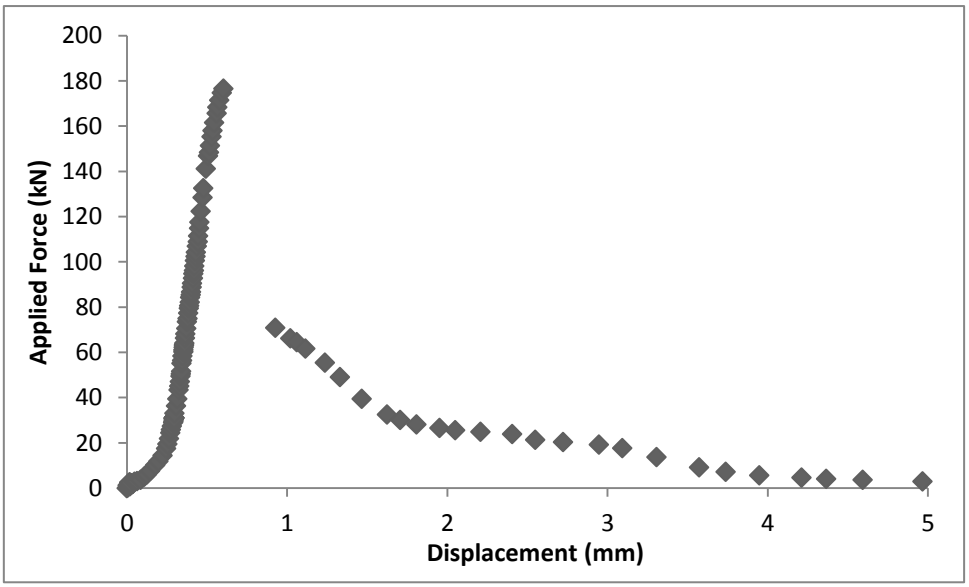

Figure 44: Graph showing applied force vs displacement for test piece 2d

6.2.4 Glass Fibre Insulated Full Fit Joints

As can be seen in Table 5, the glass fibre full fit joints showed the best performance in shear during this set of testing. The average ultimate shear strength of these test pieces is 14.23 N/mm^2. All of the test samples performed better than the USA bench mark of (12.07 N/mm^2) and therefore all results are highlighted green.

Sample No.	Peak Applied Force (kN)	Ultimate Shear Strength (N/mm^2)		% above or below bench mark*
4a	215.8	12.98	P	7.61
4b	207.4	12.48	P	3.42
4d	272.8	16.41	P	36.04
4e	250.3	15.06	P	24.82

Table 5: Results of glass fibre insulated full fit joints

The failure mechanisms seen in these test pieces are similar to that show by the Kevlar and standard test pieces. Figure 45 shows that de-bonding of the glue from the rail web has occurred which is similar to the Kevlar insulated full fit joint and can be explained using the same arguments as discussed in the Kevlar results section. The image also shows delamination of the glass fibre at the fishing angles.

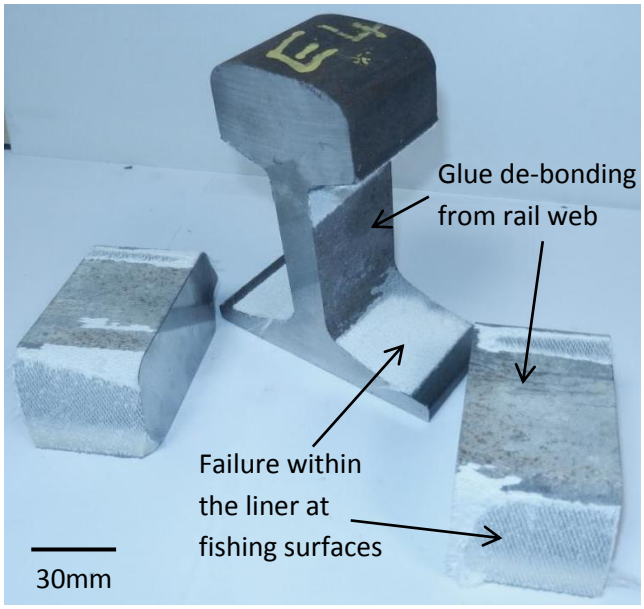

Figure 45: Test piece 4e showing different failure mechanisms at the web and the fishing angles

Upon failure of these test pieces the fishplates remained in place due to the delamination in the fishing surfaces not being complete. The test piece in Figure 45 was pushed further by the hydraulic actuator after failure so that the fishplates separated from the rail. The test piece shown in Figure 46 was not pushed through after failure. It can be seen that de-bonding has occurred between the glue and the web of the rail but the fishing surfaces are where the test piece is still held together. This indicates that de-bonding is the first type of failure to occur in this test.

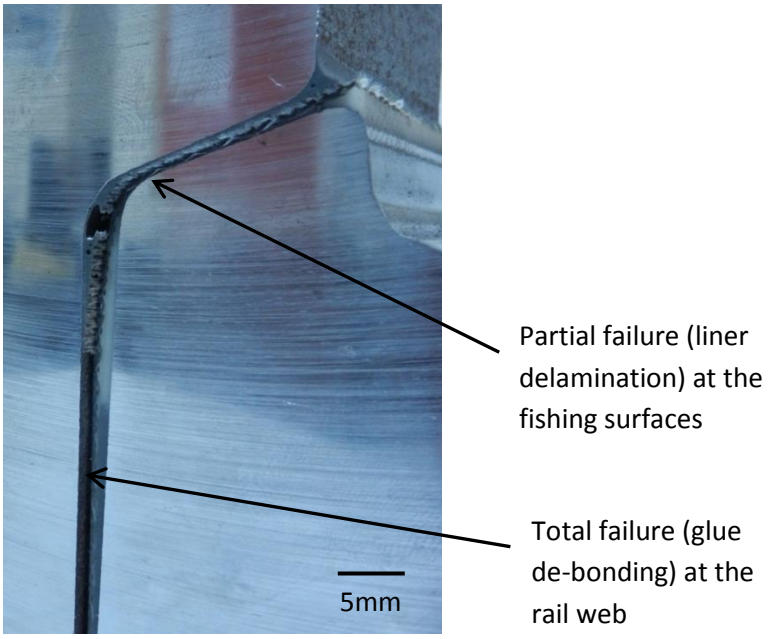

Figure 46: Test piece 4a showing different types of failure mechanism

The above conclusions are backed up by the data collected from the ultrasonic implementation. It can be seen in Figure 47 that the sensor focused on the rail web from inside the web shows a large change in reflection coefficient, suggesting de-bonding, as soon as the force is applied to the test sample. The sensor focused on the lower fishing angle shows a change in reflection coefficient when the joint starts to fail, this is also relatable to Figure 45 and Figure 46 where it has been shown that the fishing angles of the test sample de-bond after the web.

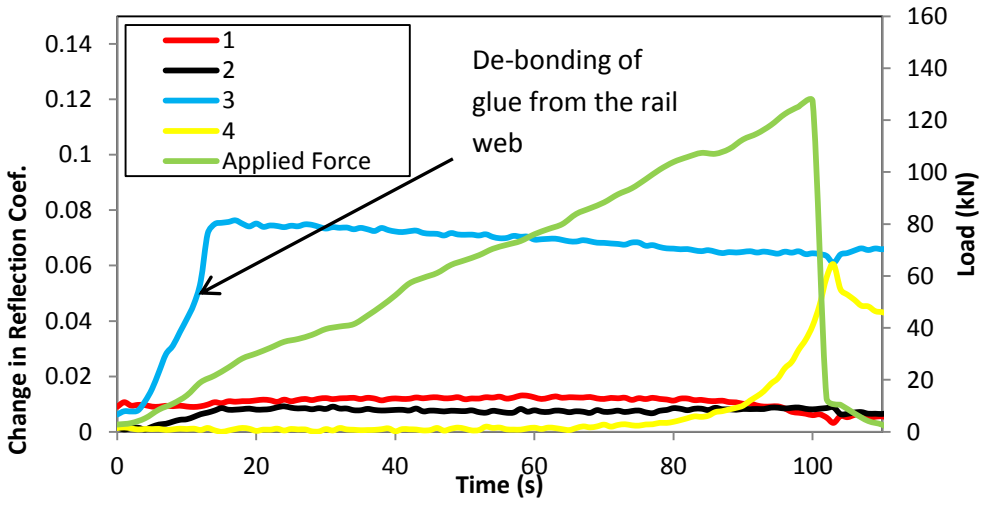

Figure 47: Plot showing ultrasonic and force data for a glass fibre insulated full fit IBJ design

The graph in Figure 48 shows that the failure of these test pieces was not sudden; on reaching the maximum applied force the test piece shows plasticity. The maximum displacement before the strength of the test piece is compromised is similar to the other test samples at around 0.5 mm.

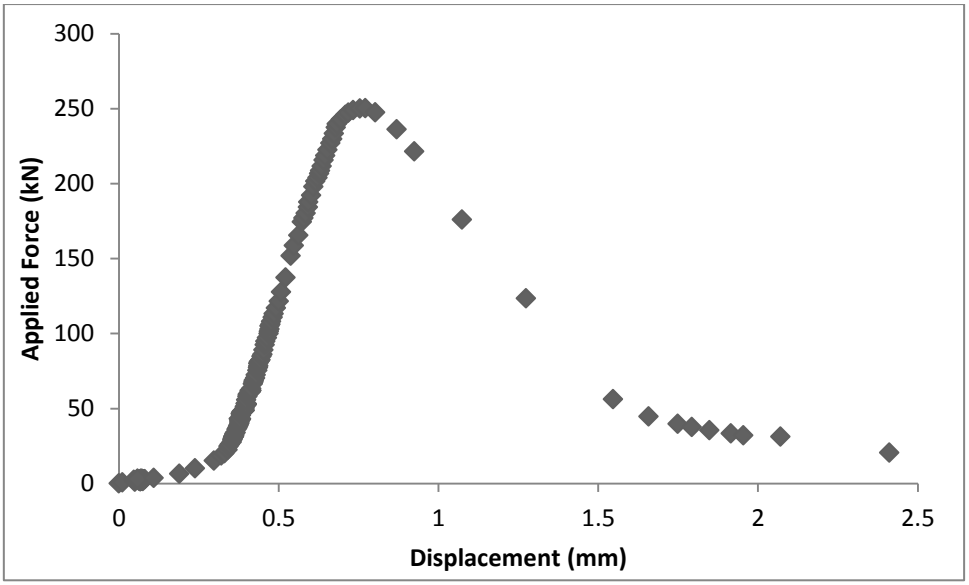

Figure 48: Graph showing applied force vs displacement for test piece 4e

6.3 Conclusions

During this testing the results clearly show that the glass fibre full fit design of joint shows the best performance in shear. This is because of the high shear strength exhibited by the epoxy impregnated glass fibre liner.

The failure of the standard UK joint test pieces, number 1, occurred in the liner itself and not the bond between the glue and adherend. This means that the maximum shear strength has been achieved using a liner of this type. The sectioning of these joints has led to the discovery of crack formation in the liner, most likely due to high clamp forces applied by the fasteners during assembly, which will reduce the performance of the joint.

The main failure of all other joints was caused by a de-bonding of the glue from the web of the rail. This has been discussed in the results section and has been attributed either to an insufficient amount of glue in the layer between the liner and the rail or poor surface condition of the rail upon assembly of the joint. Both of these problems could be addressed to improve the performance of the full fit joint design using either Kevlar or glass fibre liners. Further investigation could focus on surface treatment of the rail and fishplates, this would reduce the chance of oxidation and could improve the bond between components.

During all testing work the failure of the test pieces was either in the liner or at the interface between the liner and the glue on the rail side or the interface between the glue and the rail. Failures are never seen on the fishplate side of the liner alone. This indicates that the glue layer or surface preparation and bonding results in a better overall bond of the fishplate and liner than the rail and liner.

The ultrasonic examination of the joints shows that de-bonding of the glue from the rail can be monitored. From the results presented it can be seen that the coefficient of reflection changes as de-bonding occurs. It can also be seen, however, that sometimes the sensors do not pick up any events occurring and the reflection coefficient stays constant. These results show that ultrasonic

sensors could be used to monitor a full scale IBJ although the only sensor placement that could be achieved would be on the fishplate focusing on the web of the rail. In the above results this sensor does not often pick up activity so this method may be difficult to implement.

Further work could be conducted that would investigate the placement of the ultrasonic sensors in more detail. This would allow a more accurate assessment of the feasibility of this type of measurement for condition monitoring.

7 Specimen Testing – Experimental Modelling of Lipping

As discussed in chapter 2.3, analytical and numerical modelling has been implemented in an attempt to discover the mechanism behind lipping, the deformation or plastic flow of the rail head over the insulating gap in an IBJ. Examples of experimental modelling of the phenomenon found in the literature have so far been unsuccessful and therefore the aim of this experiment was to model lipping experimentally.

The current hypothesis that can be gathered from the literature is that lipping could be caused by two different mechanisms. The first being the high contact forces between the wheel and the railhead around the area of the endpost which result in a concentration of stress in the railhead at the rail ends subsequently leading to plastic deformation. The second is that longitudinal creep forces due to traction and braking, which lead to ratchetting, plastic flow longitudinally, also contribute towards lipping over the endpost. By using a twin disc test machine both of these mechanisms can be modelled.

An additional aim, when experimental modelling of lipping was successful, was to use the method to test different materials or designs to assess the effect they have on lipping. This includes the rail and the endpost material and the thickness or angle of the endpost.

7.1 Method

To experimentally model the contact between the wheel and the rail and therefore model the lipping behaviour of the railhead the Sheffield University ROlling and Sliding (SUROS) twin disc test machine was used. The SUROS twin disc test machine has been used previously for modelling the interface between the wheel and the rail to investigate wear and rolling contact fatigue problems (34) (41). A schematic of the rig is shown in Figure 49, the two motors control the test discs' rotation individually so that a slip (equivalent to a traction or braking force) can be generated. The hydraulic piston and load cell allows for the correct contact pressure to be created between the two discs.

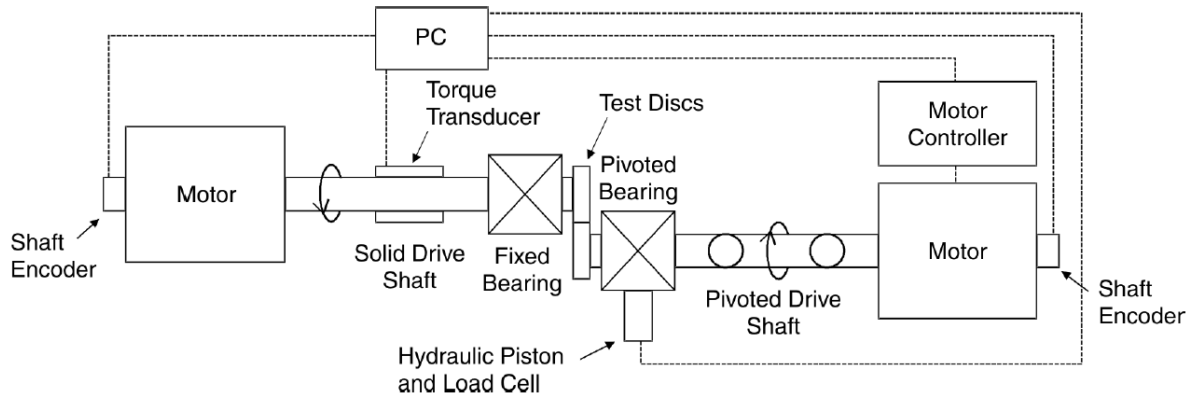

Figure 49: Schematic of the SUROS test rig (34)

To ensure the correct materials are used in the test set-up, the discs were machined from the railhead and wheel steel. The rail discs used in this experiment had slots cut in the running surface which were then filled with an endpost material to simulate the rail ends and middle of an IBJ in service, this type of test sample can be seen in Figure 50. The discs were 47mm in diameter and 10mm wide across the contact area. The endpost slots that were cut into the rail disc have a depth

of 3mm, this set-up gave a good method to test the hypotheses mentioned above but did not give a complete and accurate model of the contact at an IBJ. As discussed in chapter 1, the IBJ is a weak point in the track and this will lead to the vertical deflections at the IBJ which may have an effect on lipping, but were not investigated in this test set-up.

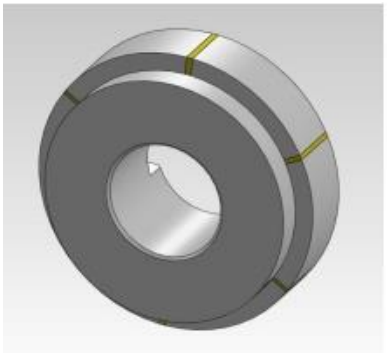

Figure 50: Rail disc with endpost inserts

Hertzian contact theory, Equation 1, was used to calculate the width of the contact patch between the two discs used in the twin disc machine.

$$a = \left(\frac{4PR}{\pi E^*}\right)^{1/2} \quad (1)$$

The twin disc testing was conducted using a maximum contact pressure of 1500 MPa which corresponds to a load (P) of 7.19 kN. This created a contact width of 0.6 mm between the two discs. The normal contact width between a wheel and rail is around 12 mm and, therefore, the endpost inserts used in the rail disc were scaled down also. In the UK endposts installed into insulated joints are usually 6 mm or 9 mm. There is a practical limit to how small the endpost inserts can be made and therefore the smallest insert was made to a width of 0.5 mm.

The SUROS rig was used to run the test at a speed of 400 rpm, a slip of 0.5% and contact pressure of 1500 MPa. The contact pressure is a standard value used for rolling contact fatigue (RCF) testing on the SUROS test rig which is higher than the value generally used to model the tread contact, 900 MPa. The higher value was chosen in order to accelerate the testing regime. The slip value was chosen to represent tread contact conditions of a driven wheel. Tests were run at first for 2000 cycles and further testing was carried out to a total of 96000 cycles. A table of all different test samples can be seen in Table 6.

Sample Number	Rail Material	Endpost Material	Endpost Thickness (mm)	Number of Cycles
1	R260	Epoxy Glass	0.5	2000
2	R260	Epoxy Glass	0.75	2000
3	R260	Epoxy Glass	1.0	2000
4	R260	PA6	0.5	2000
5	R260	PA6	0.75	2000
6	R260	PA6	1.0	2000
7	R350	Epoxy Glass	0.5	2000
8	R350	Epoxy Glass	0.75	2000
9	R350	Epoxy Glass	1.0	2000
10	US Premium	Epoxy Glass	0.5	96000
11	US Premium	Epoxy Glass	0.75	96000
12	US Premium	Epoxy Glass	1.0	96000
10	Stellite 6 clad	Epoxy Glass	0.5	96000
11	Stellite 6 clad	Epoxy Glass	0.75	96000
12	Stellite 6 clad	Epoxy Glass	1.0	96000

Table 6: Twin disc test samples

7.2 Results and Discussion

7.2.1 Experimentally Modelling Lipping

The first testing was carried out to prove the concept of modelling lipping using the twin disc test rig. The rail disc used was manufactured from steel grade R260, the standard grade of rail used in the UK. The discs were run for periods of 400 cycles before the test was stopped and the rail disc was checked for signs of any lipping. After a total of 2000 cycles lipping could be seen where the gap that the endpost occupies was closing up, this can be seen in Figure 51 where the endpost can be seen before and after testing for 2000 cycles. In image (b) the gap that is more apparent in image (a) has closed up due to metal flow. Also in image (b) damage to the railhead can be seen which appears similar to that shown in a real IBJ that has been damaged shown in Figure 8.

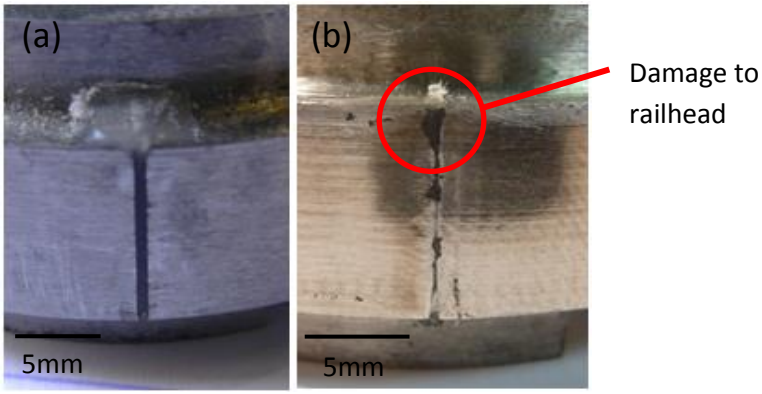

Figure 51: Surface image showing endpost in a rail disc: (a) pre-testing; (b) post testing

Once lipping had been seen on the surface of the joint the discs were then cross sectioned so that a better understanding of the depth of the steel deformation could be gained. An image of the sectioned disc can be seen in Figure 52 where material flow is clearly visible at the running surface of the disc.

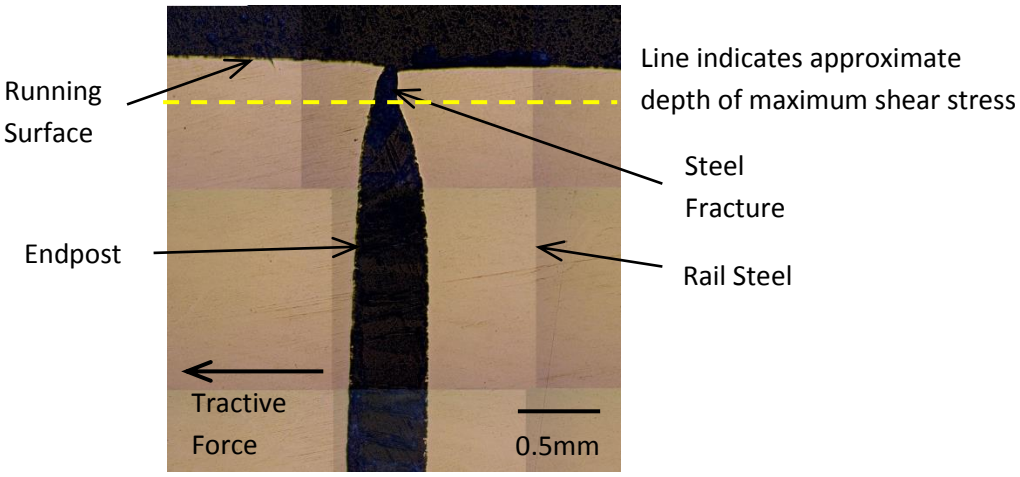

Figure 52: Sectioned view of 0.5mm epoxy/glass endpost in 260 grade steel disc.

The steel fracture that is indicated in Figure 52 is part of the running surface of the disc that has broken off after lipping has formed. It is thought that this is due to the high contact pressure of the wheel disc on the rail disc which is greater than the lip can support and therefore the lip has

fractured. The maximum shear stress at a depth below the running surface is explained below in Equation 2 and Figure 55.

The sectioned discs were mounted so that etching could take place and images were easier to obtain. The mounting material was of similar colour to the endpost material and therefore the endpost is not clearly visible in the images.

The sectioned discs have been etched so that the grain boundaries of the steel can be seen and therefore the hypothesis that lipping is due, in some part, to ratchetting behaviour can be tested. The etched steel at the running surface of the rail disc can be seen in Figure 53. From this image it can be seen that there is no deformation of the rail steel in the direction of the tractive force, this suggests ratchetting has not occurred. This is most likely because the discs were only run for a total of 2000 cycles at a low slip of 0.5%, which is not long enough for ratchetting to become visible. It has therefore been concluded that the lipping generated in this testing, which can be seen in Figure 52, is due to the bulk deformation of the steel caused by the high contact pressures between the wheel and rail discs. It is possible, however, that if ratchetting were to have occurred during this short test period and very thin layers of material flowed over the endpost they would have been easily broken off or worn away after a few cycles. More cycles are required to accumulate greater strain and more surface flow.

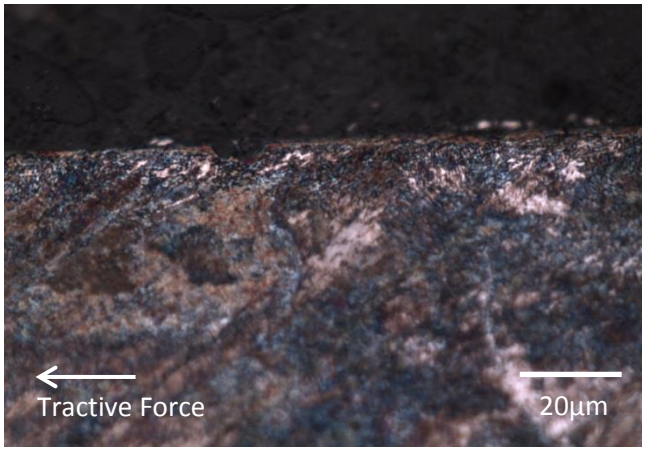

Figure 53: Etched cross section of 260 grade rail disc after testing

The lack of ratchetting that is seen in these discs can be explained by analysis of a shakedown plot. This is a plot of the coefficient of traction against the load factor. The R260 grade discs falls into the lower left side of the graph which represents a subsurface elastic condition and therefore ratchetting is unlikely to occur in these discs with the test parameters that have been applied.

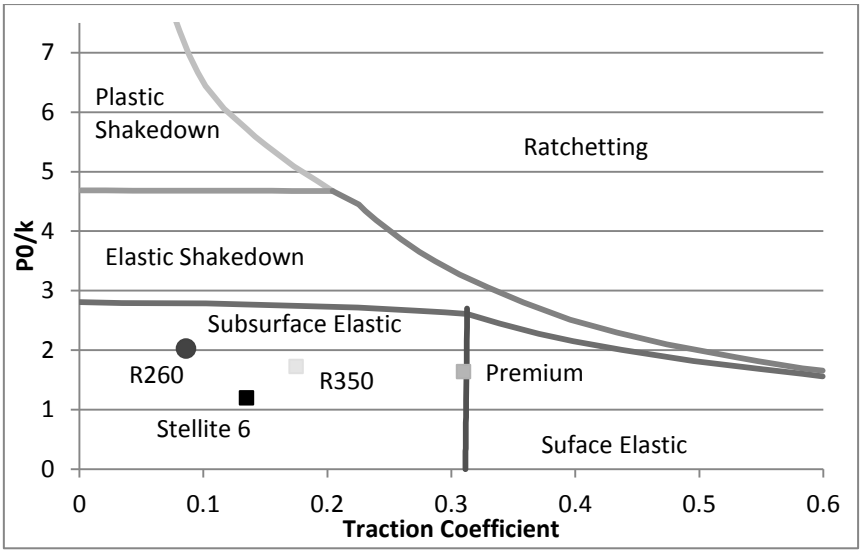

Figure 54: Shakedown plot with different rail materials

The bulk deformation of the steel below the running surface can be explained by the shear stress distribution in the disc. The highest shear stress is below the running surface of the disc as is shown in Figure 55. The graph, a plot of equation 2 which calculates the shear stress in the disc, shows the maximum shear stress at a depth of approximately 0.25mm. This plot does, however, assume no friction in the contact which is not true, the friction involved would decrease the depth of the maximum shear stress slightly. The level of the coefficient of friction required to bring the peak shear stress to the surface is 0.3. As seen in the plot in Figure 55, the R260 disc has a coefficient of friction of 0.08, and therefore the peak shear stress would still be below the surface. The peak shear stress at a depth of 0.25mm, or slightly less than this when taking friction into account, corresponds well with the deformation seen in Figure 52.

$$\tau_1 = \frac{p_0}{a}\{z - z^2(a^2 + z^2)^{-0.5}\} \quad (2)$$

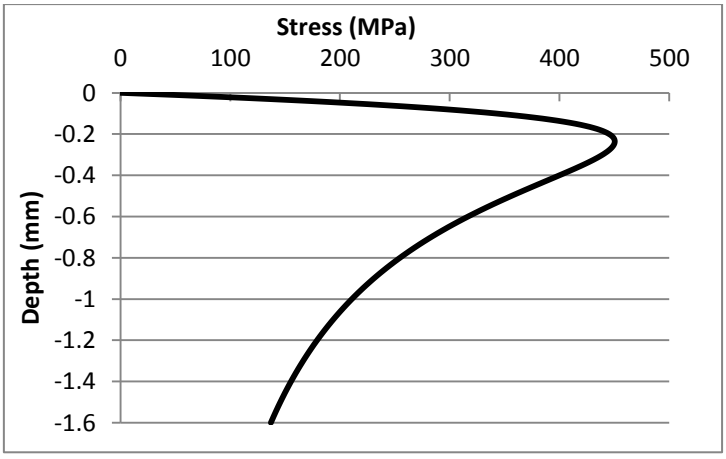

Figure 55: Shear stress distribution in the rail disc below the running surface

A comparison of the testing in the twin disc machine and in-situ joint studies can be made by comparing the two images in Figure 56. In addition to the fracture of the steel due to high contact pressures discussed above, damage is apparent on the running surface of the disc. This can be

compared to shelling that has been noticed to occur around the endpost of IBJs in the field. Similar shelling or cracking can be seen on the surface images of the disc in Figure 51.

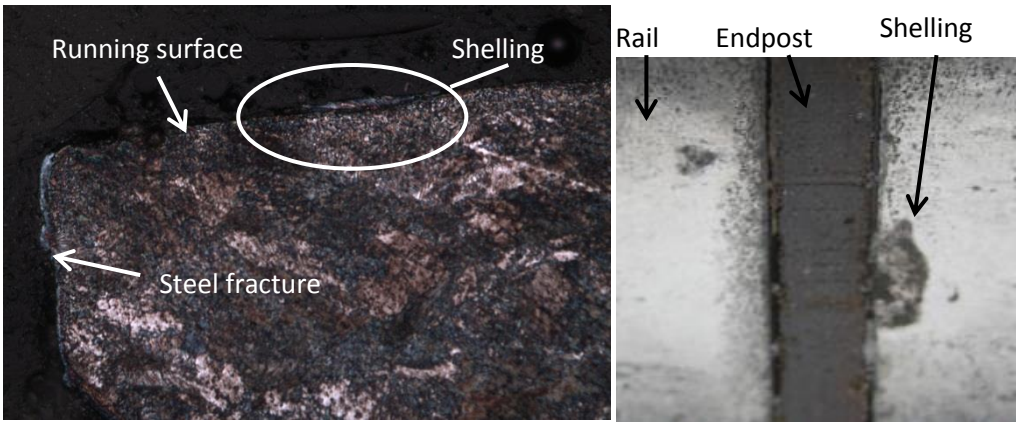

Figure 56: Comparison of shelling in a) the twin disc test and b) in the field (42)

7.2.2 Effects of Changing the Endpost Thickness

As discussed in chapter 7.1 the practical limit for the smallest endpost inserted into the rail disc is 0.5mm. To assess the effect of endpost thickness a disc was manufactured with endpost slots of 0.5, 0.75 and 1.0mm in thickness. The test was run for 2000 cycles again. In Figure 57, images of the sectioned disc with the three endpost thicknesses can be seen; (a) shows a 0.5mm endpost, (b) a 0.75mm endpost and (c) a 1.0mm endpost. The lipping that occurs on the left side of the endpost, opposite to the direction of the tractive force, has been marked. It can be seen that the magnitude of the lipping is similar in each case at 0.25mm.

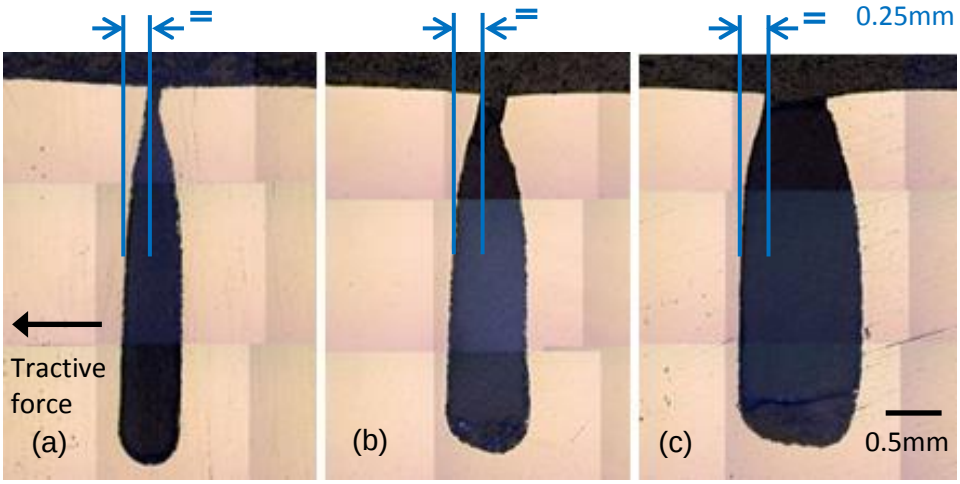

Figure 57: Varying endpost thickness showing similar amounts of lipping of the left side of the endpost.

Looking at the right side of the endpost, lipping in the direction of the tractive force, it is easy to see that the magnitude of the lipping varies and appears to be greater when a thicker endpost is used. However, when analysed more closely in Figure 58 it can be seen that in two cases the steel has fractured in a similar manner to that described in chapter 7.2.1, this occured in (a) and (b), the 0.5mm and 0.75mm thick endpost samples. If this fracture had not occurred during the testing process it can be estimated that the magnitude of lipping would have been similar in each case as

shown by the dashed lines in Figure 58. This leads to the conclusion, therefore, that the thickness of the endpost does not affect the rate of lipping in the direction of the tractive force.

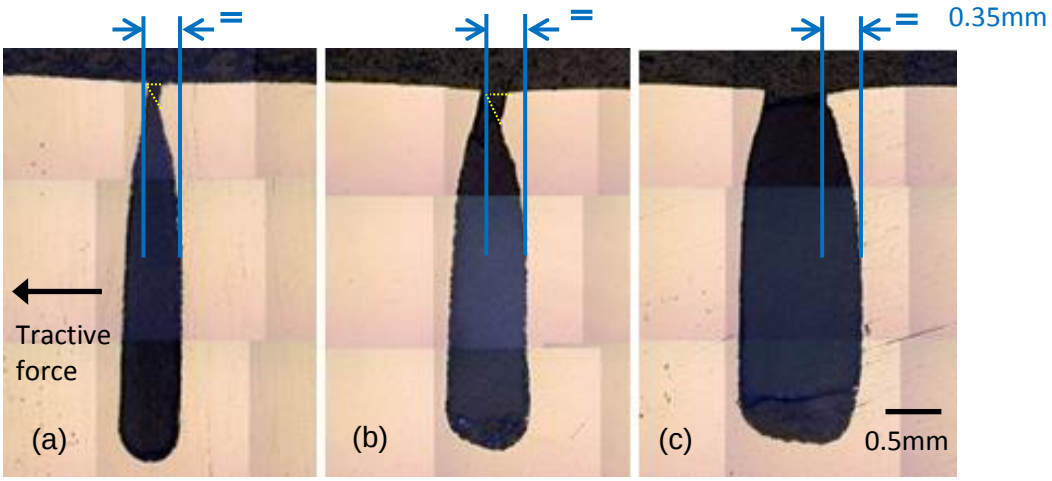

Figure 58: Varying endpost thickness showing varying amounts of lipping of the right side of the endpost.

The result that endpost thickness does not affect the rate of lipping of the railhead would lead to the conclusion that a thicker endpost would be beneficial as a steel lip would take longer to bridge the gap between the two rail ends. A thicker endpost can lead to other issues within the IBJ though, for example the wider the gap between the two rail ends the weaker the joint becomes and, consequently, this could lead to other failure modes associated with the IBJ or the support structure.

7.2.3 Effects of Changing the Endpost Material

The two most common endpost materials used in the UK are an Epoxy-glass composite material, used mostly in glued IBJs and a polyamide (PA6) used more commonly in non-glued IBJs. These two materials were inserted as endposts into the rail disc and the same testing procedure was followed to assess the effect these materials have on lipping performance. The effect of changing the endpost material can be seen in Figure 59 where the epoxy-glass composite was used for the test reported in image (a) and the PA6 material was used in (b). It can be seen that the steel of the disc deforms more and closes more of the gap in image (b), suggesting that the PA6 material is less able to resist the steel and more lipping occurs as a consequence. This is most likely because of the higher compressive strength of the epoxy-glass composite material.

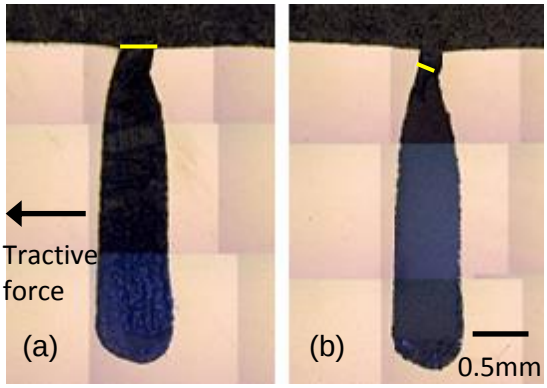

Figure 59: The effect of endpost material on lipping a) epoxy/glass b) PA6 (0.75mm endpost thickness)

The lines shown in Figure 59 mark the height of the endpost after testing has been carried out. From this it can be seen that the PA6 material has worn more than the epoxy-glass material and therefore a gap is present between the steel on either side of the endpost. The wear debris that this created built up on the disc and can be seen in Figure 51. This gap left between what would be the rail ends in a full IBJ could cause problems as it may fill with rail wear debris or other conductive material and lead to electrical failure due to contamination.

7.2.4 Effects of Changing the Rail Steel

Differing rail steels have been tested so a comparison could be made between them on their lipping performance. UK standard R260 grade rail steel has been compared with R350 heat treated rail steel. R350 grade rail steel is advertised as having a tensile strength of 1175 MPa, higher than R260 grade at 880 MPa (43). The hypothesis is that tougher rail steel will reduce lipping of the rail head. Hardness measurements of the two types of steel were taken and can be seen in Figure 60, this has confirmed that the R350 grade steel has a higher hardness than the R260 grade.

The graph in Figure 60 shows the hardness of the discs after 2000 cycles. The plots show very little or no evidence of work hardening, a harder layer of material at the surface of the disc. This would further support the conclusion that no ratchetting has occurred during this short test time.

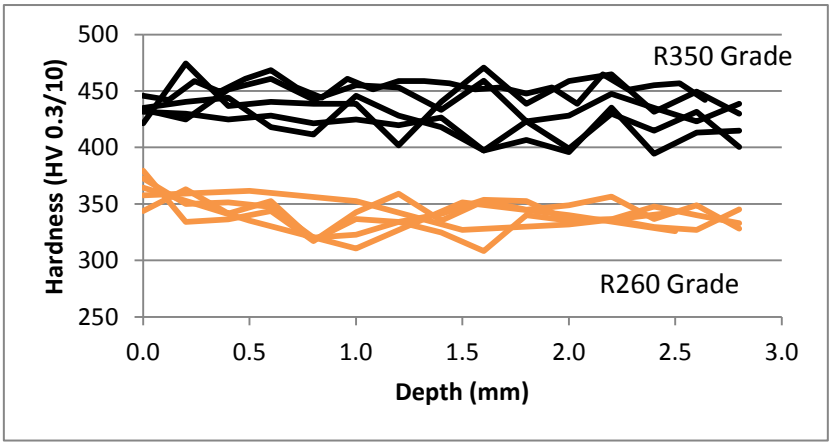

Figure 60: Hardness trace of R260 and R350 grade discs

Figure 61 shows a cross section image of the endpost in both a standard R260 grade rail disc and in a heat treated R350 grade rail disc. It is clearly seen that the heat treated rail steel lipped much less

than the standard rail steel. This is thought to be because the tougher rail steel is able to better withstand the high vertical and tractive forces exerted on it by the wheel disc.

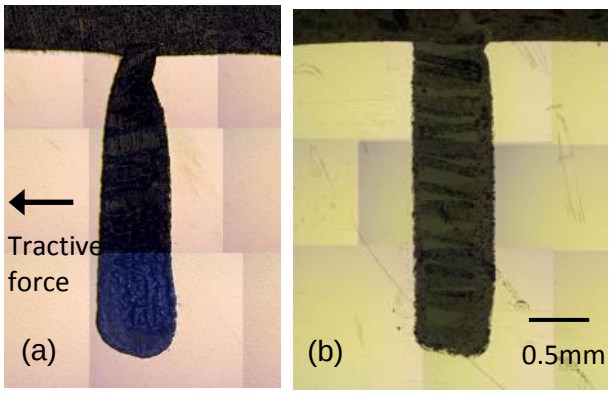

Figure 61: The effect on lipping of harder / tougher rail steel R350 grade (b) and R260 grade (a)

The tested R350 grade discs were also etched for comparison with R260 grade discs, an example of which is shown in Figure 62. It can be seen that no ratchetting was present as in the R260 grade discs. This is again backed up by the information provided by the plot in Figure 55 where the R350 grade disc is also in the subsurface elastic region where no ratchetting is expected. No shelling of the running surface near the endpost is observable where it was in the case of the R260 grade discs.

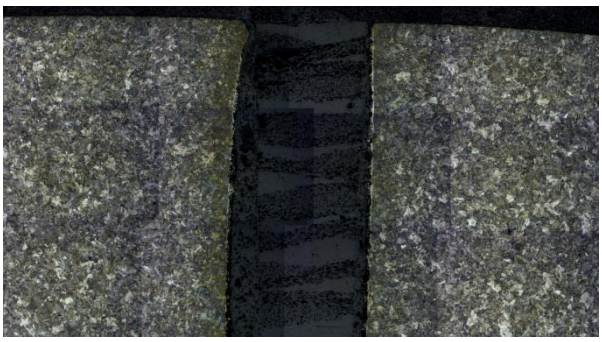

Figure 62: Etched R350 rail disc, no ratchetting or shelling is present

Further measurements were taken to assess the performance of the two rail steels in comparison with one another. A profilometer was used to measure the surface of the discs so that the vertical plastic deformation of the steel could be evaluated as well as the longitudinal lipping effect. Figure 63 shows profiles of the head hardened and standard grade steel in comparison to the profile of an ideal disc. The profile was measured around the circumference of the disc. In an actual IBJ the equivalent measurement would be the profile of the railhead longitudinally along the rail in the direction of traffic. It was seen that the deformation of the standard grade steel was much greater than that of the head hardened rail. The discrepancies in the centre of the graph are the locations of the endpost.

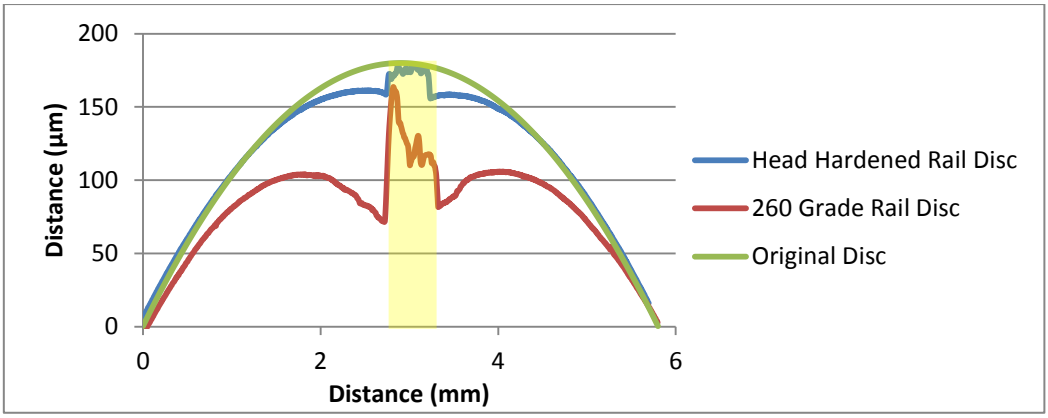

Figure 63: Profiles of the two different rail steels tested in comparison to the ideal disc profile, the shaded area denotes the location of the endpost. Profile around the circumference of the disc.

The vertical plastic deformation of the steel around the centre of an IBJ leads to a dip in the track. Dipped joints are usually associated with track structure degradation and are problematic because they cause the passing wheels to exert high dynamic forces on the IBJ and the surrounding track structure. This leads to further damage and premature failure of the system as discussed in the introduction. Dipping of the joint because of material flow could be one cause of initial structural degradation.

7.2.5 Investigating Laser Clad Materials on the Rail Surface

In addition to testing different rail steels, materials that have been laser clad onto the test samples have also been assessed for their performance benefits. A tougher material can be laser clad on top of the rail as discussed in the literature in chapter 2.3.

To begin this testing a grade R260 rail disc was clad with Stellite 6 material, a cobalt based alloy commonly used for hardfacing and wear protection of components. Stellite 6 has a higher hardness and strength than the R260 rail steel, the hardness of the laser clad layer of the samples being approximately 600HV whilst the grade R260 rail steel measured at approximately 350HV, this can be seen in Figure 65. Stellite 6 material was chosen due to previous investigations seen in the literature where different materials laser clad onto twin disc specimens were tested. Stellite 6 showed the lowest wear and good RCF performance (32).

The samples were tested using the same parameters as in previous tests so that comparisons could be made between them. It must be mentioned, however, that the pressure between the two discs may not have been 1500 MPa as used for the previous tests. The force applied to the discs was kept at the value of 7.19 kN but because of the discs differing material properties it is likely the contact patch was smaller and therefore a slightly higher pressure was experienced between the two discs. It is difficult to assess the change in contact pressure, especially in the laser clad disc that has a layered structure and this is outside of the scope of the current research. After 2000 cycles the laser clad specimens showed little to no sign of lipping, very similar to the results gained by using grade R350 discs. Cross section images of these discs can be seen in Figure 64.

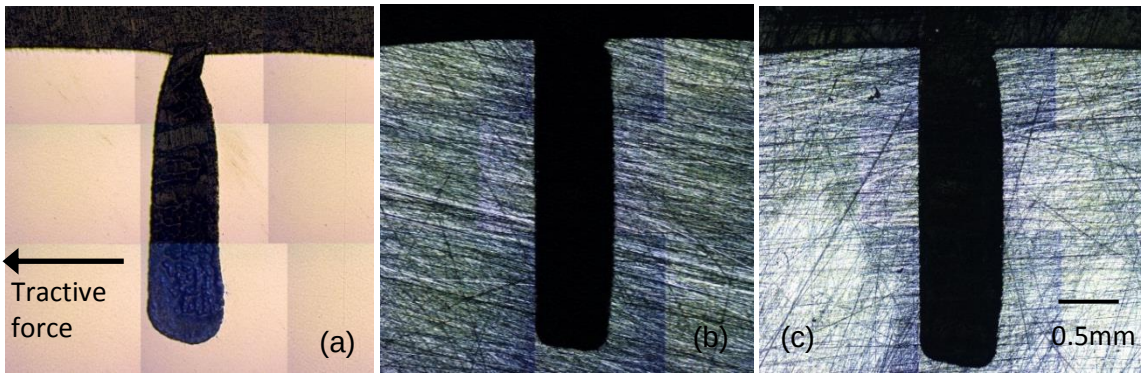

Figure 64: Different disc samples tested under the same conditions (a) R260 rail steel (b) R350 rail steel and (c) R260 rail steel with laser clad layer of Stellite 6

The reduction in lipping of the laser clad sample compared to the R260 sample can clearly be seen in Figure 64. The improvement in lipping performance is due to the same reasons that the R350 grade discs show better qualities, the laser clad layer is harder and tougher and so resists the high contact pressures better. The increase in hardness between the different materials can be seen in Figure 65, from this graph it can be seen that the laser clad layer has a higher hardness than the R350 and R260 discs and the layer is around 0.5mm in thickness. Underneath the laser clad layer the hardness of these discs is increased over the bulk material from a depth of 0.5 to 1.5mm. This is the heat affected zone where the properties of the R260 material have been changed by the laser cladding process and are roughly the same hardness value as the R350 discs. Beyond this heat affected zone the hardness is similar to that of the R260 grade discs.

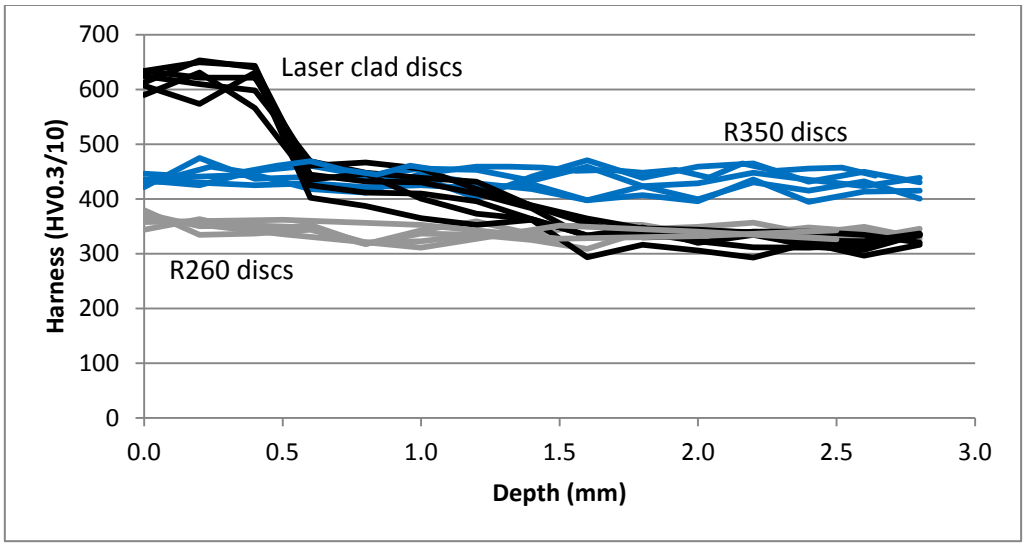

Figure 65: Harness of grade R260, R350 and laser clad twin disc samples

The tests above have been run for 2000 cycles, which was not enough to cause severe lipping in either the R350 rail disc or the laser clad rail disc. Therefore, further tests were carried out for a greater number of cycles so that an assessment could be made of possible benefits of laser clad rail over hardened rail steel. For this testing samples of premium rail steel from the US were used, this rail steel is very similar in properties to that of R350 grade rail steel used above. The laser clad material that is used is kept as the same material as in the above tests, Stellite 6 cobalt alloy. The

tests in this case have been run for a total of 96000 cycles at the same slip value as previous tests of 0.5%.

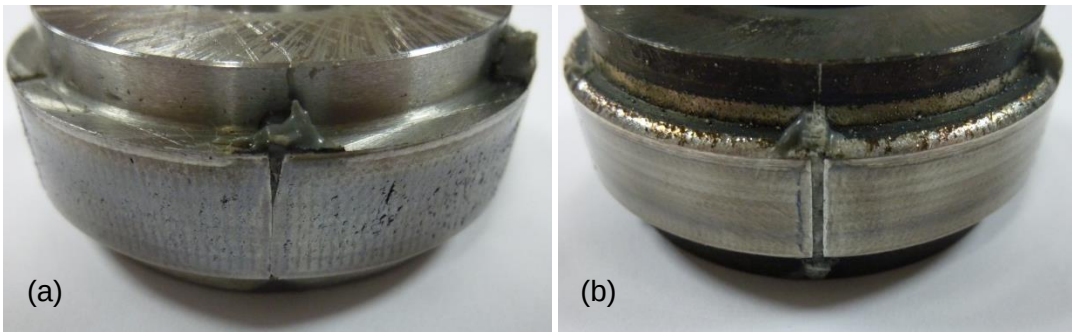

Figure 66: Surface images of the premium rail (a) and laser clad (b) twin disc samples after 96000 cycles

From image (a) in Figure 66 it can be clearly seen that a full lip has formed over the endpost gap in the premium rail steel sample. In comparison, the laser clad sample in image (b) shows the endpost is still visible and very little or no lipping appears to have occurred. This is further highlighted by the cross section images in Figure 67.

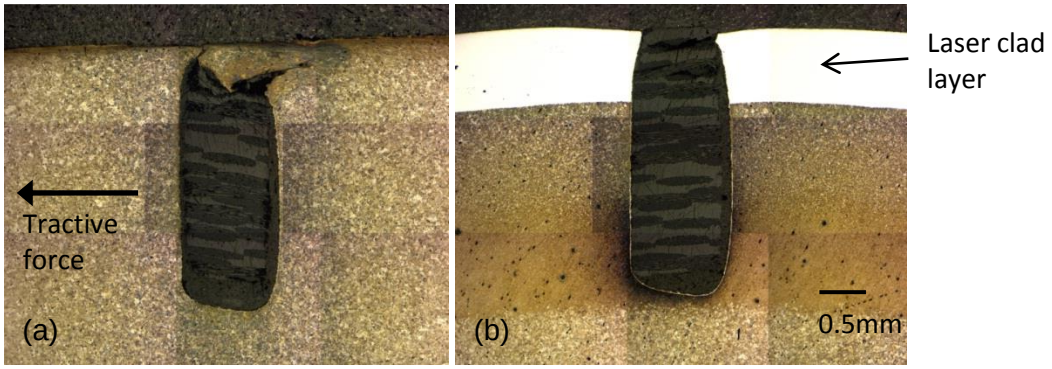

Figure 67: Cross sectional images of premium rail steel (a) and laser clad (b) twin disc samples after 96000 cycles

In Figure 67 the laser cladding layer can clearly be seen in image (b). The steel in these images has been etched to display the grain boundaries and the Stellite 6 layer is visible because of this process. A closer image of the surface of the premium rail disc in cross section can be seen in Figure 68. This image shows the ratchetting behaviour of the disc to a depth of around 0.3mm. The total depth of deformation of the steel in Figure 67 (b) is around 0.7mm, this would suggest that bulk deformation is still occurring, as was displayed in the previous results. However, the bulk deformation is heavily influenced by the tractive force as there is a much greater lip formed in this direction than is formed against the direction of the tractive force.

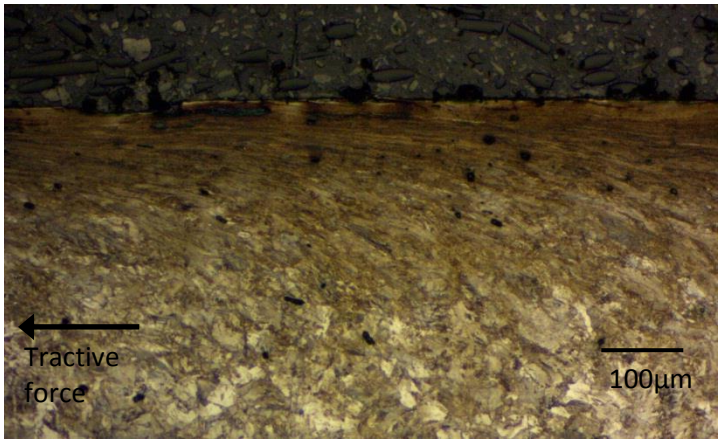

Figure 68: Image of the running surface of the premium rail disc in cross section displaying ratchetting behaviour

In Figure 69 a plot of the coefficient of traction can be seen of the premium rail disc test. This shows that the traction coefficient is higher than for other discs to start with compared to the values shown in Figure 54, the coefficient then slowly drops throughout the test. This helps to explain the ratchetting seen in these discs as the increase in friction brings the maximum shear stress in the disc towards the surface. It also explains why ratchetting was not seen in the R350 grade rail. The R350 grade discs were only run for 2000 cycles meaning that the traction coefficient did not reach the value required to cause ratchetting. The traction coefficient does not reach its peak value until around 8000 cycles.

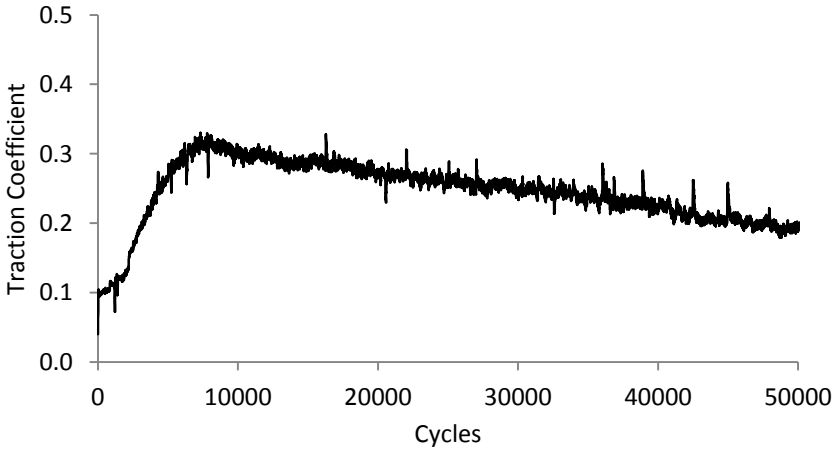

Figure 69: Graph showing the coefficient of traction for the premium rail steel disc

Profile measurements were also taken of the discs used in this test which can be seen in Figure 70. The results are similar to that shown in Figure 63. The laser clad rail disc which shows an increased performance in lipping also displays less vertical deformation at the running surface than the premium rail disc. As in the previous measurement the profile is measured around the circumference of the disc.

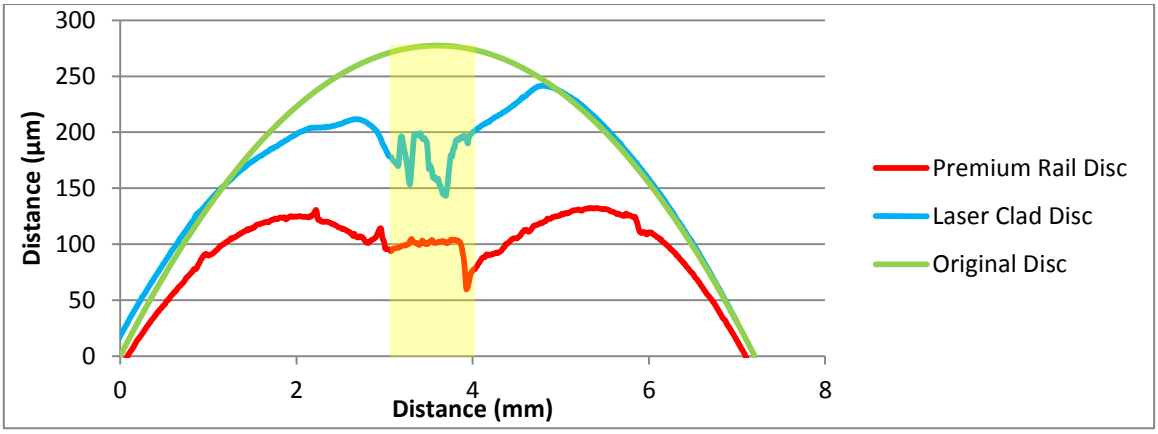

Figure 70: Graph showing the different profiles of the tested rail discs in comparison with a new disc, the shaded area denotes the location of the endpost

7.3 Conclusions

The testing that has been carried out has led to a number of conclusions:

- Lipping of the steel railhead over the endpost has been simulated successfully using the Sheffield University ROlling and Sliding twin disc test machine.
- The effect of changing the endpost thickness was investigated. The thickness was not found to affect the speed of lip formation. A thicker endpost provides a greater distance between the two rail ends and should therefore lead to a greater time before electrical failure due to lipping. However, the effect of overall joint deformation also needs to be considered.
- Changing the endpost material from PA6 to epoxy glass altered the lipping / plastic deformation seen over the endpost. The PA6 endpost led to more deformation in the steel. This also led to a higher wear rate in the PA6 endpost than the epoxy glass.
- Increasing the hardness and strength of the rail steel was found to reduce the lipping over the endpost. The vertical deformation of steel at the endpost position was also reduced. The performance was increased further by using a toughened laser clad layer on the running surface of the disc.
- Lipping in these tests has been caused by both the bulk deformation of the steel at the endpost and influenced by the tractive force and ratchetting of the steel at the running surface.

The benefits of laser cladding a harder material onto the surface of the rail were beneficial to lipping performance. Further work could concentrate on using this method to reduce lipping and investigate possible problems with this implementation. The transition between the standard rail steel and the laser clad layer needs to be investigated.

8 Comparison of Experimental Modelling of Lipping with Results of an Alternative Test Method

Experiments carried out by other researchers using an alternative test method to assess the benefits of laser cladding the rail surface with a harder material with respect to lipping performance are outlined and analysed in this chapter. A comparison of the results of this method and the twin disc testing method of chapter 7 has been made.

8.1 Experimental Method

The test rig in this experiment uses a full scale railway vehicle wheel and rail to experimentally model the forces that are experienced in the contact between these components in a real life situation. The rig, which can be seen in Figure 71, can apply a force between the wheel and rail in the vertical direction simulating the weight of a train (F). The rail is pulled by a horizontal actuator which simulates the movement of the train over the rail (R). The wheel can also be pulled by another actuator (W) to generate creep between the wheel and rail and simulate a tractive / braking force. The wheel is fixed in place about its central point but is free to rotate. Multiple wheel passes can be generated by this test method. The rig applies a force to the wheel and then pulls the rail and wheel to simulate wheel movement on the track. The vertical load is then released so that the rail can be returned and the cycle can start again.

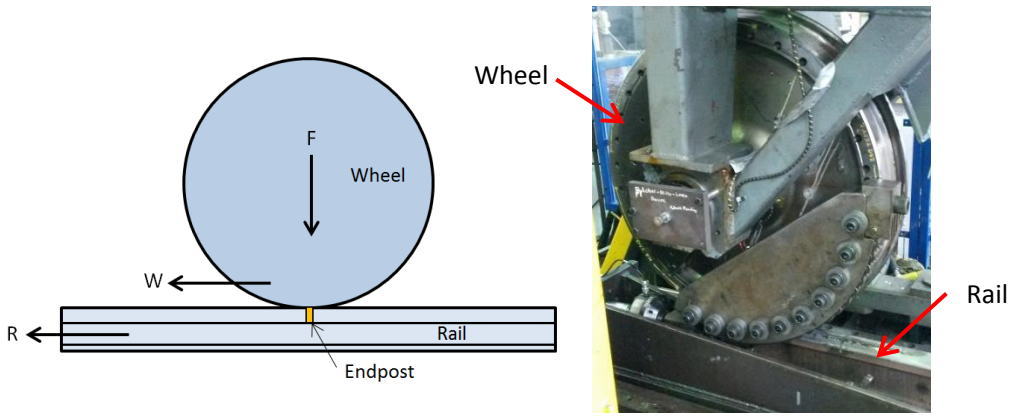

Figure 71: Test rig schematic and photo

Due to space limitations within the test rig a full IBJ could not be tested and therefore test samples were created where a gap was machined into the rail head and endpost material was inserted into the gap. This is similar to the methodology used in chapter 7, however this was a full scale endpost and a flat rail rather than a curved disc.

Testing was carried out on two types of rail, one standard R260 grade rail and one R260 grade rail with a layer of laser clad Stellite 6 material on the rail head. Both rail samples had 6mm epoxy glass composite endpost inserts. To decrease the testing time and speed the lipping process a high slip was used between the rail and the wheel to simulate a high traction / braking force. The vertical load on the wheel was 110 kN which is equivalent to a contact pressure between the wheel and rail of around 1500 MPa. This contact pressure is similar to that generated in the twin disc testing in chapter 7.

8.2 Results and Discussion

The first tests were carried out on standard R260 grade rail at 3% slip between the rail and the wheel to accelerate any lipping. After 5000 cycles photographs were taken of the running surface of the rail which show that lipping occurred. In Figure 72 below it is shown that the gap between the rail either side of the endpost has reduced from 6.4mm to 3.0mm because the railhead has deformed over the endpost material. If left to continue this is the lipping behaviour that would eventually lead to the rail either side of an IBJ to touch which would cause electrical failure of the IBJ. It cannot be seen easily in the below image but as well as the lipping created in this experiment wear debris also formed. The debris in this case accumulated within the gap where the endpost wore away and could lead to electrical failure in the case of an IBJ.

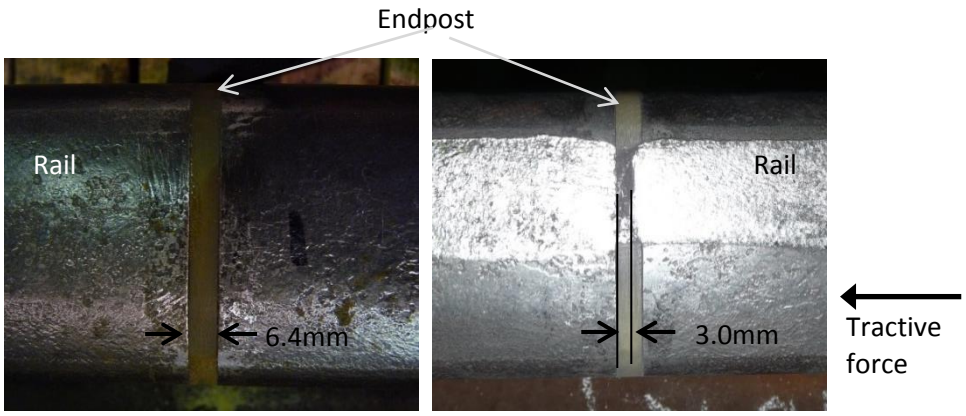

Figure 72: Images of the R260 grade railhead before (left) and after (right) testing for 5000 cycles

The above images can be compared to those in Figure 51 taken after the twin disc testing with the same grade of rail. The deformation in the contact area in both cases appear quite similar which suggests that the twin disc testing method is a good representation of a real wheel / rail contact as is generated in this full scale experiment. It can be seen in the above image the deformation of the railhead is only in one direction (the right rail head has deformed to the left). This directionality is because the slip applied to the wheel simulates a tractive force from right to left. The same was true in the twin disc samples in chapter 7 where a slip / tractive force was also applied.

The test was then carried out on the laser clad rail with a layer of Stellite 6 on the head of the R260 grade rail. The test was again conducted at 3% slip between the rail and the wheel. The test was carried out for a total of 20,000 cycles and photographs taken of the railhead after every 5000 cycles.

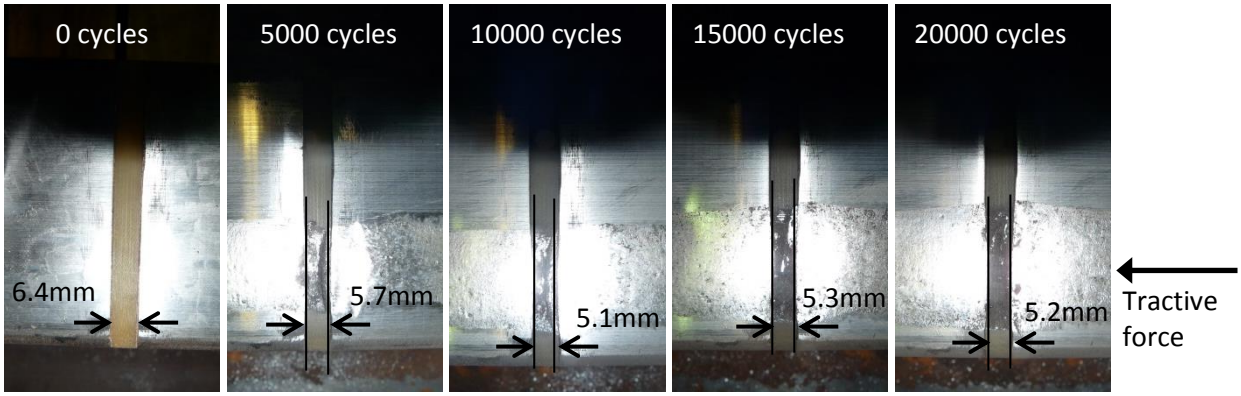

Figure 73: Images of Stellite 6 laser clad railhead before and during testing

The images in Figure 73 showed that some lipping formed over the endpost in the laser clad rail as the gap between the two rail ends closed up slightly. This lipping is much less severe than the deformation experienced by the non-laser clad R260 grade rail under the same conditions. The wear debris was also reduced in this test meaning that electrical failure due to debris bridging the gap over the endpost is less likely.

Another test was conducted with the standard R260 grade rail using a slip between the rail and the wheel of 1%. In Figure 74 it can be seen that the laser clad Stellite 6 sample exposed to 3% slip performed in a similar manor to the R260 grade rail when only at 1% slip. It can also be noticed that the gap in the laser clad Stellite 6 sample has stopped reducing. This could be because of work hardening of the Stellite 6 material which resists lipping further. The gap in the R260 grade continues to grow.

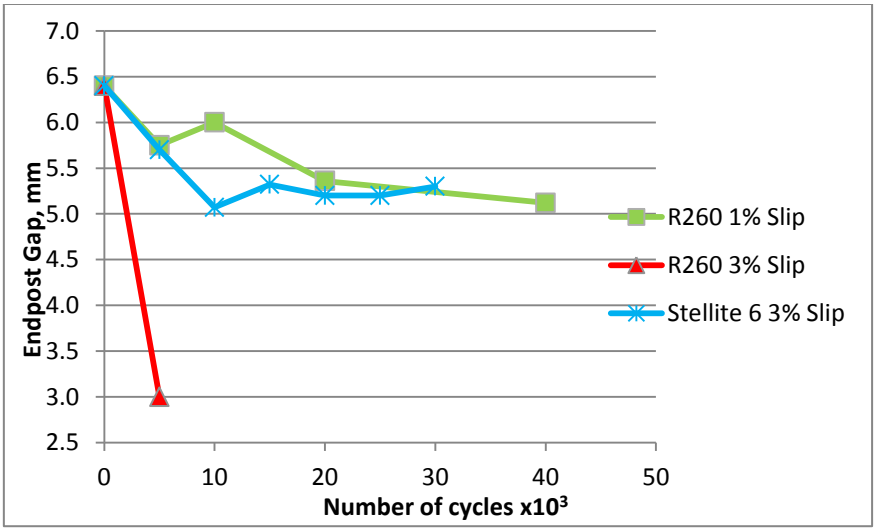

Figure 74: Change in the gap between rail ends in full scale lipping tests

These results match well with those gained in the twin disc testing in chapter 7.2.5 where the laser clad twin disc specimens displayed a much better performance in respect to lipping than the plain rail specimens.

8.3 Conclusions

By comparing the test method and results described in this chapter with the twin disc test method and results laid out in chapter 7 a number of conclusions can be gained.

- The twin disc test method gives a good representation of the wheel / rail contact. Similar lipping and deformation can be seen in the twin disc method than in the full scale method where a real wheel / rail contact is generated.
- Performance improvements seen in twin disc testing by using different rail head materials have been replicated in this full scale test method.

Gaining the knowledge that twin disc testing can be used to accurately predict performance gains in full scale experiments using different rail materials is important. Twin disc testing is a much quicker and less expensive process than full scale testing. Therefore more materials can be tested and evaluated prior to use in full scale tests or trials in the field.

This testing could also be used for further work investigating the transition between the standard rail steel and the laser clad layer. It would be beneficial to understand this interface in order to avoid and design out problems such as rail shelling which may occur in service.

9 Full Assembly Testing – Cyclic Fatigue Testing of Comparison IBJs

Full scale testing of IBJs was carried out to extend the shear testing that has been completed and reported upon in chapters 5 and 6. The aim of the testing was to compare the performance of two IBJ designs whilst also assessing the method under consideration and comparing this with the standard qualification tests discussed in chapter 3.

The following test method was used so that the life cycle of the joint could be assessed. This involved testing to a more onerous loading regime than in the qualification test methods discussed in chapter 3.2. Taking this approach, testing to failure was carried out and this gave a better understanding of the IBJ.

9.1 Method

The testing method used to assess the performance of design changes made to an IBJ was a four point bend set-up that cyclically applied a vertical force onto the rail. The endpost of the IBJ was positioned centrally between two hydraulic actuators that applied a force to the railhead. An LVDT was used to monitor the deflection of the joint at the endpost. Due to the constraints of the test rig being used the distance between the two actuators was set at 600 mm. The supports which the IBJ were positioned upon could be altered and in this experiment were set to a spacing of 1600 mm, a diagram of the test set-up can be seen in Figure 75.

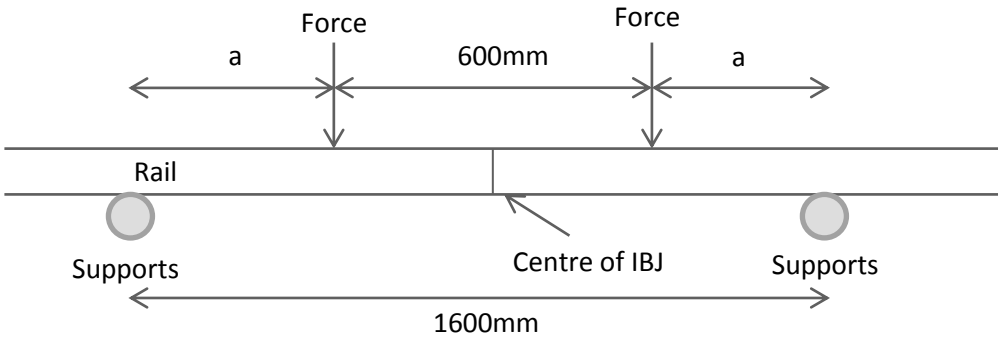

Figure 75: Diagram of four point bending set-up

An image of the test set-up showing the actuators and support position can be seen in Figure 76. It can be seen that the actuator supports are attached to the rig base on which the rail supports are also attached. The rig base has been designed to withstand high forces but this type and the reaction forces in the rig means that the rig will deform when forces are applied. This is discussed further in the results section below.

Figure 76: Image of four point bending set-up

The load was applied to the IBJ cyclically in order to fatigue the joint in a similar manner to that occurring in service where IBJs are repeatedly loaded by passing wheels. In order to test the life cycle of the joint and test it in more severe conditions than in current qualification tests a test regime was devised where the load was increased throughout the test. Table 7 shows the loads applied at various numbers of cycles throughout the test.

Number of cycles (million)	Load applied (kN)	Equivalent bending moment (kNm)
0 – 0.5	161	40
0.5 – 1.0	270	67
1.0 – 1.5	337	84
1.5 – 2.0	404	101

Table 7: Loading regime for cyclic testing of IBJs

The loads were calculated so that a bending moment was applied to the joint as specified in Table 7. The bending moment of 40 kNm was calculated using beam on elastic foundation theory aiming to represent a rail with the maximum static force applicable on the UK rail network (25 ton axle load) where the rail is on a 'soft' foundation (low track modulus) according to the literature (18). The calculation for the bending moment in the rail from a beam on an elastic foundation theory is shown below, equation 3.

$$M = \frac{Ql_c}{2} e^{-\frac{x}{l_c\sqrt{2}}} . \cos\left[\frac{x}{l_c\sqrt{2}} + \frac{\pi}{4}\right] \quad (3)$$

$$where\ l_c = \sqrt[4]{\frac{EI}{K_T}} \quad (4)$$

K_T = Track modulus. (7.83N/mm^2 for 'soft foundation' (18))

Using beam on elastic foundation theory and equations 3 and 4 to calculate the bending moment in the rail did not yield an accurate answer because the rail is not a beam on an elastic foundation. The bending moment in the rail will change depending on whether the wheel load is applied over a sleeper or midway between the sleepers. To take this into consideration and calculate a better

estimate of the bending moment in the rail, when the applied force is midway between sleepers, equations 5 and 6 were needed.

$$M_0 = M_n - \left(\sum_{j=1}^{j=n-1} F_j - \frac{Q}{4}\right) s \quad (5)$$

$$where\ F = -\frac{Q}{2} e^{-\frac{x}{l_c\sqrt{2}}} . \cos\left[\frac{x}{l_c\sqrt{2}}\right] \quad (6)$$

By gaining a figure for the bending moment in the rail the force to be used in the four point bending set-up to induce the same moment was calculated using equation 7.

$$Q = \frac{2M}{a} \quad (7)$$

The next bending moment of 67kNm was chosen to equal that of the most stringent qualification test that could be found for a similar sized rail section (37). The final bending moment of 101kNm was chosen as a 2.5 factor of safety over the first bending moment that aims to replicate in service conditions. This loading was also close to the limits of the test rig being used. The third bending moment was chosen midway between the second and final moments.

During the cyclic testing procedure, after each 0.5 million cycles, static testing was carried out to assess the stiffness of the joint and whether the IBJ was losing stiffness or strength during the test. The deflection at the centre of the IBJ was also monitored throughout cyclic loading.

9.1.1 Test Samples

The full scale testing was carried out on two joint samples, a standard UK joint which is currently manufactured and approved for use in the UK and a new design based on the shear testing results carried out in chapters 5 and 6. The new IBJ design consisted of a full fit fishplate with a flexible glass fibre insulating liner. The fishplate was glued to the liner using Temperange II adhesive. For commercial reasons the glue used to install the pre-insulated fishplates into the rail was the same in both test samples, this glue was not tested in the shear testing process. Both IBJs were fastened using the current UK standard fastening system of 1.1/8" swage fasteners. The IBJs chosen for testing were of the four hole design as it was decided these are weaker than the six holes joints and therefore any joint failure would be accelerated.

Ultrasonic transducers were attached to the fishplates of both test samples so that monitoring of the joint could take place during the test. The transducers were not placed on the head, foot or in the web of the rail as was the case during the shear testing; this is because these placements would not be achievable on IBJs that are installed in service. An image of the test samples with the attached ultrasonic sensors can be seen in Figure 77. Four ultrasonic sensors were placed on each fishplate (eight per joint), two of the four sensors were placed in the middle of the joint just either side of the endpost where de-bonding was more likely to occur, the other two sensors were placed further away on either side of the IBJ centre.

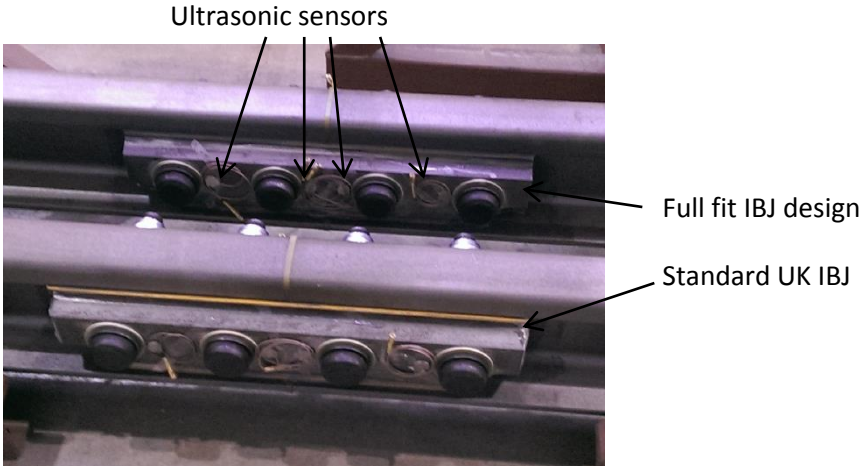

Figure 77: Two full scale test samples with ultrasonic sensors

After assembly and installation of the IBJs, electrical testing was carried out to the Network Rail standard that all IBJs have to conform to in the UK (38). Both test samples passed the electrical testing procedure.

9.2 Results and Discussion

9.2.1 Static Testing

Before the IBJs were cyclically tested a measure of their static stiffness was taken in the test rig and compared with a piece of standard, non-jointed, rail tested in the same manner. Increasing loads were applied to the test samples and the deflection at the centre of the IBJ measured so that a stiffness value could be determined. The results of the testing can be seen in Table 8. The raw results gained from the LVDT mounted to the rig and measuring the centre of the IBJ or rail have been corrected due to the rig movement. During the tests that have been carried out the rig and actuators moved by a small amount independently from the supports of the rail. This was measured and a correction factor was applied to the results to cancel out this movement.

Force Applied (kN)	Displacement (mm)			Corrected Displacement (mm)			Theoretical displacement (plain rail)
	Plain Rail	Standard IBJ	Full Fit IBJ	Plain Rail	Standard IBJ	Full Fit IBJ	
20	0.41	0.37	0.41	0.33	0.29	0.33	0.29
50	1.06	1.00	1.05	0.86	0.80	0.86	0.73
100	2.04	1.99	2.05	1.65	1.60	1.66	1.46
150	2.97	2.97	3.04	2.39	2.39	2.46	2.18
200	3.92	3.95	4.03	3.15	3.17	3.26	2.91
Stiffness (kN/mm)				64.52	62.50	61.73	68.71

Table 8: Results of static testing on IBJs

The above results show that the stiffness of the IBJs is lower than that of the plain rail which is expected as discussed in chapter 1. It also shows that the full fit joint is less stiff than the standard

UK wedge fit IBJ. The stiffness of the standard IBJ is 97% that of the plain rail and the stiffness of the full fit IBJ is 96% of that of the plain rail. These stiffness values are close to that of plain rail and match the aims of Network Rail that were discussed in chapter 2.4. The right hand column of Table 8 shows the theoretical deflection of the centre of the plain rail in the testing set-up calculated using beam bending theory. This shows that not all of the rig deflection may have been taken into account as the theoretical value for the rail stiffness is higher than the measured value.

9.2.2 Cyclic Testing

Cyclic testing was conducted as per the method discussed in chapter 9.1. The deflection of the centre of the IBJs was measured during the test at intervals and the results can be seen in Table 9. The figures in this table have been corrected in the same manner as for the static testing due to the movement of the rig during the tests. The deflection of plain rail was also tested dynamically at the same loads for a comparison with the IBJs. It can be seen that the IBJs are closer to the stiffness of the plain rail at lower loads (around 95% or above) but at higher loads the stiffness of the IBJs is reduced to around 87% of that of the plain rail.

Applied Force (kN)	Deflection (mm)		
	Standard IBJ	Full Fit IBJ	Plain Rail
160	2.27	2.36	2.24
270	3.88	4.20	3.85
337	5.18	5.43	5.09
404	7.12	7.05	6.18

Table 9: Average IBJ deflection during cyclic testing

The figures in Table 9 indicate that the standard IBJ is stiffer than the full fit IBJ at lower loading because the deflection was lower in the standard IBJ. However, as the test was continued the standard IBJ lost strength compared to the full fit IBJ, the deflection becomes greater in the standard IBJ than the full fit IBJ. Looking more closely at the deflection of the IBJs during the test it can be seen in Table 10 that the standard IBJ starts to weaken during the 337 kN loading cycle. The deflection of the IBJ increases during the 0.5 million cycles where this load was applied, suggesting that the joint was breaking. The full fit IBJ, although showing slightly higher deflections, performs in a more consistent manner whilst being loaded with 337 kN, the deflection stays more constant. Whilst being cyclically loaded at 160 kN and 270 kN both IBJs performed consistently and the deflection throughout these loading regimes was constant.

Cycles (thousands)	Average Deflection at centre of IBJ (mm)			
	Standard IBJ		Full Fit IBJ	
	337 kN	404 kN	337 kN	404 kN
0	4.98	6.32	5.38	7.05
100	5.18	7.74	5.36	-
200	5.21	7.92	5.36	-
300	5.23	-	5.4	-
400	5.24	-	5.37	-
500	5.24	-	5.38	-

Table 10: Table showing the change in deflection during cyclic testing

In Table 10 some results from the loading at 404 kN are missing, this is because of the failure of both test samples at this load. The deflection of the standard IBJ was again increasing over time and eventually, failure occurred in the fishplate at approximately 250,000 cycles into this loading regime. The full fit IBJ experienced a failure of the rail at approximately 95,000 cycles into the final loading regime.

During the test the deflection of the IBJs was filmed so that a closer analysis of the rail ends and the endpost could be gained. It is seen in Figure 78 that at the foot of the rail a gap opens up at the endpost when the joint is under load. Both the images are taken from footage when the joint was under the maximum load of 404kN. The gap in the standard IBJ appears to be larger than that formed in the full fit IBJ which suggests the full fit IBJ is stiffer, or bonded to the rail with more strength, as it is restricting the movement of the two rails relative to each other more than the standard IBJ.

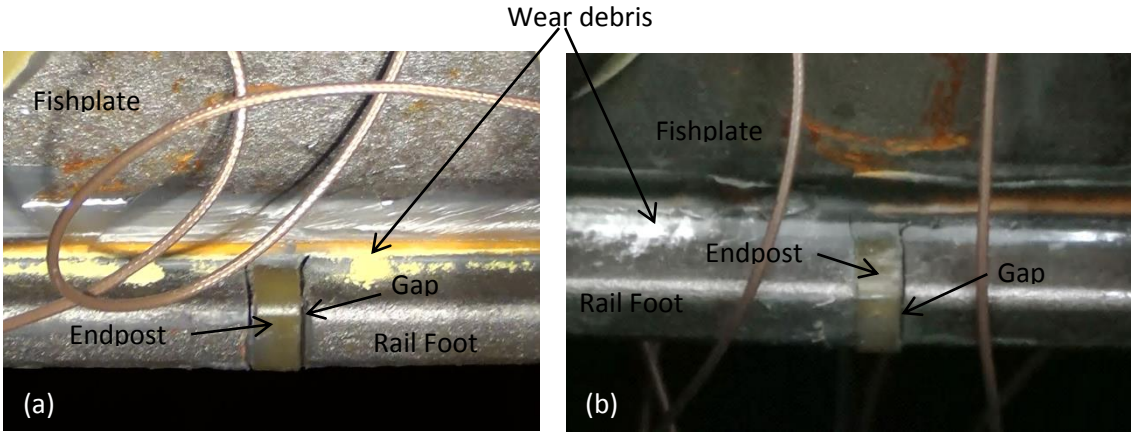

Figure 78: The rail foot at the centre of the IBJs in test (a) standard IBJ, (b) full fit IBJ

The gaps seen in Figure 78 are allowed to open up because the fishplate has de-bonded from the rail. The wear debris seen in the images shows that de-bonding has occurred; the insulating liner is being worn away by the differential movement of the rail and the fishplate. More wear debris can be seen in the standard IBJ, along with the larger gap, suggesting that this IBJ has de-bonded more than the full fit IBJ. Wear debris started accumulating from both IBJs during the 337kN load cycle, indicating that de-bonding started occurring around this time, quite a long time before the complete failure of the IBJs.

The two comparison IBJs failed in different ways as can be seen in Figure 79 and Figure 80. One of the standard IBJ's fishplates failed, seen in Figure 79, and in the full fit IBJ the rail failed just outside the fishplated area, seen in Figure 80.

Figure 79: Failure of the standard IBJ due to fishplate failure

Figure 80: Failure of the full fit IBJ due to a failure of the rail

The initial assessment of these failures suggest that the full fit IBJ is stiffer than the standard IBJ due to the design of the joint and less de-bonding that occurred during the test as discussed above. The stiffer IBJ means that more force is transferred into the rail causing the rail to fail before the fishplates.

Looking more closely at the failure of the standard joint it can be seen in Figure 81 that the fishplate failed after fatigue crack growth from the bottom of the fishplate. This failure was due to the de-bonding of the fishplate from the rail which caused greater movement and therefore stress in the fishplate.

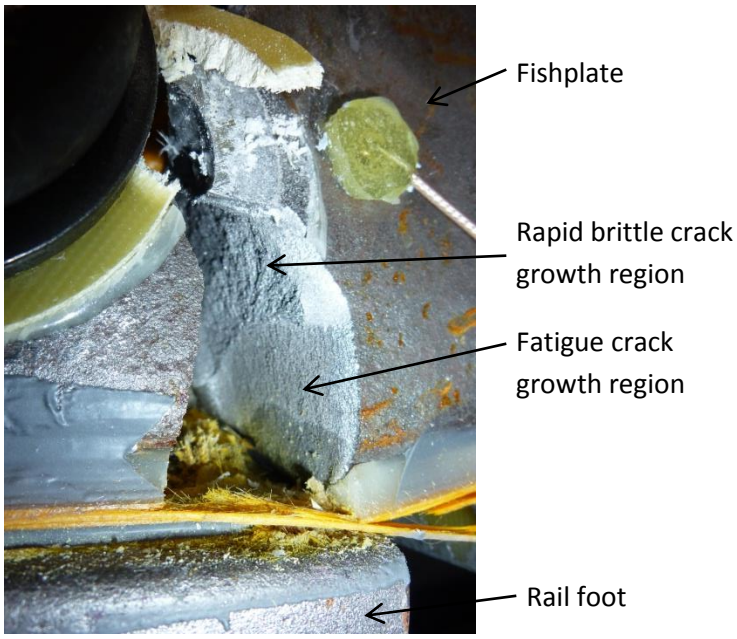

Figure 81: Failure of the standard IBJ showing a fatigue crack region

The opposing fishplate in the standard IBJ did not fail in the same manner as the fatigue crack shown in Figure 81. As can be seen in Figure 82 the fishplate is still intact but bent because of the extra stress it has had to cope with once the other fishplate failed. It can be seen in this image, however, that there is a lot of damage to the insulating liner at the centre of the joint where the de-bonding has taken place.

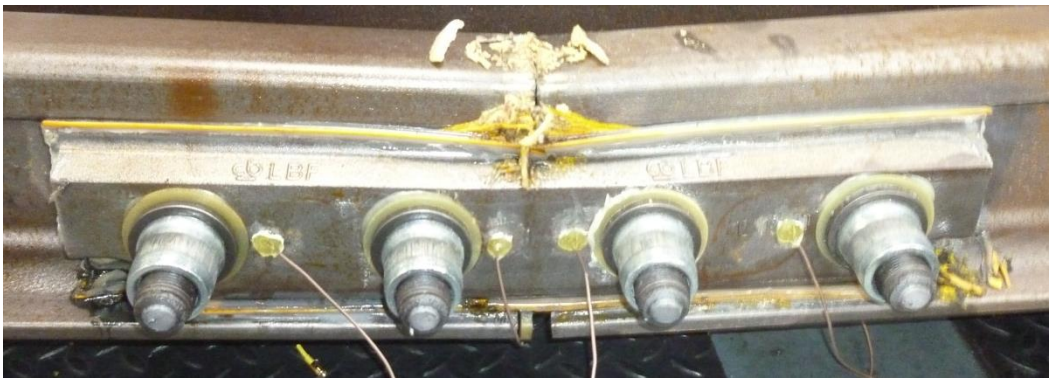

Figure 82: Fishplate of standard rail joint that did not fail due to cracking

Electrical testing of the rail joint was carried out after every 0.5 million cycles. Up until the failure occurred in the standard IBJ the two rails were still electrically insulated from each other.

The failure of the full fit IBJ occurred in the rail as seen in Figure 80. Figure 83 shows the failure in the rail that originated from a fatigue crack in the foot of the rail before rapid fracture of the rest of the section. The underside of the head of the rail shows where the liner has de-bonded from the glue layer and a layer of glue is left on the fishing surface.

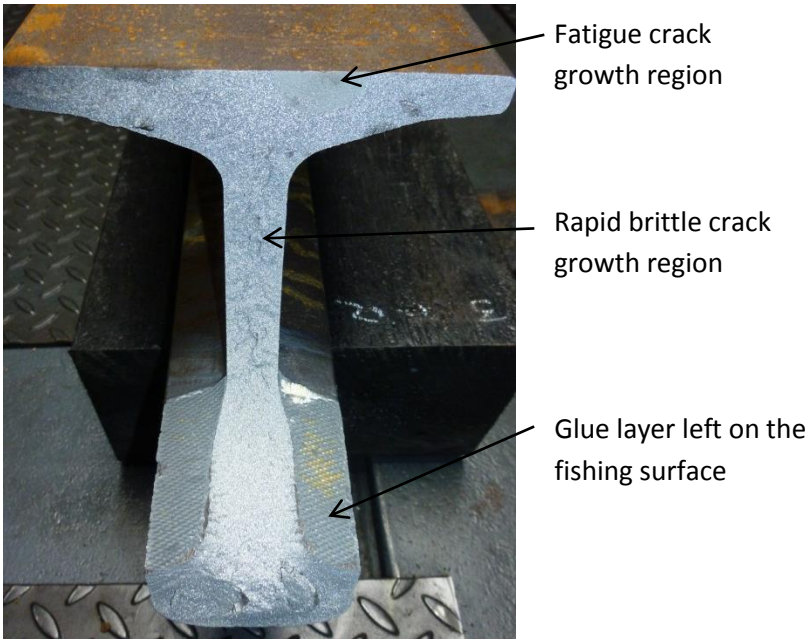

Figure 83: Failure in the rail in the full fit IBJ

The failure of the rail occurred just outside the fishplated area of the joint and almost directly underneath one of the loading points of the four point bending set-up. The fatigue crack initiated and propagated from a notch in the foot of the rail. However, the notch was not out of the ordinary for the foot of the rail as can be seen in Figure 84.

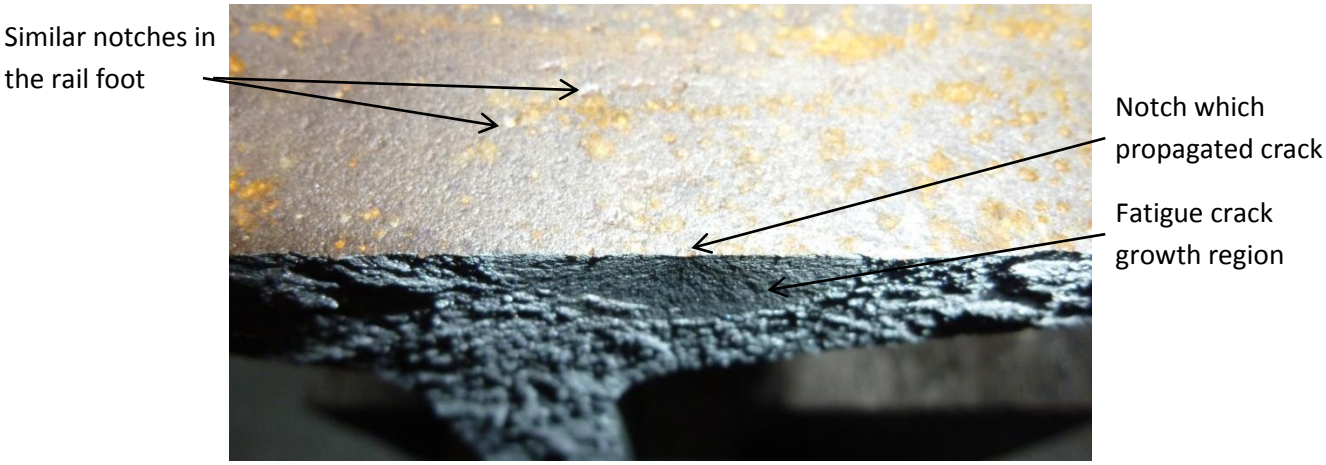

Figure 84: Fatigue crack in the rail and notches in the rail foot

The fishplates of this full fit IBJ showed no signs of fatigue cracking which was the cause of failure for the standard IBJ. The joint was tested electrically every 0.5 million cycles and was insulating throughout. The IBJ also passed electrical testing once the failure had occurred in the rail.

9.2.3 Ultrasonic Monitoring

Ultrasonic monitoring of the IBJ was carried out to give an understanding of the de-bonding of the glue layer in the joint and also to assess the possibility to develop a condition monitoring system based on the use of this technology. The use of ultrasound to measure the de-bonding of the glue layer was discussed in chapter 6.1 and similar sensors were used in this set-up and these were glued onto the fishplates of the IBJ as stated above.

During the cyclic testing, data was gathered from the ultrasonic sensors at intervals and this data was used to calculate the reflection coefficient. The average reflection coefficient could then be calculated for each interval and these have been compared to give an understanding of the degradation of the glue / insulating layer in the IBJ. It is worth noting that cyclic testing was carried out continuously due to time constraints within the project. Intervals for ultrasonic data gathering were dictated by equipment availability and also normal working hours and therefore these intervals, as seen in the results below, were not evenly spaced throughout the test period.

The plot shown in Figure 85 displays the change in reflection coefficient observed from sensors on the standard UK IBJ. The sensors displayed here are channel two, three, six and seven which are the sensors placed in the middle (nearer the endpost of the IBJ) of both fishplates. As is shown in the plot, the reflection coefficient does not change greatly until the IBJ enters the final loading regime and is close to the point of failure. The failure point is indicated by the vertical line on the plot.

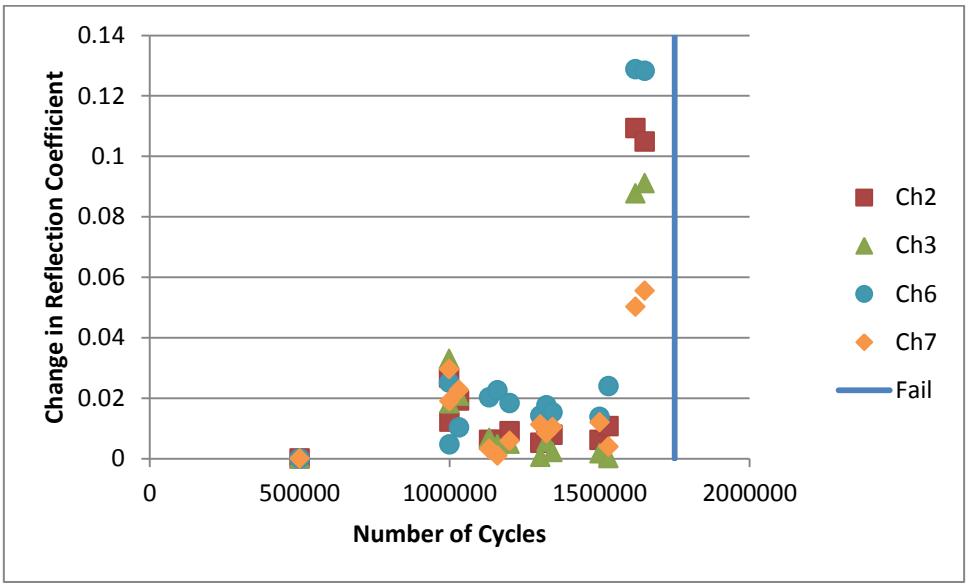

Figure 85: Change in reflection coefficient of ultrasonic sensors during cyclic testing of the standard IBJ

The above plot indicates that de-bonding occurred in the 404 kN load cycles and failure occurred soon after. This opposes what was seen during the test and documented in chapter 9.2.2 where wear debris from de-bonding started to accumulate during the 337 kN load regime. It is assumed, then, that this was due to de-bonding of the glue layer between the web of the rail and the insulating liner. This de-bonding was not detected because using sensors on the outside of the fishplate means that only the bond between the fishplate, glue and insulating liner can be detected. To detect the interface between the web of the rail and the glue and insulating liner layer then a sensor needs to be placed in the web of the rail as was carried out in chapter 6.

In Figure 86 the plot shows the change in reflection coefficient observed from sensors on the full fit design IBJ. It can be seen that the results are more scattered and random than those gathered from the standard UK joint, however, there is a general trend of increasing change in the reflection coefficient as the test was carried out.

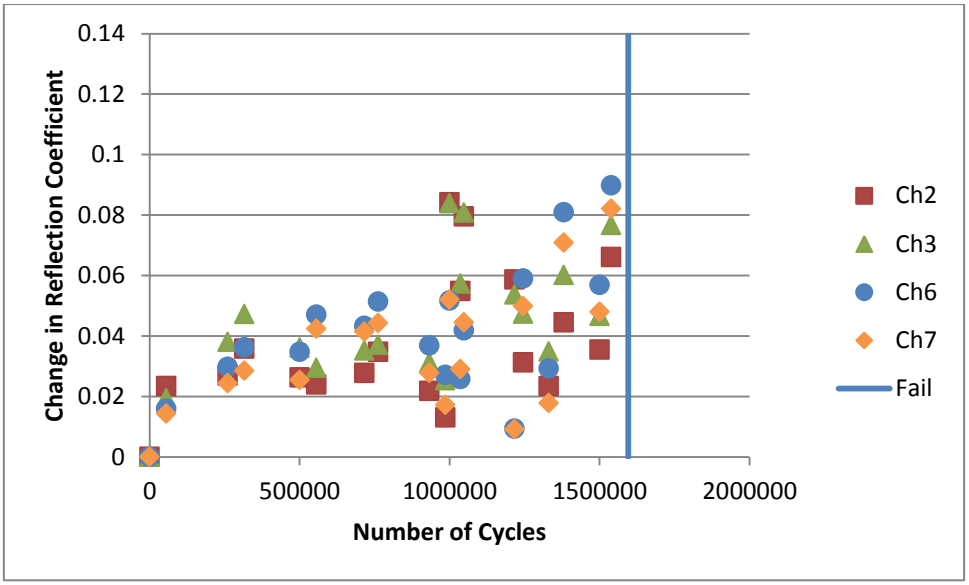

Figure 86: Change in reflection coefficient of ultrasonic sensors during cyclic testing of the full fit IBJ

The results in Figure 86 suggest that de-lamination of the full fit design joint progressively increased throughout the test. The design of this IBJ uses a flexible glass fibre liner that is impregnated with epoxy glue upon assembly of the components. It is believed that this glass fibre liner slowly degrades under the forces imparted upon the IBJ during the test. This causes small voids to form and therefore a change in the reflection coefficient is observed. This is opposed to the standard UK joint which is constructed from a stiff pre-formed insulating liner. From the results shown in Figure 85 it appears this liner fractures more suddenly causing a sharp change in the reflection coefficient rather than a gradual change over time. This matches well with the observations of the component shear testing discussed in chapter 6. In this previous testing the standard UK design fractured rapidly whereas the full fit design that incorporated the glass fibre liner experienced a more plastic behaviour, where the liner gave way gradually.

9.3 Conclusions

During the testing process there were no external signs that either of the IBJs were weakening during the first million cycles of the test which comprised the first and second loading regimes. From the ultrasonic analysis, however, it can be seen that the full fit design IBJ experienced some de-bonding at this time where the standard UK IBJ showed less signs of this happening. This explains the slightly higher deflection of the full fit IBJ.

During the third and fourth loading regimes the IBJs showed signs of de-bonding which was assessed by the build-up of insulating liner wear debris on the foot of the rail. From visual inspection the standard joint appeared to undergo more de-bonding and subsequently the failure of the fishplate occurred. This is seen in the ultrasonic results as a more sudden de-bonding of the insulating liner than that seen in the full fit IBJ which occurred just before failure of the fishplate.

The full fit IBJ offered a stiffer design at higher loads and less de-bonding was visually seen. The ultrasonic results show that de-bonding was more progressive and, as in the component shear testing, the first signs of de-bonding did not lead to overall failure. Due to this the IBJ held together

better at higher applied loads where the stress was transferred to the rail, causing failure there rather than in the fishplate.

The test method and test rig used were successful in testing both of the rail joints to the limits of their capability. The method allowed analysis of the IBJs at lower loads but also allowed analysis up to failure. This is an improvement on standard qualification test methods used currently. It is of benefit to test the IBJ to failure and to understand the failure mode so that improvements in design can be made.

Further investigation of the ultrasonic technology used should be carried out in order to obtain the most useful results possible. Alteration of the frequency and bandwidth used may lead to a higher degree of accuracy in measurement and enable the technology to be implemented in the field as a monitoring technique more easily. Also, placement of the sensors should be further investigated so it is ensured that they are placed where delamination will occur first and therefore capture the first point of failure of the IBJ.

10 Full Scale Testing - Monitoring and Comparing Lab Tests with Field Measurements

Further measurements have been taken in order to compare the difference between the standard and new joint design that were compared in chapter 9. This measurement technique has also been used to compare how the test rig performs when compared to real rail deflections under a passing train.

10.1 Method

The method that has been used for the laboratory testing is the same in set-up to that used in chapter 9. IBJs, supported at 1.6m spacing, were subjected to load from 2 actuators each spaced 300mm either side of the centre of the joint. This 4 point bending set-up is shown in Figure 75. Cyclic loads of the same magnitude as the previous tests were applied to the joints, these are shown in Table 11.

Load applied (kN)	Equivalent bending moment (kNm)
161	40
270	67
337	84
404	101

Table 11: Loads applied to the laboratory tested joints

Measurements were taken by video analysis methods. Targets are applied to different areas of the joint that can be filmed as shown in Figure 87. A software program records footage of the targets as the IBJ is cyclically loaded and real time displacements of the joints can be seen because the video equipment can be calibrated against a known measurement on the surface of the IBJ. Footage can also be analysed post experiment in order to gain a full understanding of the displacements of various parts of the IBJ.

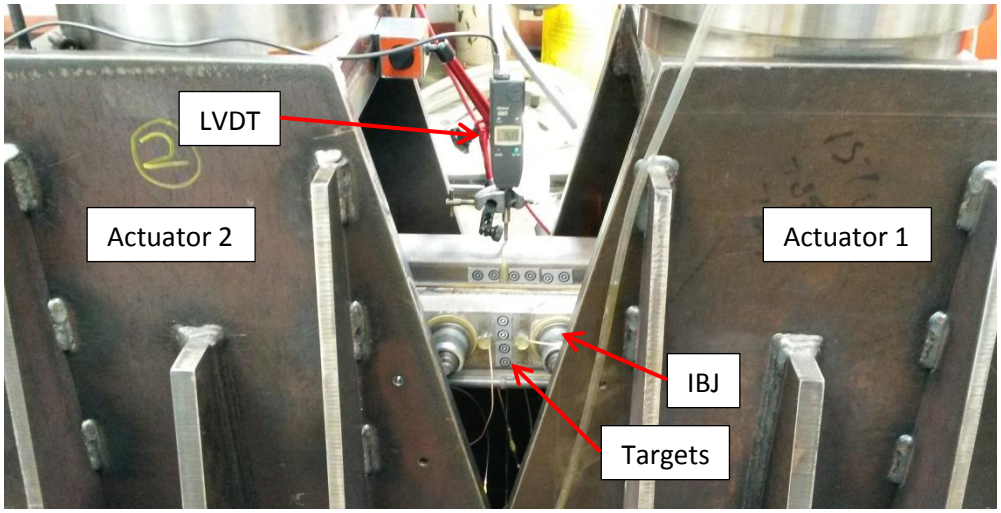

Figure 87: Testing set-up with targets for video analysis and LVDT.

An LVDT was also used throughout the testing to compare values with the video analysis software. This was mounted on the rig and measured displacement at the midpoint of the IBJ.

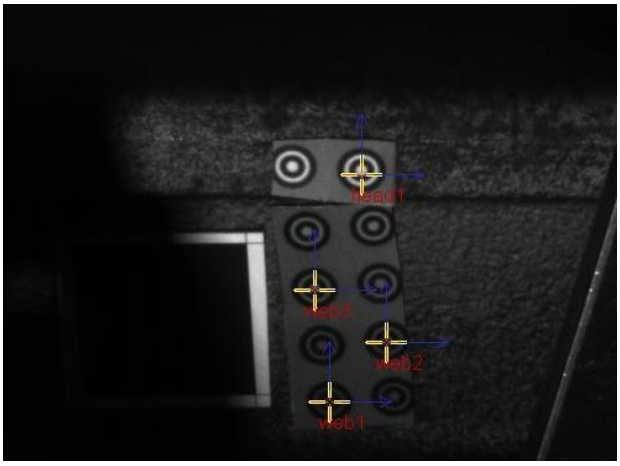

Figure 88: Targets on the web of the rail as seen by the video camera

Figure 88 shows a still image from the video camera, the targets are picked up in the software and are tracked to allow for the measurement of displacement.

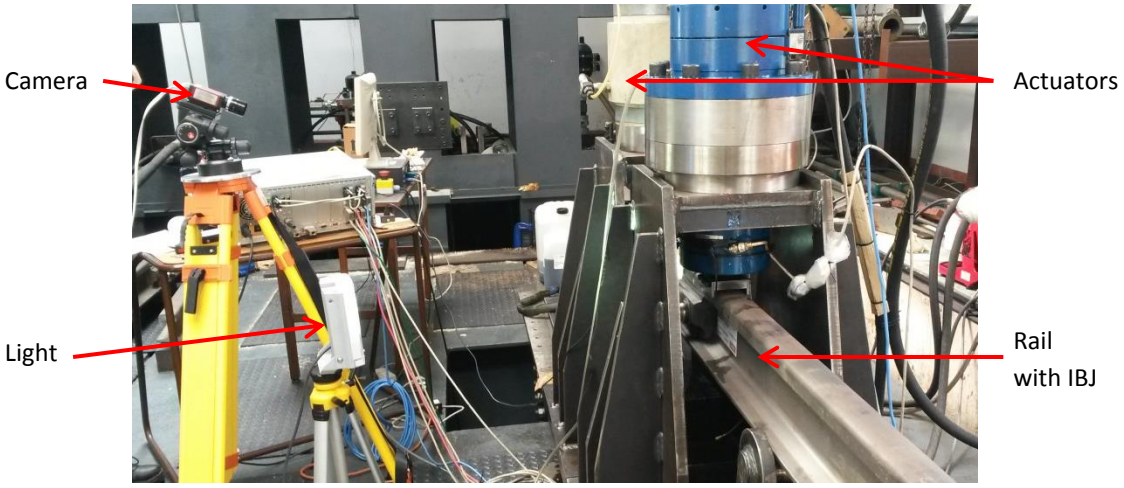

Figure 89: Test set-up showing camera position for laboratory testing

During the setting up of the test the distance from the camera to the targets on the IBJ was measured and input into the software. This information along with information on the angle of the camera is used by the software so that deflections in the vertical direction are calculated rather than just the deflection seen by the camera which would be at an angle to vertical. An image of the test and measurement set-up is shown in Figure 89.

The laboratory testing was carried out on test sample IBJs that were of the same design and materials as the IBJ test samples in chapter 9. Both of these were 4 hole glued IBJs, one being the standard current design and the other being a new design full fit IBJ. Laboratory testing was also carried out on a sample of plain rail.

The same technique was applied to rail installed in the field. Measurements of the deflection of this rail were taken so that these could be compared to the results gained from laboratory tests. This test set-up is similar to that in the lab with targets applied to the rail to enable monitoring of the rail using video analysis equipment. An image of the field based measurement set-up is shown in Figure 90.

Figure 90: Image of measurement set-up - video analysis of a section of rail

10.2 Results and Discussion

Firstly, the results of the laboratory testing are presented and a comparison between the two IBJ types is made. This is also compared with the results of the testing in the previous section with further analysis of the test rig. The results of plain rail laboratory testing are then compared to the in-field analysis of rail and a more accurate conclusion of the test rig performance is given.

10.2.1 Laboratory Testing

The table below shows the results that were gained from LVDT measurements during this experiment. As in chapter 9 the displacement of the rig has been taken into account in these measurements and a correction factor applied based upon this to ascertain the true rail deflection.

Applied Force (kN)	Displacement (mm)	
	Standard IBJ	Full Fit IBJ
161	2.54	2.39
270	4.56	4.20
337	5.91	5.61
404	7.19	6.97

Table 12: Full scale deflection test on different IBJ designs, LVDT measurements

It has been shown in Table 12 that the full fit IBJ deflects less than the standard IBJ. Comparing these results with those gained in chapter 9 and displayed in Table 9 it was seen that the full fit IBJ shows a similar performance in both cases. The standard joint in this case, however, has performed less well and higher deflections were seen in this test sample than that tested previously. This could indicate that the standard joint is more susceptible to slight variations in the manufacturing procedure. This could be because of cases like that shown in Figure 38 where the assembly process caused the insulating liner to split, therefore weakening the IBJ.

Using the video analysis software a similar set of results can be displayed for the two IBJ types.

Applied Force (kN)	Displacement (mm)	
	Standard IBJ	Full Fit IBJ
161	2.75	2.29
270	4.66	3.99
337	5.92	5.01
404	7.11	6.11

Table 13: Full scale deflection test on different IBJ designs, video analysis measurements

The values that have been displayed in Table 13 give the same general results as those presented in Table 12. Using both methods of measurement the standard IBJ experiences a greater deflection than the full fit IBJ. There are differences in the values however. When measuring the Standard IBJ the values of the LVDT measurements and the video analysis measurements are very close. For the full fit joint the values for the video measurement are close to those measured using the LVDT but are consistently lower. This may be due to small inconsistencies in the set-up of the LVDT and the movement of the rig.

The rig movement has not been taken into account whilst looking at the displacements calculated by video analysis. Unlike the LVDT which is attached to the rig whilst measuring the rail joint the camera for the video analysis is totally separate from the rig set-up and therefore no corrections need to be calculated.

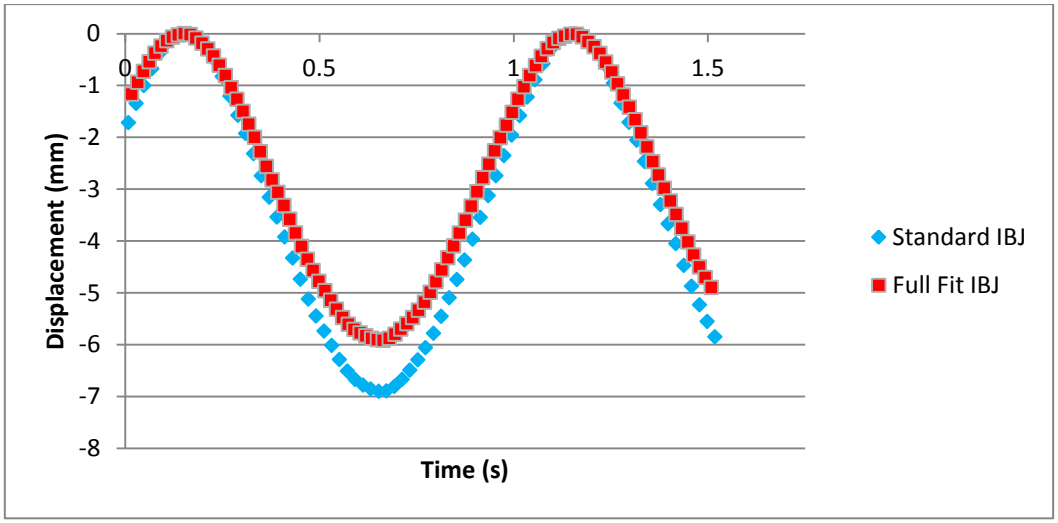

Figure 91: Graph showing the displacement over time of two different IBJ designs in laboratory testing under a cyclic load of 404 kN.

In Figure 91 a graph is shown of the displacement of the IBJ over time measured using the video analysis software. The video was set-up during the experiment to 50 frames per second meaning that 50 measurements are taken every second which allows the plot in Figure 91 to be generated. In the tests the load was applied to the joint cyclically in a sinusoidal wave form. It can be seen in the plot that this waveform has been transferred to the IBJ. Both IBJs deform in a very similar way, the only difference in the two plots being the amplitude of the displacement which has already been discussed from the results shown in Table 14. It is worth noting that the displacement that is shown in the plot in Figure 91 is negative because the IBJ were being pushed downward by the rig.

10.2.2 Field Measurements compared to Laboratory Measurements of Plain Rail

Measurements, using the video analysis technique, of a section of rail were taken so that the displacements and rail shape under load could be compared to laboratory testing. The rail that was measured was subject to a train passing over with an axle load of 12 tons travelling at roughly 18m/s. This would be considered a normal axle load in the UK for commuter traffic and would translate to a 6 ton load on each rail. The condition of the track at the measurement location was good with no voids or anomalies.

The plot in Figure 92 shows the displacement of the rail when the first bogie of the train passes over. The first difference that can be noticed between this measurement and that taken of the laboratory testing is the hogging of the rail. This is the upward movement of the rail before the first wheel reaches the point that is being measured. This phenomenon is not modelled in the laboratory testing as it would necessitate a much more complex test set-up. The deflection in the upward direction, however, is small compared to that in the downward vertical direction and it can be assumed that this movement would have little effect on the overall fatigue of the IBJ. Figure 93 displays the displacement of the plain rail when in the test rig. The plain rail was subjected to a cyclic force with maximum amplitude of 161kN, equal to the first test regime of the IBJ tests earlier in this chapter.

Another key difference between the field measurements and the laboratory testing measurements is the superposition of displacement due to wheels being close together in the field. This is clearly seen and is highlighted in Figure 92 where the rail reaches a point of maximum displacement twice in quick succession without returning to the starting point, or zero deflection, in between. It would be possible to alter the laboratory testing so that the test rig also loads the rail in this way but it was much simpler to load as a sine wave. The maximum displacement would not be affected by loading with the shape seen in Figure 92 and therefore this was not deemed necessary.

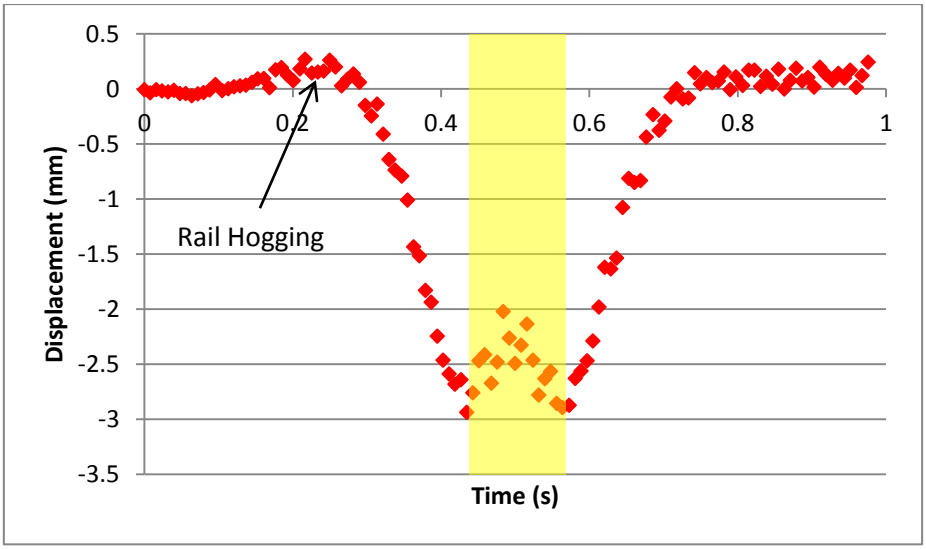

Figure 92: Graph showing the displacement of the rail with one bogie pass.

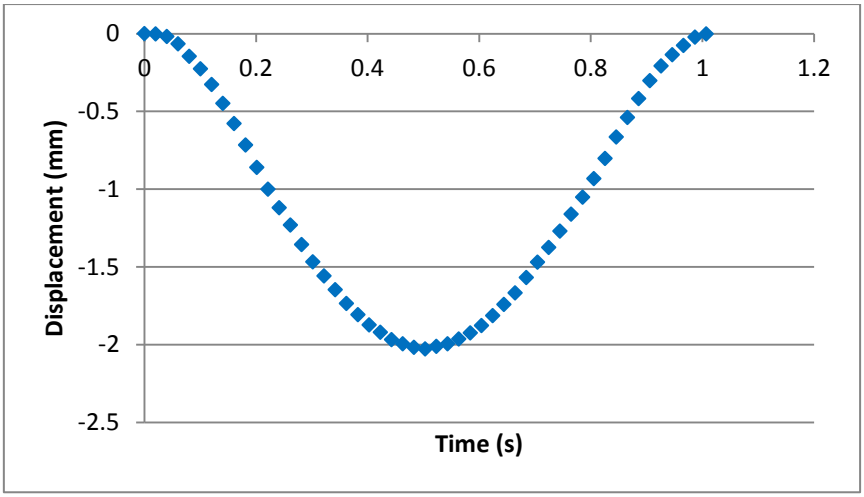

Figure 93: Graph showing displacement of rail in laboratory testing, load of 60kN

In order to compare the different results and understand the differences better the highlighted section in Figure 92 can be removed. This means that the plot would show the results if just a single wheel passed over the rail. In addition to this the displacement vs time plots can be altered to display the shape of the rail. This is achieved by including the speed of the train, converting the time into distance.

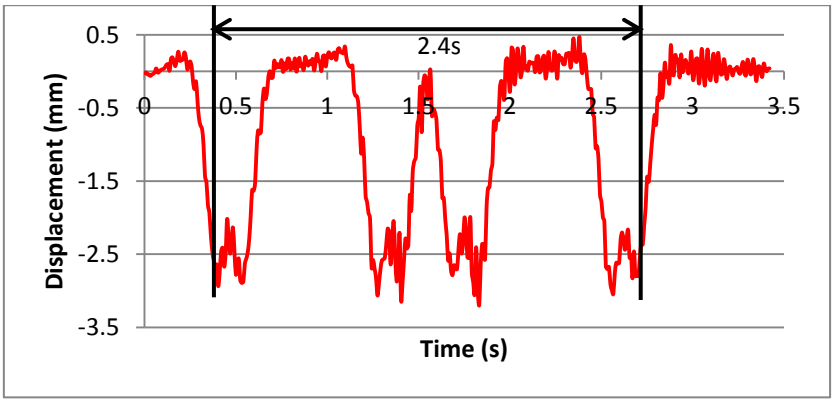

Figure 94: Rail movement due to a passing train

The speed of the train has been calculated from the video analysis results shown in Figure 94. The distance between the first and last wheel is known to be 43 metres and the time between these events is 2.4 seconds, equating to a speed of 18m/s. For the laboratory measurements the test rig cycled at a frequency of 1 Hz with a support spacing of 1.6m. Therefore equivalent to a train speed of 1.6m/s. In Figure 95 the shape of the rail in field and laboratory measurements are compared. Not as many data points are available to view for the field measurements compared to the laboratory measurements because of the higher train speed.

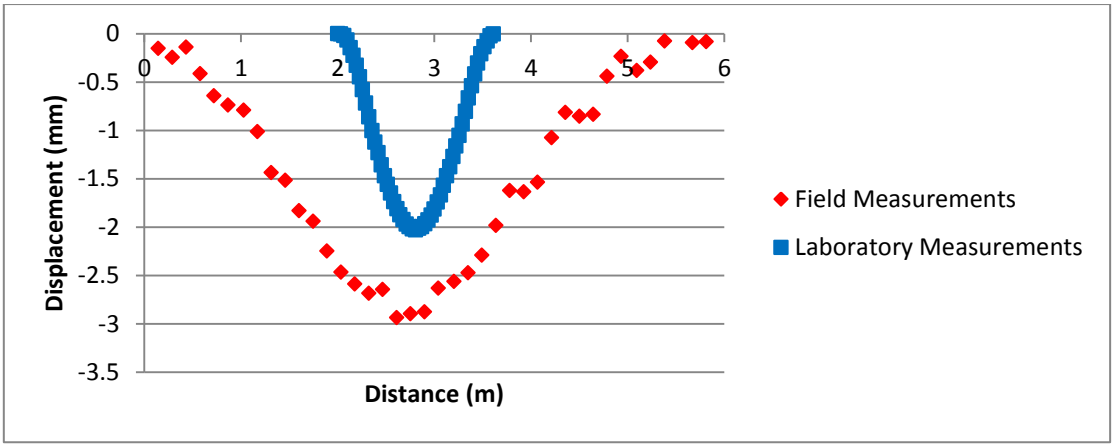

Figure 95: Rail shape from different laboratory and field measurements

Figure 95 displays the shape of the rail under load over a distance. The shape is important because it is related to the bending moment and therefore the forces seen within the rail. The field measurements show a shallower curve of the rail meaning there is less bending moment in the rail and therefore reduced stress compared to the rail tested in the lab. This is expected because the force applied to the rail in the laboratory test aimed to model a 25 ton axle load (as discussed in chapter 9) whereas the field measurements were taken under a 12 ton axle load. This comparison indicates that the lowest load used in the test regime in chapters 9 and 10 was onerous when compared to normal UK commuter traffic.

The laboratory testing loaded the rail cyclically in a sign wave pattern which is clear to see in the plot in Figure 95. The rail measured in the field seems to show a fairly sinusoidal shape (similar to the laboratory measurements) indicating that this loading pattern is suitable when trying to replicate real conditions.

10.3 Conclusions

Using the video analysis method to monitor the IBJs has produced similar results to measuring the displacement with an LVDT setup. It has been shown that the full fit IBJ is stiffer and does not deflect under load as much as the standard IBJ.

The benefit of using the non-intrusive video measurement is that displacement can be measured at a distance without the need to contact the rail. This has meant that plain rail measured in the laboratory can be compared to results gathered in the field. The shape of the rail in both situations has been compared and it has been shown that the laboratory testing imparts a higher bending moment on the rail when compared to standard UK commuter traffic. This means that the testing carried out is more onerous than the standard UK operating conditions. This is beneficial because higher axle loads or poor track structure could lead to increased bending moments in the rail and the testing has an included factor of safety to account for this.

11 Conclusions and Recommendations

11.1 Conclusions

The testing in this work has been successful in analysing the materials and designs used in IBJ manufacture and has also worked towards the life cycle assessment of insulated joints.

Specimen testing was carried out on materials which concluded that a different glue and insulating liner to that currently used in a standard IBJ would result in improved shear strength. By increasing the shear strength of the glue and insulating liner layer this would improve the stiffness of the IBJ and increase its life in service.

Component testing was carried out to further the results of the specimen testing. This procedure found that using a full fit glass fibre insulated fishplate provides increased shear strength to the IBJ. The testing process also showed that ultrasonic monitoring of the IBJ gives the ability to see when areas of the IBJ de-bond. This was useful in setting up full scale testing and could be worked on further to develop an in service inspection device with the ability to tell if an IBJ is damaged internally where no sign of the damage can be seen externally.

Full scale testing was carried out which utilised a new and bespoke testing regime and aimed to test an IBJ more rigorously than in current qualification testing regimes. Tests were carried out on two IBJs, one standard UK IBJ and one full fit design that was prepared on the basis of the specimen and component testing. The testing resulted in the failure of both IBJs but through different mechanisms. The full fit IBJ was found to be stiffer at higher applied loads which caused the stress to be diverted into the rail which failed. The standard IBJ was less stiff at higher applied loads and the de-bonding of the fishplate from the rail led to high stresses in the fishplate which failed through propagation of a fatigue crack. Ultrasonic monitoring of the IBJs during the full scale testing gave an insight into the de-bonding of the insulating layer and helped identify the causes of failure. The results showed a more rapid de-bonding in the standard IBJ while the full fit design experienced a more progressive de-bonding. These results backed up the initial ultrasonic data taken from the component shear testing. Again, this shows in-service inspection using ultrasonic technology could be developed, however, this may be limited due to the ability to only mount sensors on the outer edge of the fishplates and not within the web of the rail.

The testing that has been carried out has resulted in an improved design of IBJ which has been shown to be stiffer at higher loads and does not de-bond rapidly, as the standard IBJ does.

Further full scale testing was used to assess a new measurement technique where video analysis software measured the displacement of the IBJ. The results that this technique gave were similar and comparable to the results gained when measuring using an LVDT. This technique was used to measure the deflection of rail in real life with a train passing over. The shape of the rail under load could then be compared to the laboratory full scale testing. It was found that the full scale testing imparts a higher bending moment and therefore a higher stress into the rail than in real life under the conditions observed.

Specimen testing was also carried out to assess lipping at an IBJ and what could be done to reduce this type of failure in the railway system. It was shown that lipping could be experimentally modelled using twin disc testing which is a novel method in the attempt to achieve this. It was

found that endpost material with a higher compressive strength resists the lipping of the rail steel better than materials with lower compressive strengths. The endpost width did not affect the rate of lipping of the rail steel. The change that had the biggest effect on the lipping of the rail head was the rail material, hardened rail steel was found to be better than standard grade rail steel. Laser cladding of a harder material layer on top of the rail steel improved the performance of the rail head further. The advantages of these materials were not only to reduce lipping in the longitudinal direction but also to reduce dipping or material flow in the vertical direction. This has a benefit to the life of an IBJ due to the reduced vertical forces imparted upon it if there is less dipping.

The twin disc testing method was compared to a full scale test method. In this experiment the laser cladding technique was again tested and proved successful in reducing the lipping seen in the gap where the endpost sits. This comparison gives more confidence that the twin disc test can be utilised to investigate the performance of different rail materials with respect to lipping.

Using the results from this research a new IBJ concept has been developed with an increased life cycle compared to the current UK IBJ. The shear and full scale testing has determined the materials and joint design used in order to increase the shear and fatigue strength of the IBJ and reduce the risk of mechanical failure. The twin disc testing has shown how lipping and dipping at the endpost of an IBJ can be reduced, increasing the time to electrical and mechanical failure of the IBJ. New methods of testing have been developed and it has been proved that using these can improve understanding of the IBJ and the failures that occur.

11.2 Recommendations

It is recommended that further testing is carried out on the new joint design using the test regime that was developed in this work. The testing should be completed to confirm the IBJ's performance. A six hole joint of the same design should also be tested to confirm the design benefits in this configuration. The concept of ultrasonically monitoring the IBJ should be carried on in laboratory tests but also implemented and monitored in the field to determine the effectiveness of this method. Further study into ultrasonic measurements should include investigation of different ultrasonic frequencies and bandwidths to find out if this can give a more detailed view of the delamination process. Also, investigation of the position of the sensors to ensure that they are placed strategically and that they detect the first point of failure within the IBJ should be carried out on further tests.

Further video analysis should be carried out to measure IBJs that are in service. This would give a baseline of joint stiffness that can be compared to the stiffness of IBJs in laboratory tests and also new designs that are installed in service.

The laser cladding of the railhead to improve the lipping performance of the IBJ should be taken forward into field testing where an IBJ with a laser clad railhead is installed adjacent to a standard rail joint. These joints can then be compared and a better understanding of the life cycle improvement of an IBJ using this material improvement can be gained. Investigation needs to be carried out to determine the configuration of the laser clad layer on the rail head, including the layer thickness and the length that the layer extends either side of the joint. Some of these investigations could be achieved using the test methods described in chapters 7 and 8. These methods would be

especially helpful in determining the possible problems at the transition between the laser clad layer and the standard rail steel. Where this transition happens there will be a sudden change in rail head hardness which could cause many problems. The design of the transition t is important and could mitigate any perceived issues, designs can be tested first using the twin disc method to enable comparison of different designs at different slip and contact pressures. This testing should highlight any initial concerns due to railhead shelling or delamination. The design can then be tested further and proven in the full scale wheel test rig to ensure a prototype is safe to install in the field.

11.3 Publications Arising From the Work

1. P. Beaty, R. Lewis, B. Temple and M. B. Marshall, “Experimental Modelling of Rail End Lipping in Insulated Joints,” in *Proceedings of WCRR*, Sydney, Australia, 2013.

2. P. Beaty and P. Insley, “Looking at Lipping,” *The Rail Engineer,* p. 39, October 2013.

3. P. Beaty, R. Lewis, B. Temple and M. B. Marshall, “Experimental Modelling of Rail End Lipping in Insulated Joints,” in *Proceedings of Railways 2014*, Ajaccio, Corsica, France, 2014.

4. P. Beaty, R. Lewis, B. Temple and M. B. Marshall, “Experimental Modelling of Rail End Lipping in Insulated Joints,” *Proceedings of the Institution of Mechanical Engineers, Part F: Journal of Rail and Rapid Transit,* Accepted, yet to be published.

12 References

1. **Network Rail.** IRJ (Insulated Rail Joint) Head Repair from Selectequip - YouTube. [Online] Network Rail, 28 September 2012. [Cited: 23 January 2014.] http://www.youtube.com/watch?v=vbpjPLKWJ24.

2. **The Permanent Way Institution.** Rail Joints. *British Railway Track.* Great Britain : The Permanent Way Institution, 2007, pp. 201-219.

3. **Akhtar, M, Davis, D and O'Connor, T.** *Revenue Service Evaluation of Advanced Design Insulated Joints.* Pueblo : Transportation Technology Centre Inc. (TTCI), 2008.

4. **Sporer, Petr.** Styk podlozeny izolovany.JPG. [Online] Wikimedia Commons, 22 February 2007. [Cited: 19 December 2013.] http://commons.wikimedia.org/wiki/File:Styk_podlozeny_izolovany.JPG.

5. **Network Rail.** Identified failure modes of IBJs (based on Trust output). 2010.

6. **Hanna, M, Mutton, P and Mutton, A.** *Metallurgical Examination of Failed Joint Bars from Insulated Rail Joints.* Melbourne : Institute of Railway Technology, Monash University, 2008.

7. **Chalmers.** *D4.2.3 Improved model for loading and subsequent deterioration of insulated joints.* s.l. : Innotrack, 2009.

8. *Insulated Rail Joint Maintenance Review.* 3M, 1972.

9. **Voestalpine BVG GmbH.** Insulated Rail Joint IVG30. [Online] Voestalpine. [Cited: 26 January 2014.] http://www.voestalpine.com/bwg/en/products/sondersysteme/ivg30.

10. **Mospan, John W, Remington, James A and Urmson, Jr, W Thomas.** *Lap Joint. US 8113441 B2* United States of America, 14 February 2012.

11. *Innovative Design Concepts for Insulated Joints.* **Charlton, Zachary I.** April 2007, Master of Science Thesis.

12. **Ciloglu, Korhan.** *Structural Finite Element Analysis (FEA) of Insulated Rail Joints.* Pittsburgh : LB Foster, 2008.

13. **Chandra, T, et al., et al.** *Rail CRC-Project 75, A Novel Approach to Insulated Rail Joints.* Wollongong : University of Wollongong, 2006.

14. **Jackson, Tony.** New-Endpost-Tenconi.pdf. [Online] Network Rail, 2012. [Cited: 27 January 2014.] http://www.tenconi.ch/fileadmin/user_upload/news/New-Endpost-Tenconi-1.pdf.

15. **London Underground Track Engineering.** *Technical Bulletin No. HOE-TRK-TB-2012-0074-2.0.* London : London Underground, 2012.

16. **LB Foster.** Insulated Rail Joints Catalog. [Online] 21 October 2009. [Cited: 27 January 2014.] http://www.lbfoster-railproducts.com/rail_pdf_profiles/Insulated%20Rail%20Joints%20Catalog.pdf.

17. **Martinus Rail.** Hercules L4. [Online] 2012. [Cited: 20 01 14.] http://www.martinusrail.com.au/products-and-services-app/hercules-l4.

18. **The Permanent Way Institution.** The Railway Track as a Structure. *British Railway Track.* Great Britain : The Permanent Way Institution, 2007, pp. 471-486.

19. *Finite Element Analysis of Bonded Insulated Rail Joints.* **Himebaugh, Anne K, Plaut, Raymond H and Dillard, David A.** 2008, International Journal of Adhesion and Adhesives, Vol. 28, pp. 142-150.

20. *Development of TPC railroad ties for rail joint use.* **Nishihara, Takato.** Sydney : s.n., 2013. World Congress on Railway Research.

21. **LB Foster.** L.B. Foster Insulated Tie Plates. [Online] LB Foster. [Cited: 29 January 2014.] http://www.lbfoster-railproducts.com/Insulated_Tie_Plates.asp#mstto=.

22. **Sandström, J, et al., et al.** 5.3.4 Insulated Joints. *INNOTRACK Concluding Technical Report.* Paris : International Union of Railways (UIC), 2010, pp. 117-119.

23. *Deterioration of insulated rail joints – a three-year field study.* **Sandström, Johan, et al., et al.** Chengdu : s.n., 2012. Proceedings of the 9th International Conference on Contact Mechanics and Wear of Rail/Wheel Systems (CM2012).

24. *Microstructural characterisation of railhead damage in insulated rail joints.* **Rathod, C, et al., et al.** 2012, Materials Science Forum, Vols. 706-709, pp. 2973-2942.

25. *Laser Cladding for Railway Repair and Preventative Maintenance.* **Clare, A, et al., et al.** 3, 2012, Journal of Laser Applications, Vol. 24.

26. *Experimental studies on the performanceof rail joints with modified wheel/railhead contact.* **Zong, N and Dhanasekar, M.** 2013, Proc. IMechE Part F: J Rail and rapid transit, pp. 1-21.

27. *Experimental Investigation of Wheel/Rail Rolling Contact at Railhead Edge.* **Bandula-Heva, T M, Dhanasekar, M and Boyd, P.** 2013, Experimental Mechanics, Vol. 53, pp. 943-957.

28. *Contact-impact stress analysis of rail joint region using the dynamic finite element method.* **Wen, Zefeng.** 2005, Wear, Vol. 258, pp. 1301-1309.

29. *Effects of insulated rail joint on the wheel/rail contact stresses under the condition of partial slip.* **Yung-Chuan Chen, Li-Wen Chen.** 2006, Wear, Vol. 260, pp. 1267-1273.

30. *Rolling contact fatigue predictions for rails and comparisons with test rig results.* **Kabo, E, et al., et al.** 2010, Proc. IMechE, Part F: Journal of rail and rapid transit, Vol. 244, pp. 303-317.

31. *Investigation of the rolling contact fatigue resistance of laser cladded twin-disc specimens: FE simulation of laser cladding, grinding and a twin-disc test.* **Ringsberg, J, Skyttebol, A and Lennart Josefson, B.** 2005, International Journal of Fatigue, Vol. 27, pp. 702-714.

32. *Assessment of Laser Cladding as an Option for Repair of Rails.* **Lewis, S R, Lewis, R and Fletcher, D I.** Chengdu : s.n., 2012. Proceedings of CM2012 9th International Conference on Contact Mechanics and Wear of Rail/Wheel Systems.

33. *Fatigue evaluation of surface coated railway rails using shakedown theory, finite element calculations, and lab and field trials.* **Ringsberg, J W, et al., et al.** 2005, International Journal of Fatigue, Vol. 27, pp. 680-694.

34. *Wear mechanisms and transitions in railway wheel steels.* **Lewis, R and Dwyer-Joyce, R S.** 2004, Procedings of the Institute of Mechanical Engineers Part J: Engineering Tribology, Vol. 218, pp. 467-478.

35. **Hawley, C.** *Draft performance specification for factory made insulated block joints (IBJs).* s.l. : Network Rail, 2012.

36. **Network Rail.** Company Standard Ref: NR/SP/TRK/023. London : Network Rail, 1996.

37. **Standards Austalia.** AS1085:12 Railway Track Material Part 12: Insulated Joint Assemblies. Sydney : Standards Australia International Ltd., 2013.

38. **Network Rail.** *NR/SP/TRK/064 Assembly of BR MkIII 4- and 6-hole insulated joints.* London : Network Rail, 2003.

39. *The Ultrasonic Pulse-Echo Technique as Applied to Adhesion Testing.* **Tattersall, A G.** 1973, Journal of Physics D: Applied Physics, Vol. 6, pp. 819-832.

40. *An Approach for Contact Stress Mapping in Machine Joints and Concentrated Contacts.* **Marshall, M B, et al., et al.** 4, 2004, Journal of Strain Analysis for Engineering Design, Vol. 39, pp. 339-350.

41. *Development of a machine for closely controlled rolling contact fatigue and wear testing.* **Fletcher, D I and Beynon, J H.** 4, 2000, Journal of Testing and Evaluation, Vol. 28, pp. 267-275.

42. **Sandström, J, et al., et al.** Field study of insulated rail joint degredation on Västkustbanan. [Online] [Cited: 10 10 2013.] http://www.railwaygroup.kth.se/polopoly_fs/1.347141!/Menu/general/column-content/attachment/Johan%20Sandstr%C3%B6m%20et%20al.pdf.

43. **Tata Steel.** Rail Technical Guide. [Online] 2013. [Cited: 10 06 2013.] http://www.tatasteelrail.com/file_source/StaticFiles/Business_Units/Rail/Rail%20Technical%20Guide%20Final.pdf.

44. **Ekberg, Anders and Paulsson, Björn.** *Innotrack - Concluding Technical Report - page 118.* Paris : International Union of Railways, 2010.